Assessment of Climate and Hydrological Changes in Bhutan Using CMIP6

August 2025

National Centre for Hydrology and Meteorology and Department of Forest and Park Services, Ministry of Energy and Natural Resources, Royal Government of Bhutan

Assessment of Climate and Hydrological Changes in Bhutan Using CMIP6

National Centre for Hydrology and Meteorology and
Department of Forest and Park Services, Ministry of Energy and Natural Resources, Royal Government of Bhutan

August 2025

Authors
Ms. Pema Syldon, Senior Hydromet Officer, NCHM
Mr. Ugyen Chophel, Deputy Chief Statistician, NCHM
Mr. Pema Dendup, Deputy Chief Forestry Officer, DoFPS, MoENR
Ms. Monju Subba, Senior Hydromet Officer, NCHM
Mr. Chimi Namgyel, Senior Statistical Officer, NCHM
Mr. Jigme Wangchuk, Sr. Forest Ranger, DoFPS, MoENR
Mr. Dorji Phunthso, Senior Forestry Officer, DoFPS, MoENR
Mr. Thinley Dorji, Forestry Officer, DoFPS, MoENR

Published by:
National Centre for Hydrology and Meteorology and Department of Forest and Park Services, Ministry of Energy and Natural Resources, Royal Government of Bhutan

Suggested citations:
NCHM and DoFPS. (2025). Assessment of Climate and Hydrological Changes in Bhutan Using Downscaled CMIP6 Projections.

Funded by: Royal Government of Bhutan, Bhutan For Life Project

Forward

It is with a profound sense of responsibility and dedication to national development that I present this technical report on the projected future climate and hydrological changes in the country. The National Centre for Hydrology and Meteorology (NCHM) remains steadfast in its commitment to delivering authoritative scientific assessments that inform evidence-based policy formulation and the sustainable management of Bhutan's vital water resources.

Given Bhutan's complex topography, understanding the anticipated impacts of climate change on temperature, precipitation patterns, and river discharge is of paramount importance. This report offers a comprehensive analysis based on climate models and hydrological simulations across various Shared Socioeconomic Pathways providing critical insights into temporal and spatial variations that will influence water availability, flood risk, and ecosystem resilience.

The findings detailed herein reflect rigorous research and collaborative efforts by the dedicated officials at NCHM and Department of Forest and Park Services, Ministry of Energy and Natural Resources. It is our earnest hope that this document will serve as a fundamental resource for policymakers, planners, and stakeholders engaged in Bhutan's climate adaptation strategies and integrated water resource management.

In light of the mounting challenges posed by climate variability and change, it is imperative that the insights and recommendations contained in this report guide future interventions to enhance the nation's resilience and safeguard its precious hydrological assets for present and future generations.

Karma Dupchu
Director

Acknowledgement

This report, "*Assessment of Climate and Hydrological Changes in Bhutan Using CMIP6*", was conducted jointly by the National Centre for Hydrology and Meteorology (NCHM) and the Department of Forests and Park Services (DoFPS), Ministry of Energy and Natural Resources, Royal Government of Bhutan.

We gratefully acknowledge the generous support provided by the Bhutan For Life Project, whose funding made this assessment possible. We also extend our sincere appreciation to the National Institute of Environmental Studies and International Centre for Water Hazard and Risk Management under the auspices of UNESCO (ICHARM), Japan, and collaborators whose expertise and dedication contributed significantly to the successful completion of this study.

Their collective efforts have been instrumental in enhancing our understanding of climate and hydrological dynamics in Bhutan, which will inform science- based decision making and sustainable resource management in the face of a changing climate.

List of Abbreviations

APLAT	Climate Change Adaptation Information Platform
CMIP6	Coupled Model Intercomparison Project Phase 6
DEM	Digital Elevation Model
DJF	December January February
ENSO	El Niño–Southern Oscillation
GCM	Global Circulation Model
GDP	Gross Domestic Product
GLOF	Glacier Lake Outburst Flood
IOD	Indian Ocean Dipole
ISIMIP2b	Inter-Sectoral Impact Model Intercomparison Project Phase 2b
JJAS	June July August September
NCHM	National Centre for Hydrology and Meteorology
NIES	National Institute for Environmental Studies
NSE	Nash- Sutcliffe Efficiency
MAM	March April May
OND	October November December
PRB	Punatshangchu River Basin
R^2	Coefficient of Determination
RRI	Rainfall Runoff Inundation
RMSE	Root Mean Square Error
SSP	Shared Socioeconomic Pathways
USGS	United States Geological Survey
WRB	Wangchu River Basin

Table of Contents

Table of Tables

Table of Figures

Executive Summary

This report *"Assessment of Climate and Hydrological Changes in Bhutan Using Downscaled CMIP6"* evaluates future climate and hydrological changes in Bhutan's Punatshangchu and Wangchu River Basins under three emission scenarios (SSP1, SSP2, and SSP3) across near-term (2021–2040), mid- term (2041–2060), and long- term (2081–2100) periods. The analysis integrates projected changes in precipitation, temperature, and river flow to understand potential impacts on water resources and inform adaptive management strategies.

Projected temperatures in the country show significant warming across all scenarios. Annual maximum and minimum temperatures are expected to rise between 1°C and 5.5°C by the end of the century, with the most pronounced warming occurring in the northern highlands during winter months. These temperature increases threaten the stability of snowpack and glaciers, which are vital to the country's water supply. Meanwhile, precipitation projections indicate substantial increases in annual and summer rainfall, particularly in southern regions. Under the high- emission SSP3 scenario, summer precipitation could increase by over 1500 mm by the late century, while winter precipitation is expected to remain low or decline. This pattern suggests more intense monsoon seasons and drier winters, with implications for flood risk, water availability, and ecosystem health.

Hydrological projections reveal distinct patterns between the two basins. In the Punatshangchu River Basin, river flows are generally expected to increase across all timeframes and emission scenarios, with particularly strong increases during the monsoon season. The upstream Kerabari station consistently shows higher flow, potentially exceeding 400 m^3/s under SSP3 in the long term. These trends imply greater water availability but also heightened flood risks. Conversely, the Wangchu River Basin shows declining or stagnant flows in the near and mid- term periods, especially under SSP1 and SSP2. Only under the SSP3 scenario in the long term do flows rise significantly, likely driven by increased rainfall and glacier melt. These contrasting trends underscore the need for tailored water management approaches in each basin.

The study acknowledges several limitations, including uncertainties inherent in climate and hydrological models, particularly in representing glacier and snow dynamics. Additionally, factors such as land use change and infrastructure development were not included, which could influence future water availability and flow patterns. Model biases, especially in simulating monsoon rainfall and extreme events, may also affect the precision of projections at the basin scale.

Based on these findings, policy recommendations include prioritizing flood management infrastructure and adaptive reservoir operations in the Punatshangchu River Basin to cope with intensified monsoon flows. In the Wangchu River Basin, emphasis should be placed on water conservation, dry season storage, and demand management to address declining flows. Nationally, expanding hydrometeorological and glacier monitoring networks is critical, alongside integrating climate projections into water resource planning, disaster risk reduction, and agricultural policies. Developing basin-specific adaptation strategies will be essential to managing increasing variability and extreme events.

In conclusion, Bhutan is projected to experience rising temperatures and more variable precipitation patterns, leading to regionally diverse hydrological outcomes. While some areas may benefit from increased water availability, others are likely to face greater water stress or flood hazards. A proactive, science-based approach to climate adaptation and water management is vital to safeguard livelihoods, ecosystems, and the country's sustainable development goals.

1. Introduction

Bhutan is a landlocked and mountainous country located in the eastern Himalayas region. The country's diverse elevation and complex topography contribute to significant climatic variability, with climatic zones ranging from subtropical conditions in the southern foothills to alpine climates in the northern highlands (Dorji et al., 2021). The southwest monsoon, which typically spans from June to September, accounts for about 73% of Bhutan's total annual rainfall, though the amount and intensity vary across regions (NCHM, 2019). While this seasonal rainfall is vital for agriculture, hydropower generation, and ecosystem functioning, it also heightens the likelihood of floods and landslides in vulnerable areas (NCHM, 2021).

The country's steep terrain and fragile geological formations make it highly susceptible to a range of hydro-meteorological hazards, including floods, landslides, slope failures, windstorms, and glacial lake outburst floods (GLOFs) (ADPC & UNDRR, 2020, Dorji et al., 2016). Among these, floods are the most frequent and damaging hazard, particularly during the monsoon season. Vulnerability is heightened by the concentration of approximately 70% of Bhutan's settlements and infrastructure including hydropower plants, roads, airports, and agricultural lands along flood-prone river valleys (MoWHS, 2015). Bhutan ranks fourth in South Asia in terms of population exposed to flood risks, with 1.7% of its population residing in high-risk zones (MoEA & WB, 2015).

Climate change is projected to exacerbate the frequency and intensity of extreme weather events, thereby increasing the severity of associated hazards. The retreat of glaciers and altered precipitation patterns are already impacting water availability, resulting in monsoon flooding and dry-season water scarcity. These hydrological changes directly affect Bhutan's key economic sectors, particularly agriculture and hydropower, which are inherently sensitive to climatic conditions (NSB, 2020). In 2020, electricity generation contributed 17.74% to Bhutan's Gross Domestic Product (GDP),

Although Bhutan maintains over 70% forest cover and is a net sequester of greenhouse gases, the impacts of climate change are becoming more visible and often transcend national borders. The country's biodiversity and forest ecosystems, which play essential ecological, cultural, and economic roles, are also under threat. Enhancing resilience through climate-adaptive infrastructure, early warning systems, and sustainable resource management is essential to protect both the livelihoods of vulnerable communities and the nation's economic stability.

1.1. Rationale for the report

Understanding and preparing for the impacts of climate change in Bhutan requires scientifically robust assessments of both climatic and hydrological changes. Given the country's complex mountainous terrain and distinct spatial climate variability, outputs from global models such as those in the Coupled Model Intercomparison Project Phase 6 (CMIP6) often contain systematic biases when compared to local observations. If left uncorrected, these biases can undermine the reliability of climate impact assessments.

To address this, the current study integrates historical meteorological data from the NCHM dataset to apply bias correction to CMIP6 climate models. This approach ensures that downscaled projections of temperature and rainfall better represent Bhutan's local climate conditions. The resulting high resolution, biased corrected climate datasets are critical for developing reliable future scenarios tailored to Bhutan's unique environmental context.

Hydrologically, Bhutan's river systems fed primarily by monsoon rainfall and snow and glacier melt are highly sensitive to changes in climatic patterns. Climate change is projected to significantly alter hydrological regimes due to shifts in temperature, precipitation patterns, snowmelt timing, and evapotranspiration (Zam et al., 2021, Mahanta et. Al., 2018)). These changes can influence river flows by reducing base flow, increasing the frequency of extreme events such as floods and droughts, and altering the seasonal timing of flows (Poff et al., 2010). These changes pose considerable challenges for key sectors such as hydropower, agriculture, disaster management, and biodiversity conservation.

This study couples downscaled climate projections with hydrological modeling to assess future water resource dynamics and associated risks. By quantifying potential climate and hydrological shifts, the report aims to support evidence- based policy formulation, climate resilient development, and adaptive natural resource management in Bhutan.

1.2. Assessment framework

The assessment framework comprises two components:

1) Assessment of Climate under CMIP6 scenario using gridded observations
2) Assessment of Hydrological Changes in Bhutan.

To understand the future scenarios under climate change, we used the bilinear interpolation method to downscale the temperature and rainfall from the nine selected Global Circulation Model (GCM) outputs and biased corrections with the historical data set for the study. The rainfall was given as input into a hydrological model, Rainfall Runoff Inundation model to simulate river flow in Punatshangchu and Wangchu River Basins.

2. Assessment of Climate under CMIP6 Scenario

2.1. Methodology

2.1.1. Historical climate data

High resolution (1 km) gridded data set from 67 weather stations in the country from 1996-2019 for precipitation and maximum and minimum temperature, from NCHM were used for the study. The average distance between the stations were from 25- 45 km, covering elevations from 170 to 3530 m, and from different time periods.

2.1.2. Global Circulation Model

In this study, nine Global Climate Models (GCMs) selected from the CMIP6 were based on the criteria established by the Inter-Sectoral Impact Model Intercomparison Project Phase 2b (ISIMIP2b), ensuring consistency with best practices for climate impact modeling. ISIMIP2b

provides a standardized framework for model selection that emphasizes the use of GCMs which effectively capture the range of global mean temperature responses, climate sensitivity, and regional climate variability. This approach aims to support impact assessments across sectors while maintaining scientific rigor and comparability (Frieler et al., 2017). The selected models represent a diversity of climate outcomes, which is essential for assessing uncertainties and providing robust climate projections under different emission scenarios.

The nine selected GCMs as shown in Table 2.1, were chosen to cover a representative range of climate responses and to avoid model redundancy by minimizing inter model correlation, which is a key recommendation in ISIMIP2b's ensemble selection strategy (Warszawski et al., 2014). Furthermore, the model selection aligns with the 2024 climate projection outputs of NCHM (NCHM, 2024). The NCHM's projections are based on both historical observations and future scenarios that reflect national climate priorities and regional dynamics. Ensuring consistency with NCHM projections allows for the integration of global climate data with localized context, which is vital for national climate impact assessments and adaptation planning. The alignment also supports the use of climate information in policy-making, infrastructure design, agriculture planning, and disaster risk management.

By adhering to ISIMIP2b's rigorous model selection criteria and harmonizing with NCHM's 2024 projections, this study ensures that the selected models are not only scientifically credible but also relevant to the Bhutanese context. This dual alignment enhances the reliability of the study's outcomes, enabling more precise estimation of future climate impacts and supporting evidence-based adaptation strategies.

The precipitation and temperature data of the GCMs (100km) were downloaded from the APLAT platform of the National Institute for Environmental Studies (NIES), Japan for three Shared Socio-economic Pathways (SSPs) which are scenarios used to model future global climate and socio-economic developments. SSP 1 2.6, SSP2 4.5, and SSP3 7.0 were chosen for this study. SP1 2.6 represents a sustainable development pathway with low challenges to mitigation and adaptation, where global cooperation and green technologies lead to low greenhouse gas emissions, peaking early and declining rapidly. SSP2 4.5, the "middle-of-the-road" scenario, assumes moderate socio-economic trends and climate policies, resulting in stabilizing emissions that lead to intermediate warming. SSP3 7.0 depicts a fragmented world with regional rivalry, high population growth in developing countries, slow economic development, limited international cooperation, and weak climate action, resulting in high emissions and significant warming. The future scenarios were simulated for three time periods: near- term (2021-2040), mid- term (2041-2060) and long- term (2081-2100).

Table 2.1: Selected CMIP6 GCMs

Model	**Group**	**Resolution**
GFDL-ESM4	primary	1.0°
IPSL-CM6A-LR	primary	2.0°

MPI-ESM1-2-HR	primary	1.0°
MRI-ESM2-0	primary	1.0°
CanESM5	secondary	2.0°
CNRM-CM6-1-HR	secondary	1.0°
CNRM-ESM2-1	secondary	1.0°
EC-Earth3	secondary	0.5°
MIROC6	secondary	1.0°

2.1.3. Downscaling climate data and bias correction

Downscaling the GCMs from 100km to 1km was performed by the bilinear interpolation method which is a commonly used spatial downscaling technique in climate science, particularly when transforming coarse resolution outputs from GCMs to finer resolutions suitable for regional or local impact studies. This method is based on estimating the value of a variable at an intermediate point using a weighted average of the four nearest grid points from the original GCM data (Hijmans et al., 2005). It assumes that changes in the variable are linear in both the horizontal (x) and vertical (y) directions, making it more accurate than nearest-neighbor interpolation while remaining computationally efficient. This method maintains continuity in the first derivative across grid cells, which helps to avoid abrupt transitions in downscaled climate variables such as temperature or precipitation.

Bilinear interpolation is widely used in regional climate applications due to its simplicity and ability to produce smooth spatial gradients, which are essential for consistent modeling of climate impacts on hydrology, agriculture, and ecosystems. However, it is important to recognize its limitations. The method assumes spatial linearity, which may not hold in regions with complex terrain, coastlines, or strong climatic gradients. Additionally, it does not incorporate physical processes or account for changes in statistical distributions, which makes it purely a geometric transformation rather than a statistical or dynamical downscaling method. Despite its limitations, bilinear interpolation remains a valuable tool in the early stages of downscaling, especially when used to provide boundary conditions for regional climate models or to interpolate coarse climate data for input into impact models. Its computational simplicity makes it especially useful in large-scale climate data processing pipelines (Wang et al., 2014). To enhance its performance, it is often combined with bias correction or more advanced downscaling techniques.

The mean bias correction method is one of the simplest and most widely used techniques for adjusting systematic biases in climate model outputs, particularly for temperature and precipitation data, which is also adopted for this study. Bias correction was applied to the 30- year monthly average data by computing the differences between historical data and GCM outputs for the baseline period of 1971–2000. GCMs often exhibit consistent overestimation or underestimation when compared to observed data due to limitations in

model structure, spatial resolution, and parameterizations (Teutschbein & Seibert, 2012). The mean bias correction method operates on the assumption that this bias is constant and can be removed by aligning the long-term mean of the modeled data with that of the observed data over a defined reference period.

The simplicity of the mean method makes it attractive for many impact studies and operational forecasting systems. It does not require complex statistical modeling or distribution fitting, making it computationally efficient and easy to implement. However, it also comes with limitations. The method assumes that the bias is time invariant and stationary, which may not hold under changing climate conditions. Furthermore, it does not adjust higher-order moments such as variance or skewness, which may be critical for extreme event analysis (Maraun, 2016). Despite these limitations, the mean bias correction remains a useful preliminary step in improving the realism of climate projections for sectors like agriculture, hydrology, and forestry. In practice, mean bias correction is often applied on a monthly or seasonal timescale to capture seasonal variability in biases. It is typically used in conjunction with other more advanced correction methods in ensemble modeling or downscaling frameworks. The use of observational datasets of high quality and resolution is critical in ensuring the effectiveness of this method. Overall, the mean method offers a straightforward and transparent approach to reduce model biases, improving the usability of climate data in impact assessment and decision-making processes.

2.2. Climate of Bhutan

Bhutan's climate is governed by the interaction of large- scale atmospheric systems and complex local topography. The primary climatic drivers include the southwest summer monsoon, the El Niño–Southern Oscillation (ENSO), western disturbances, and the Indian Ocean Dipole (IOD) (NCHM, 2021; Rupa Kumar et al., 2006; Shrestha et al., 2018). These systems, coupled with Bhutan's highly varied elevation and terrain, produce pronounced spatial and temporal climatic variability across the country (Wangchuk et al., 2020).

The southwest summer monsoon, active from June to September, is the dominant climatic force, accounting for over 70% of the country's annual precipitation (NCHM, 2021; Dorji et al., 2021). Moist air masses from the Bay of Bengal are uplifted by the Himalayan terrain, resulting in intense orographic rainfall, particularly in the southern and central regions (Phili-Sihvola et al., 2014; Dawa et al., 2015). This precipitation supports key sectors such as hydropower, agriculture, and forestry but also heightens the risk of floods and landslides during the monsoon season.

ENSO is a major driver of interannual climatic variability. During El Niño phases, the weakening of monsoonal circulation often leads to reduced rainfall and higher temperatures, increasing the likelihood of drought. In contrast, La Niña events typically strengthen monsoonal flows, enhancing rainfall and potentially increasing the risk of flood-related disasters.

Western disturbances, originating over the Mediterranean region, influence the country's climate primarily during the winter and early spring. These systems bring occasional

snowfall and rainfall to the northern highlands, playing a vital role in glacier mass accumulation and the seasonal water cycle.

Although Bhutan is geographically protected from direct tropical cyclone landfalls by the Indian subcontinent, the country is affected by the remnants of cyclones originating in the Bay of Bengal, particularly during the pre- monsoon and post- monsoon periods. These residual systems occasionally bring intense rainfall and localized windstorms, which can contribute to flash flooding and damage to infrastructure. While tropical cyclones are not considered primary climate drivers in Bhutan, their secondary impacts are relevant for understanding episodic extreme weather events within the broader regional climate context. The Indian Ocean Dipole (IOD) further modulates regional climate by altering sea surface temperature gradients in the Indian Ocean. A positive IOD phase strengthens moisture transport and enhances rainfall over Bhutan, while a negative phase may suppress monsoonal activity (NCHM, 2021; Saji et al., 1999).

Finally, the country's topography ranging from subtropical lowlands in the south to alpine mountains in the north contributes to the formation of diverse microclimates. Low- lying valleys generally experience warmer and drier conditions, whereas higher altitudes are characterized by cooler temperatures and greater precipitation. These microclimatic differences are critical in shaping agricultural patterns, biodiversity, and local weather variability across the country.

The spatial distribution of seasonal and annual precipitation over Bhutan (Figure 2.1) reveals significant variation influenced by topography and monsoon dynamics. The summer monsoon (June July August September: JJAS) contributes the highest rainfall, exceeding 5000 mm in the southern foothills, while central and northern regions receive relatively less. Pre-monsoon (March April May: MAM) precipitation also shows notable accumulation, particularly in the southern and southwestern regions, with values up to 1600 mm. Post-monsoon (October November: ON) and winter (December January February: DJF) seasons contribute minimally to the total precipitation, with maximum values around 350 mm and 100 mm respectively, mostly concentrated in isolated southern and northern zones. Seasonal precipitation can be seen in Figure 2.2.

Annual precipitation reflects the dominance of the summer monsoon, with totals reaching up to around 7000 mm in the south and gradually decreasing northwards. The spatial gradient from high to low precipitation moving from south to north is consistent across all seasons, highlighting the strong orographic influence of the Himalayan terrain on rainfall distribution.

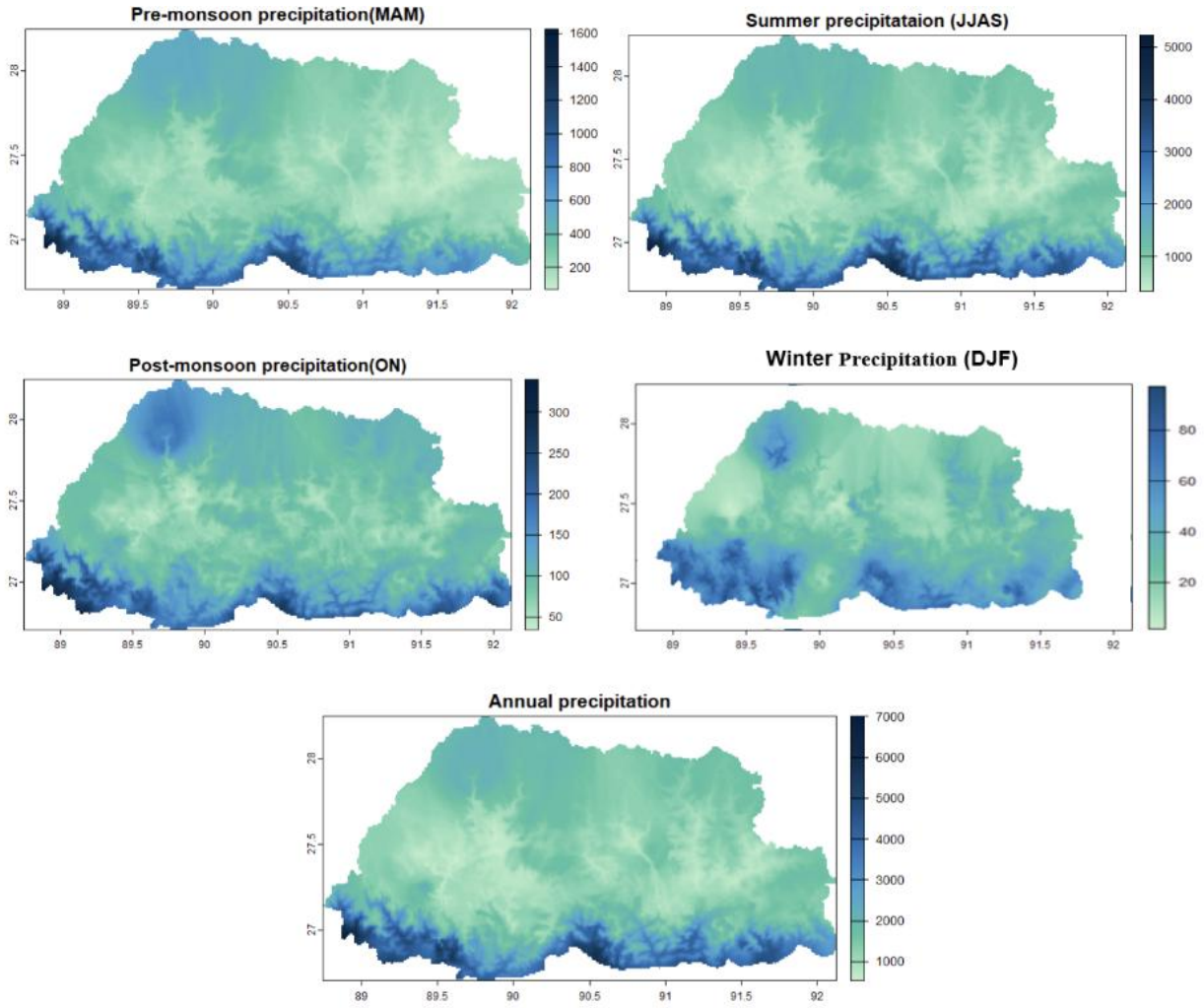

Figure 2.1: Historical seasonal and annual precipitation (mm) from 1996- 2019

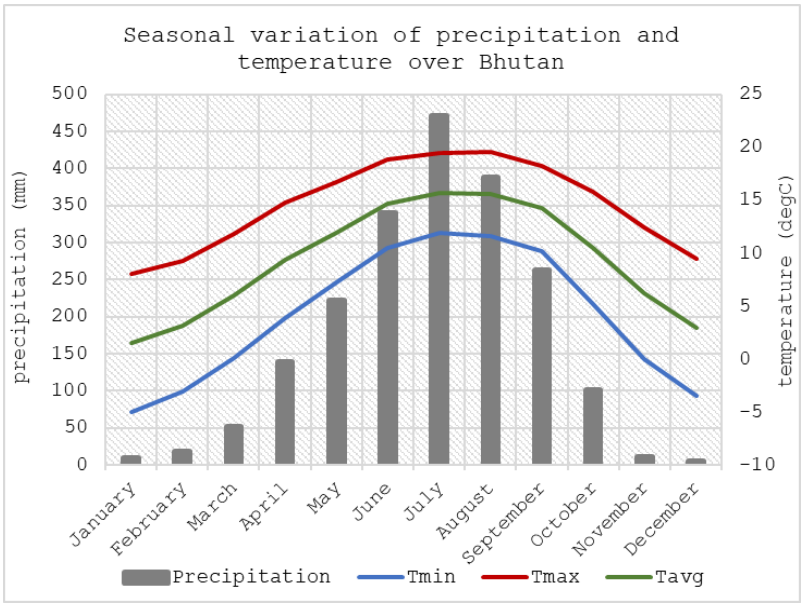

Figure 2.2: Seasonal variation of precipitation (mm) and temperature (degC) from 1996- 2019

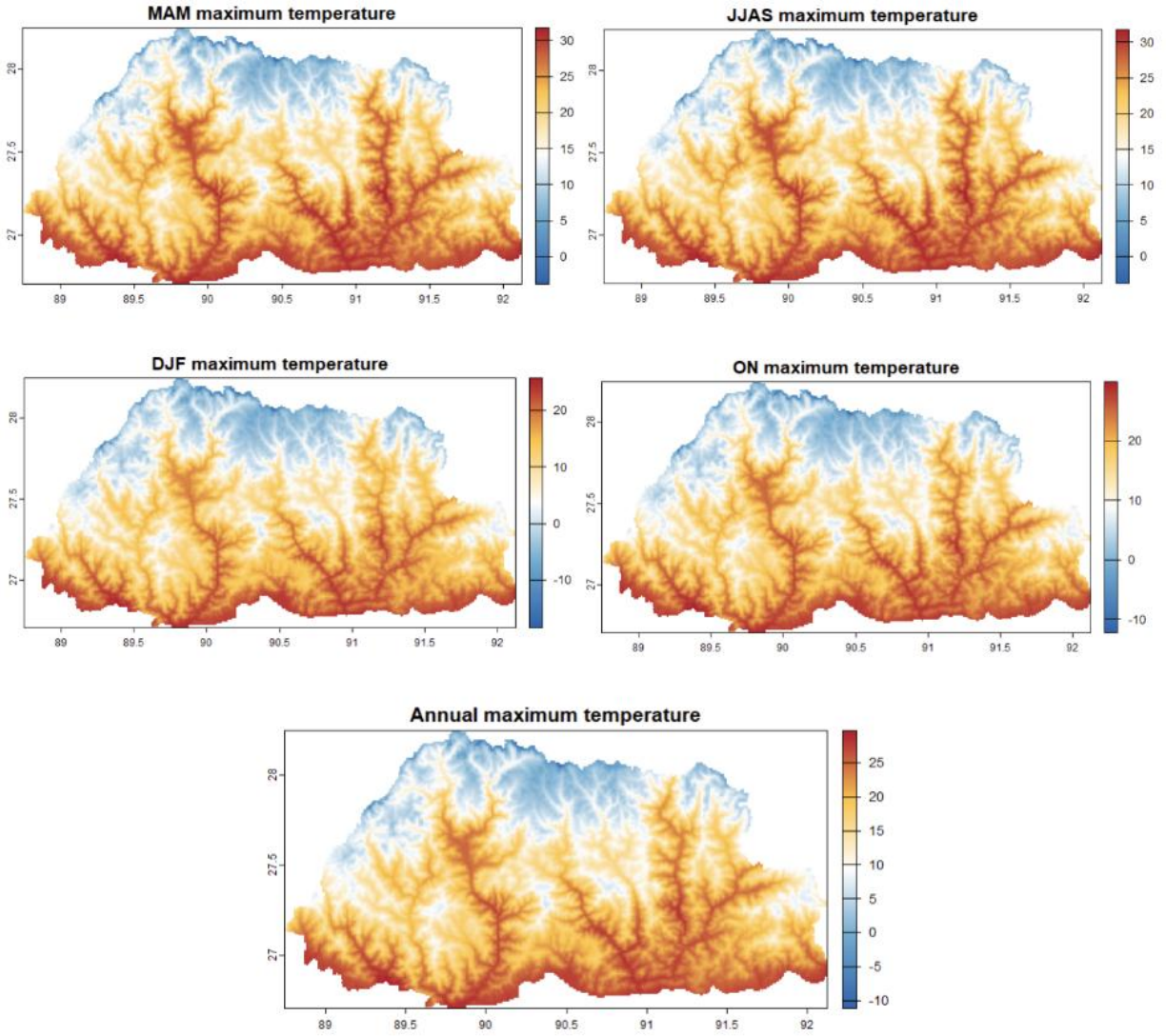

Figure 2.3: Historical seasonal and annual maximum temperature (degC) from 1996- 2019

The seasonal and annual maximum temperatures over the country (Figure 2.3) shows a clear altitudinal gradient, with higher temperatures in the southern lowlands and progressively cooler temperatures toward the northern highlands. Across all seasons, maximum temperatures exceed 30°C in southern and southeastern regions, while the northern high altitude zones consistently experience sub-zero to low positive temperatures.

Seasonal variation (also shown in Figure 2.3) is evident with the highest maximum temperatures recorded during the summer monsoon season, where much of southern Bhutan exceeds 30°C. In contrast, the winter season sees the lowest maximum temperatures, with northern areas remaining below 0°C and the southern parts rarely exceeding 20°C. The transitional seasons pre-monsoon and post-monsoon show moderate maximum temperatures, reflecting gradual warming and cooling trends. The annual maximum temperature consolidates these patterns, showing sustained high temperatures in the

southern belt and persistent cool conditions in the north, driven primarily by elevation differences.

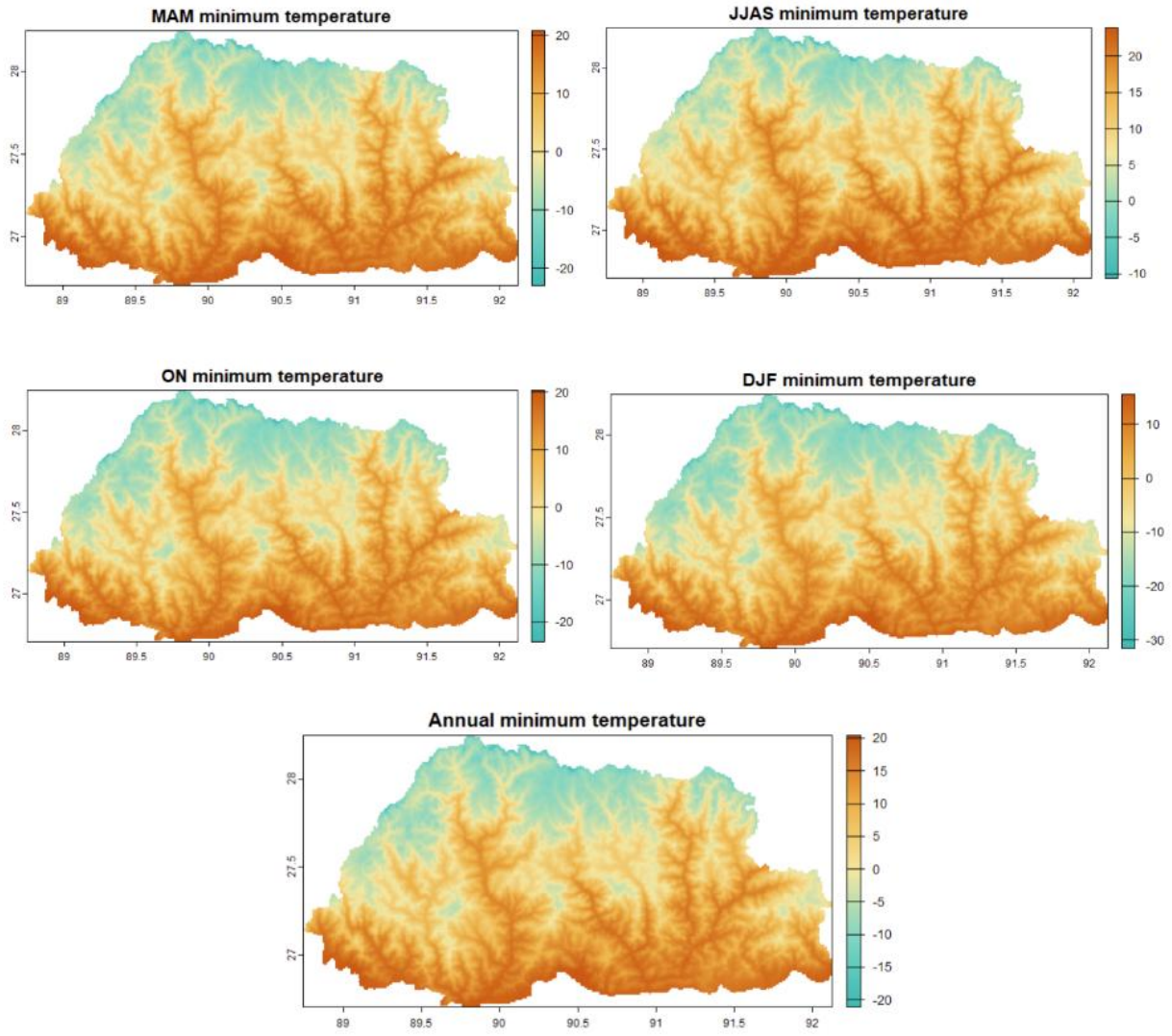

Figure 2.4: Historical seasonal and annual minimum temperature (degC) from 1996- 2019

Colder temperatures (Figure 2.4) dominate in the northern highlands and warmer conditions in the southern lowlands. Minimum temperatures in the winter season are the lowest of the year, with values dropping below -20°C in high-altitude northern regions. In contrast, the summer season shows the highest minimum temperatures, particularly in southern areas where values exceed 20°C. Pre- monsoon and post monsoon exhibit moderate minimum temperatures, generally ranging between 0°C and 15°C, with a clear north- south gradient. The annual minimum temperature map consolidates these seasonal patterns, showing persistently sub- zero temperatures in the northern regions throughout the year, while southern regions maintain much warmer minimums.

2.3. Future climate projection

2.3.1. Precipitation changes

2.3.1.1. Near- term scenario

Annual precipitation changes

Historical annual precipitation (1996–2014) (Figure 2.5) shows significant spatial variation in precipitation, with the southern and southwestern regions receiving high annual rainfall exceeding 5000 mm, while the northern highlands experience lower precipitation, typically under 2000 mm.

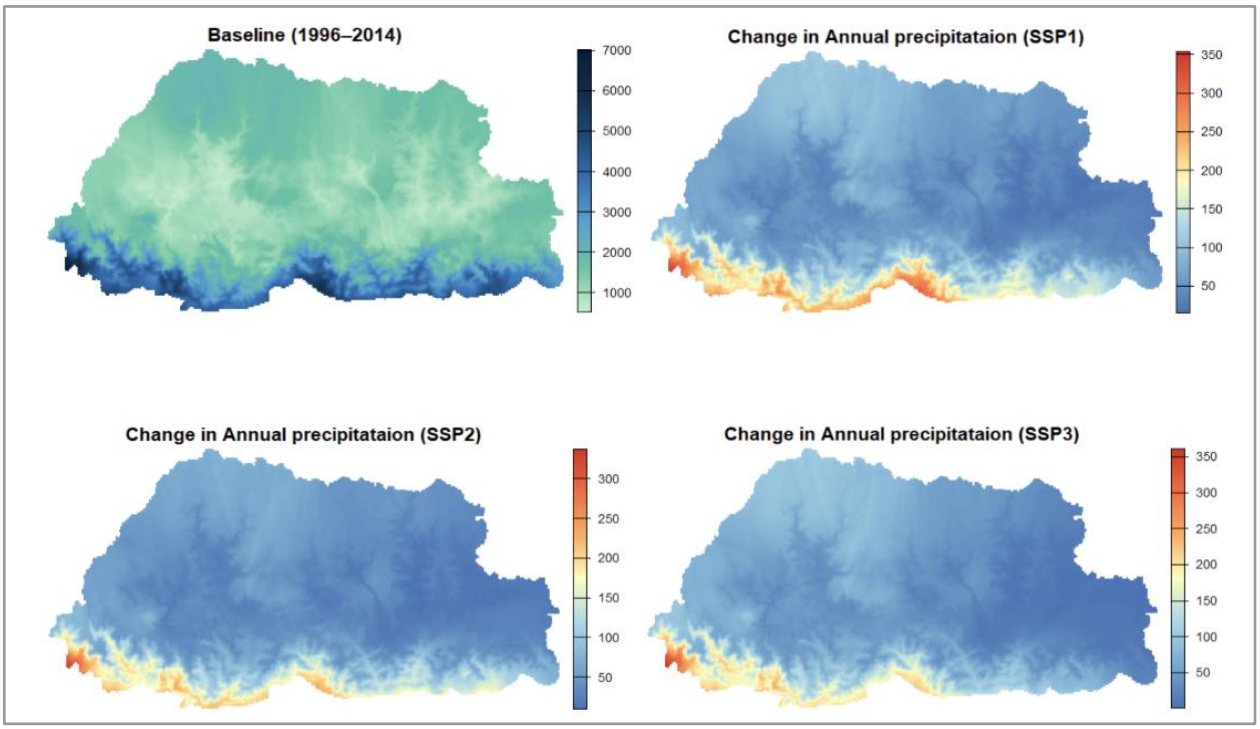

Figure 2.5: Near- term spatial patterns of baseline (top left) and projected changes in annual precipitation (mm) under SSP1 (top right), SSP2 (bottom left) and SSP3 (bottom right)

All scenarios (Figure 2.5) consistently project an increase in precipitation, particularly in the southern belt, with the highest changes around 300 mm annually. Among the scenarios, SSP3 shows the most extensive and intense increase in precipitation across the southern and southwestern regions, followed by SSP2 and SSP1. The spatial distribution of precipitation change reflects the country's topographic influence, with lowland and foothill regions expected to experience greater increases than the northern highlands.

Summer (JJAS) precipitation changes

Historical summer (JJAS) precipitation (Figure 2.6) shows high monsoonal precipitation concentrated in the southern belt, with values exceeding 5000 mm in some areas. This

spatial pattern reflects the influence of the Indian monsoon, which brings heavy rainfall to southern parts of the country due to orographic lifting along the Himalayan foothills.

Projected changes in JJAS precipitation under SSP1, SSP2, and SSP3 indicate a consistent trend of increasing rainfall, particularly in the southern and southwestern regions. SSP3 exhibits the most substantial increases, with localized changes exceeding 350 mm, followed by SSP2 and SSP1. The intensified monsoonal precipitation under these scenarios may heighten the risk of flooding, landslides, and other hydrometeorological hazards in the southern regions.

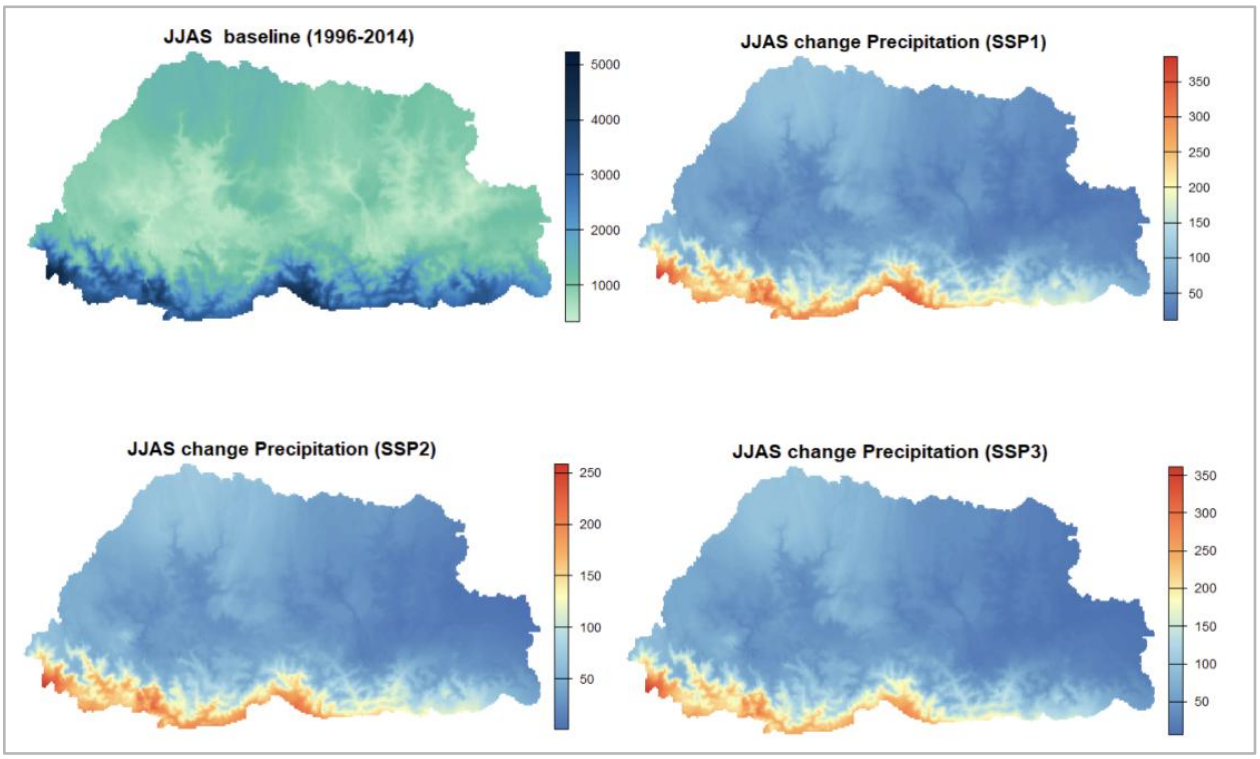

Figure 2.6: Near- term spatial patterns of baseline (top left) and projected changes in summer precipitation (mm) under SSP1 (top right), SSP2 (bottom left) and SSP3 (bottom right)

Winter (DJF) precipitation changes

Relatively low winter precipitation (Figure 2.7) is seen across the country, ranging from about 20 mm to over 100 mm, with higher precipitation concentrated in the southwestern and southern regions. All three future scenarios indicate a general decrease in DJF precipitation across the region, with the most substantial reductions observed in southern and southeastern areas.

Under SSP1 precipitation decreases by up to 14 mm, while SSP2 and SSP3 show reductions up to around 12 mm. Although SSP1 represents a low-emission future, it still shows the most severe decline, possibly due to shifts in regional climate dynamics.

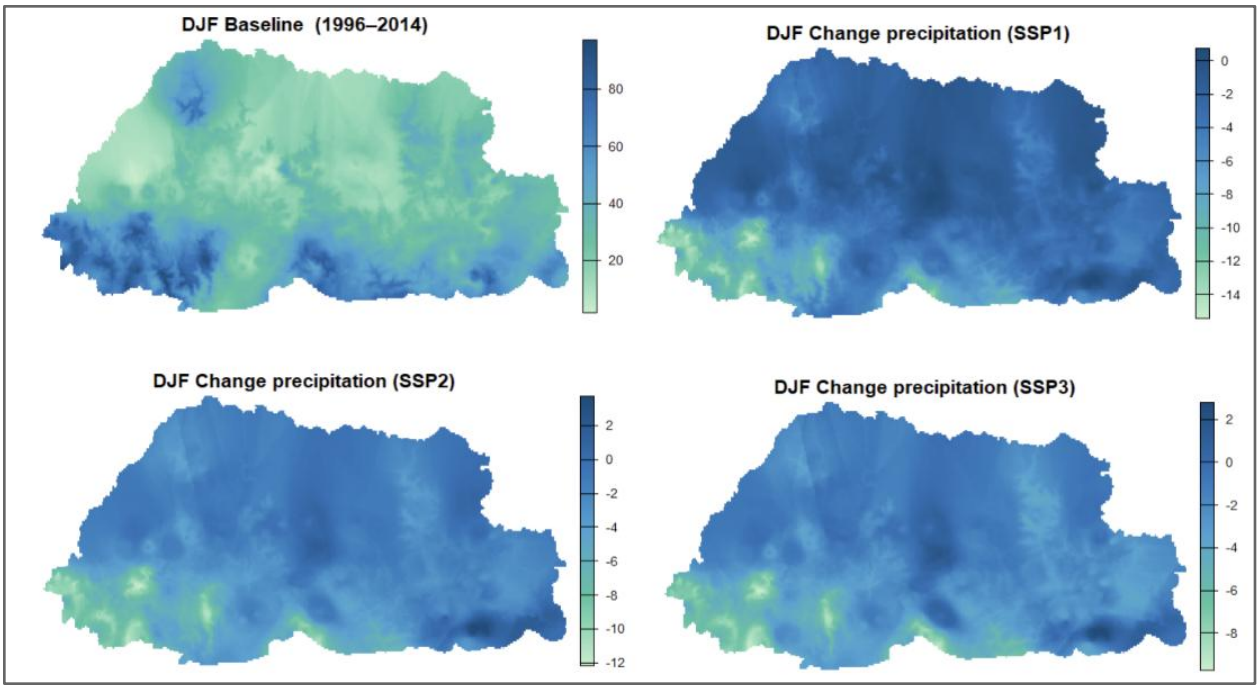

Figure 2.7: Near- term spatial patterns of baseline (top left) and projected changes in winter precipitation (mm) under SSP1 (top right), SSP2 (bottom left) and SSP3 (bottom right)

2.3.1.2. Mid- term scenario

Annual precipitation changes

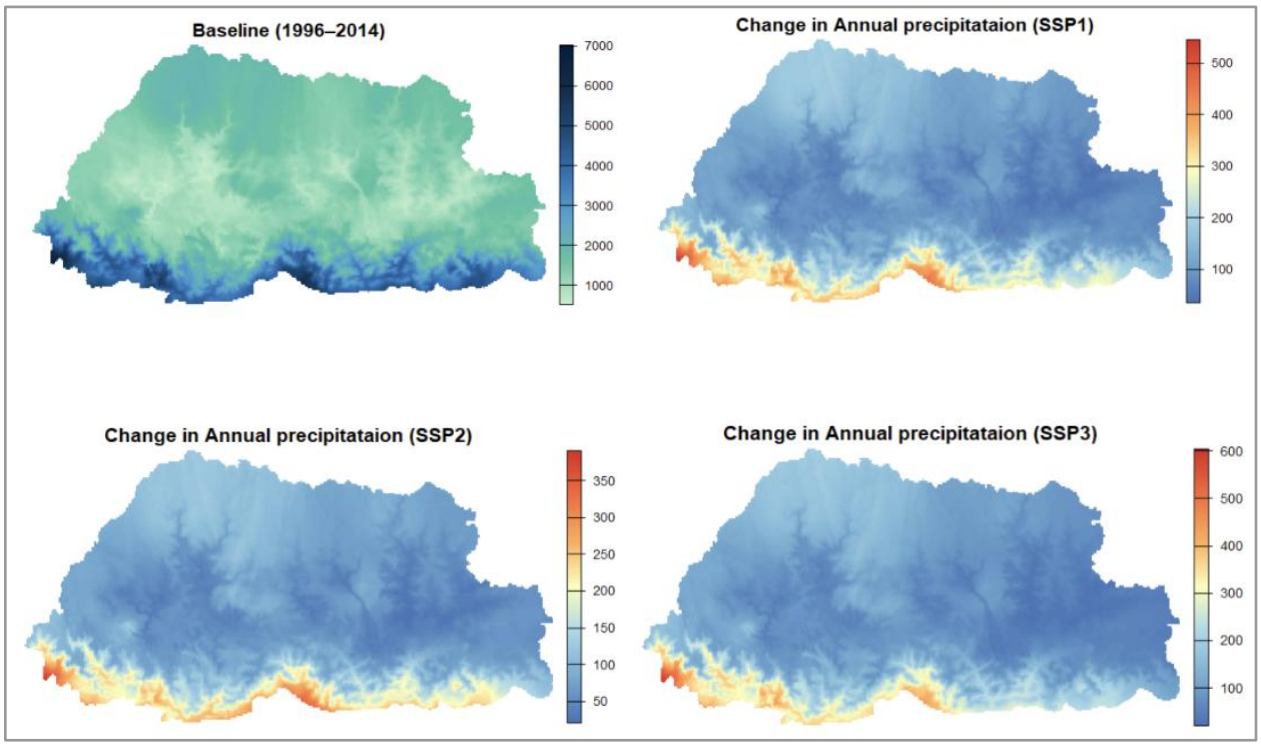

Figure 2.8: Mid- term spatial patterns of baseline (top left) and projected changes in annual precipitation (mm) under SSP1 (top right), SSP2 (bottom left) and SSP3 (bottom right)

Under projected climate scenarios, all three SSPs indicate a general increase in annual precipitation (Figure 2.8) across the region, with noticeable spatial heterogeneity. The southern regions consistently exhibit the most substantial increases, likely influenced by orographic effects and intensified monsoon activity. Under SSP1, precipitation changes predominantly range from 100- 300 mm/year, with some localized areas reaching up to 500 mm/year, reflecting a moderate yet widespread wetting trend. SSP2 projects a more conservative increase, generally between 50- 300 mm/year, but retains a similar spatial distribution, with southern and southeastern zones receiving the highest changes. SSP3 presents the most pronounced increase, with several areas in the south and southeast experiencing rises exceeding 600 mm/year. These patterns suggest that the region, particularly its southern belt, is expected to undergo increasing precipitation under all future pathways, with the magnitude of change dependent on the emissions and development trajectory.

Summer (JJAS) precipitation changes

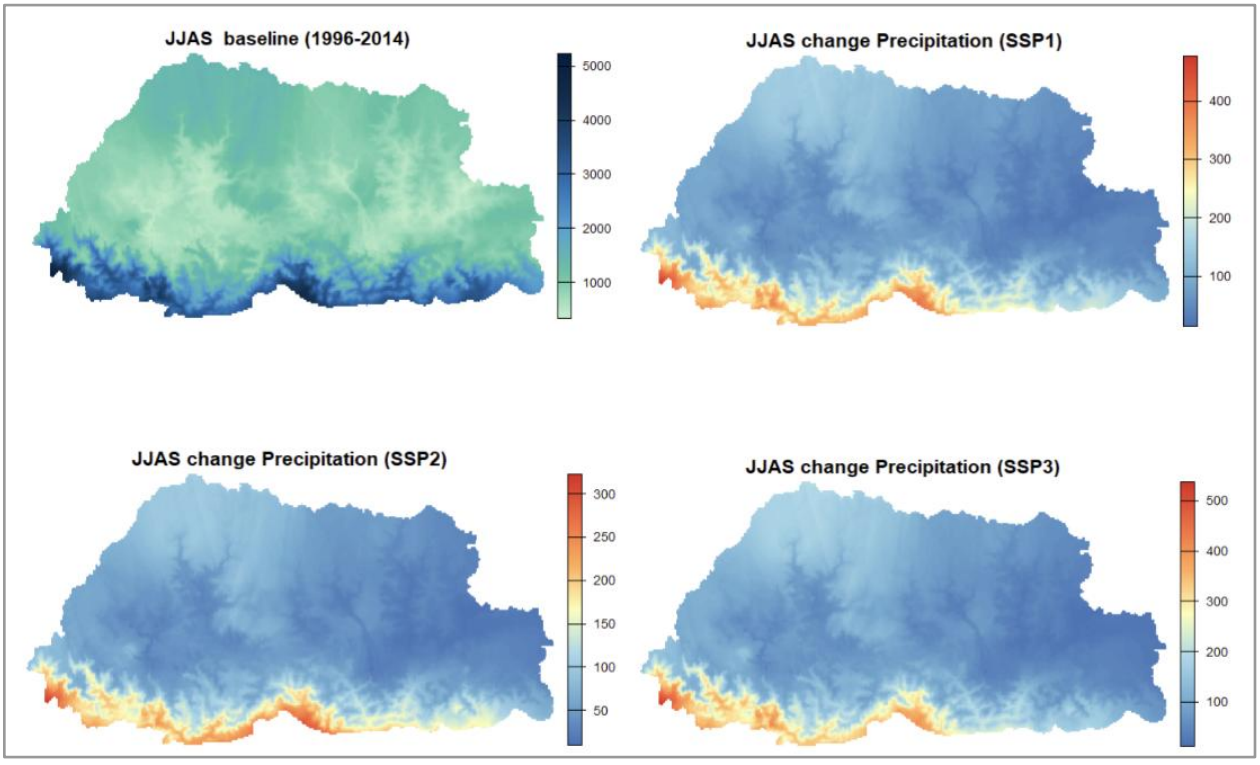

Figure 2.9: Mid- term spatial patterns of baseline (top left) and projected changes in summer precipitation (mm) under SSP1 (top right), SSP2 (bottom left) and SSP3 (bottom right)

Projected changes in JJAS precipitation (Figure 2.9) under all three SSP scenarios indicate a consistent increase in rainfall, with clear spatial concentration along the southern margins of the country. Under SSP1, increases mostly range between 100- 300 mm/season, with

isolated hotspots reaching over 400 mm, suggesting a moderately intensified monsoon. SSP2 shows a more subdued change, primarily between 50- 300 mm/season, maintaining a similar spatial distribution concentrated in southern and southwestern regions. The most pronounced increases occur under SSP3, where seasonal precipitation gains exceed 500 mm in some areas, particularly along the southern and southwestern zones. These projections underscore a strengthening monsoon regime under future climate scenarios, with the magnitude of change intensifying under higher- emission pathways.

Winter (DJF) precipitation changes

Projected changes in DJF precipitation under future climate scenarios (Figure 2.10) show relatively modest shifts compared to the monsoon season, with both spatial and magnitude changes being more subdued. Under SSP1, precipitation changes are minor, ranging between −5 to +10 mm/season, suggesting a slight increase in parts of the central and southeastern regions. SSP2 and SSP3 both project marginal decreases across much of the country, with SSP3 showing more widespread drying trends reaching −10 mm/season in several southern and southwestern areas.

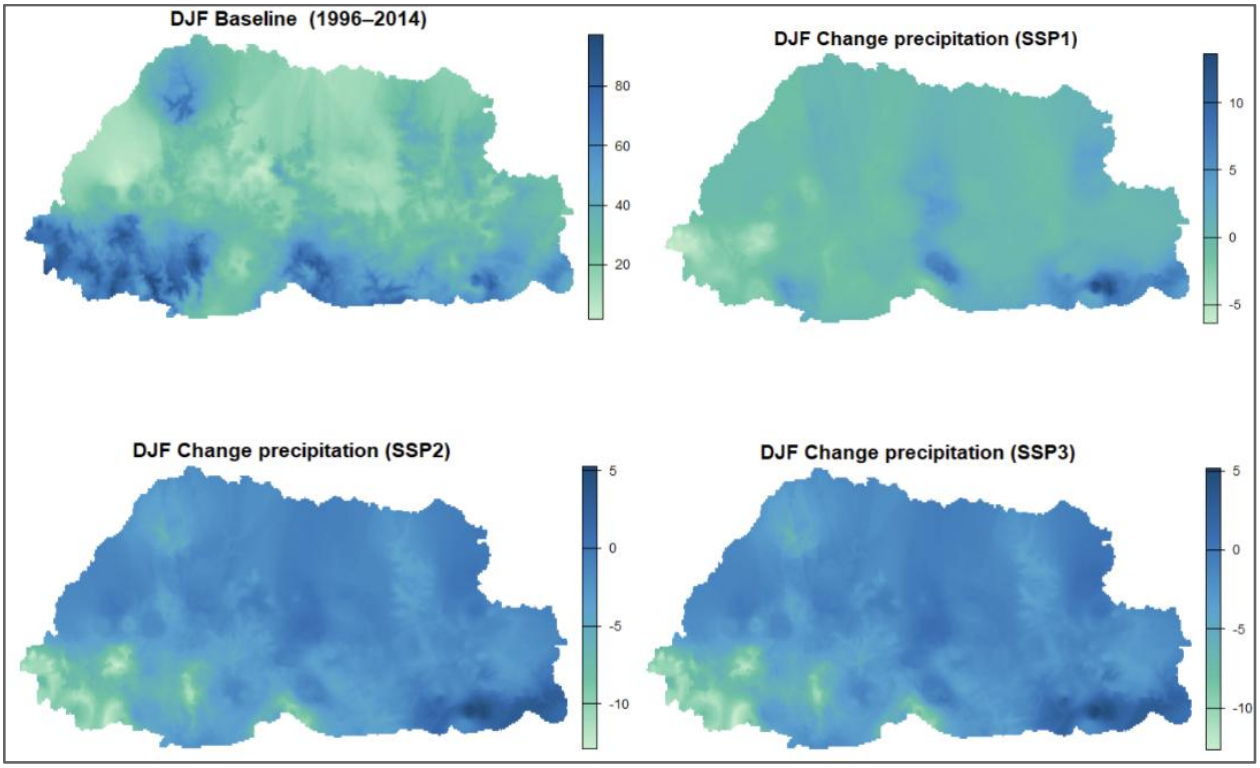

Figure 2.10: Mid- term spatial patterns of baseline (top left) and projected changes in winter precipitation (mm) under SSP1 (top right), SSP2 (bottom left) and SSP3 (bottom right)

2.3.1.3. Long- term scenario

Annual precipitation changes

Future climate projections show a consistent increase in annual precipitation (Figure 2.11) across all SSP scenarios, with notable spatial variation concentrated along the southern regions of the country. Under SSP1, projected changes range mostly between 100- 400 mm/year, with peak increases up to 600 mm in localized southern zones, reflecting a moderate intensification of the hydrological cycle. SSP2 shows a similar spatial trend but with higher magnitudes, particularly in the far south and southeast, where changes reach up to 800 mm/year. SSP3 demonstrates the most pronounced increases, with extreme precipitation gains exceeding 2000 mm/year in some southern pockets. These patterns suggest that under high-emission and less adaptive futures, the country, especially its southern lowlands, could experience substantial increases in annual precipitation, potentially intensifying flood risk, altering river flows, and challenging existing water management systems.

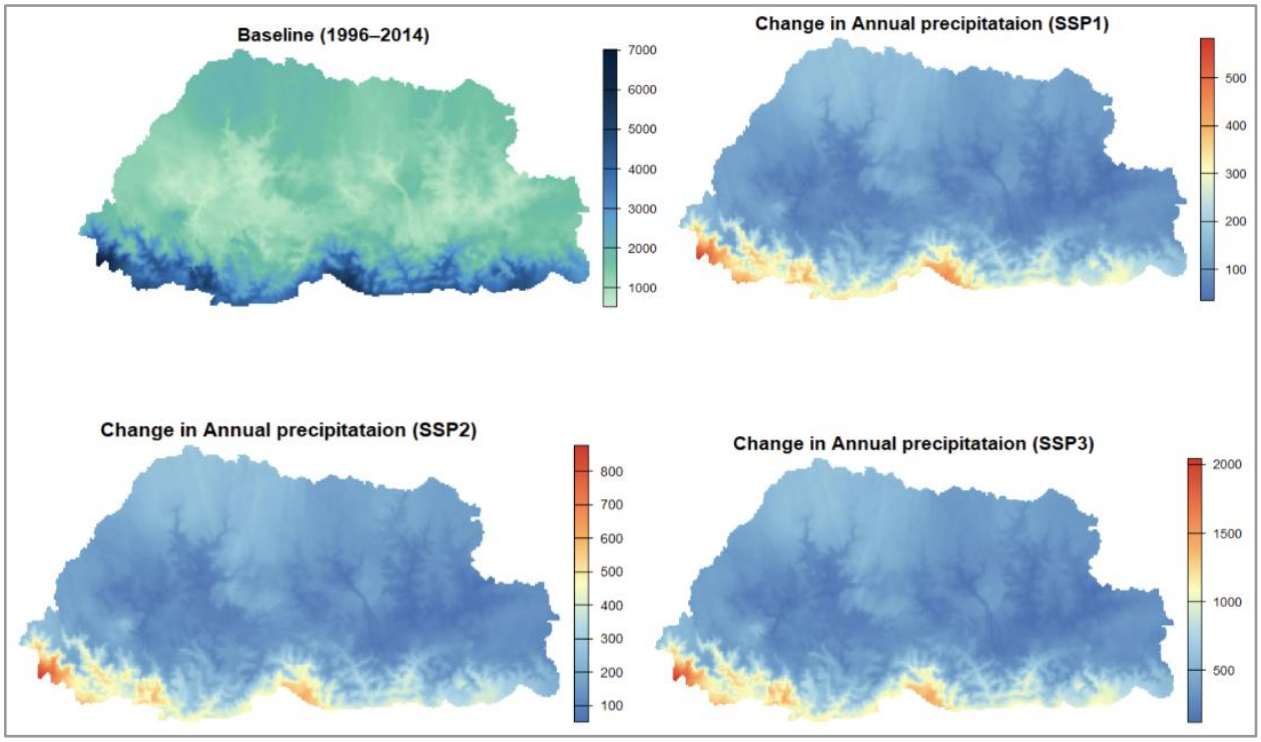

Figure 2.11: Long- term spatial patterns of baseline (top left) and projected changes in annual precipitation under SSP1 (top right), SSP2 (bottom left) and SSP3 (bottom right)

Summer (JJAS) precipitation changes

Projections for JJAS precipitation (Figure 2.12) indicate a robust increase across all SSP scenarios, with pronounced spatial variation centered along the southern regions of the country. Under SSP1, projected increases range from 100- 400 mm/season, with localized peaks exceeding 500 mm, suggesting a moderately intensified monsoon. SSP2 follows a similar spatial pattern, though with slightly lower magnitude changes, typically between

100- 350 mm. SSP3 shows the most substantial increases, with widespread gains exceeding 800 mm and some southern zones reaching up to 1500 mm/season, indicating a potentially dramatic strengthening of monsoon intensity under high-emission scenarios. These highlight a consistent wetting trend during the monsoon period, with the magnitude of change increasing under more severe climate trajectories.

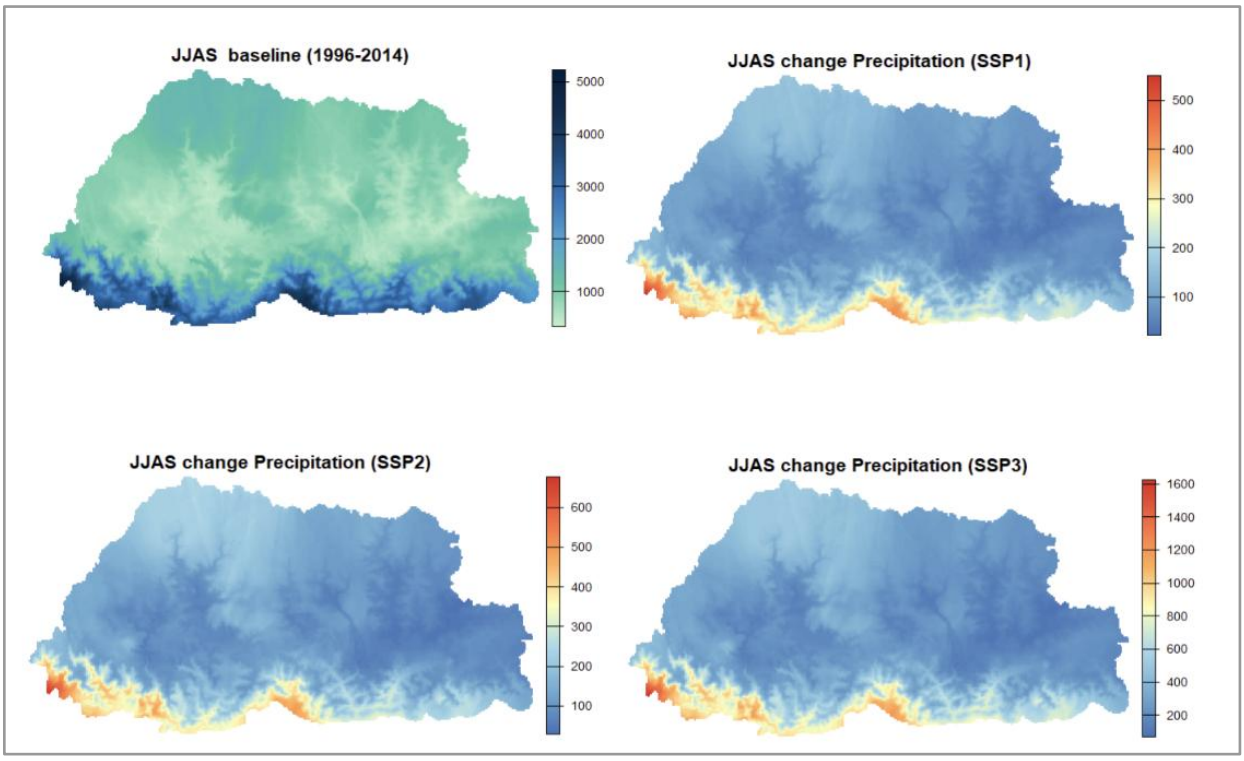

Figure 2.12: Long- term spatial patterns of baseline (top left) and projected changes in summer precipitation (mm) under SSP1 (top right), SSP2 (bottom left) and SSP3 (bottom right)

Winter (DJF) precipitation changes

Projected DJF precipitation changes across future SSP scenarios (Figure 2.13) suggest relatively minor to moderate alterations, with a general tendency toward drying under higher- emission pathways. Under SSP1, changes remain small and spatially mixed, mostly within ±10 mm/season, indicating a relatively stable winter precipitation regime. SSP2 also shows limited changes, but with a slight drying trend emerging in parts of the central and southern regions. SSP3 presents a marked shift, with widespread declines in winter precipitation reaching reductions greater than -15 mm/season across most areas.

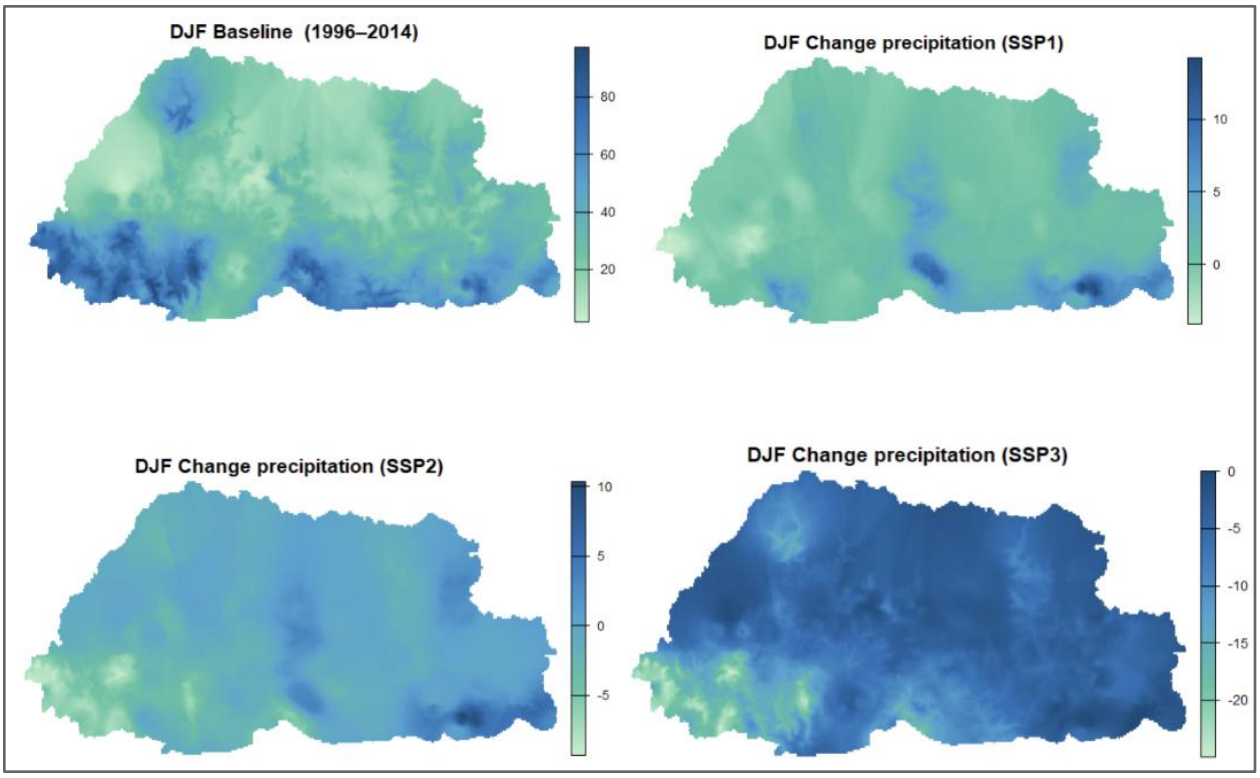

Figure 2.13: Long- term spatial patterns of baseline (top left) and projected changes in winter precipitation (mm) under SSP1 (top right), SSP2 (bottom left) and SSP3 (bottom right)

2.3.2. Maximum Temperature changes

2.3.2.1. Near- term scenario

Annual maximum temperature changes

The baseline exhibits clear altitudinal variation in maximum temperature, with warmer temperatures concentrated in the southern and low- lying regions, and cooler temperatures dominating the northern and high-elevation zones (Figure 2.14). This strong temperature gradient highlights the influence of topography on historical climate patterns.

Projected changes under all three SSP scenarios indicate an overall increase in annual maximum temperatures, with a consistent spatial pattern across scenarios: higher warming in the northern regions compared to the southern regions. Under SSP1 the projected temperature change ranges between approximately 0.75 and 1.00°C, with relatively moderate warming. SSP2 shows a slightly broader range of warming (0.60 to 1.00°C), suggesting a greater potential for regional temperature disparities. The most pronounced changes are observed under SSP3, a scenario characterized by regional rivalry and higher emissions. This pathway projects significant warming across the entire region, with a minimum increase of 0.70°C and a maximum of 1.00°C.

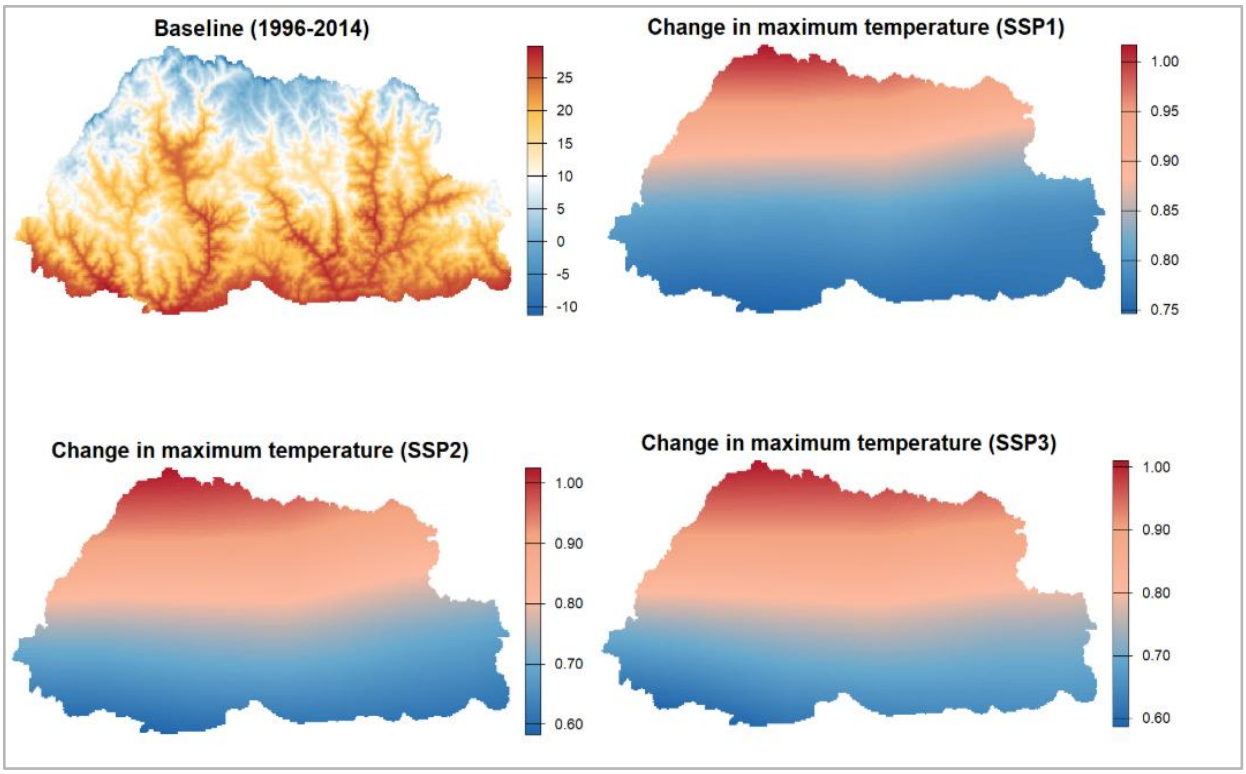

Figure 2.14: Near- term spatial patterns of baseline (top left) and projected changes in annual maximum temperature (degC) under SSP1 (top right), SSP2 (bottom left) and SSP3 (bottom right)

The consistent north- south gradient in all scenarios suggests that northern, typically cooler regions may experience more rapid warming compared to the already warmer southern areas. This could have important implications for regional climate adaptation strategies, particularly in managing thermal stress on ecosystems and human systems. The increasing gradient of temperature change from SSP1 to SSP3 also emphasizes the critical role of emissions mitigation efforts in moderating regional climate impacts.

Summer (JJAS) maximum temperature changes

Historical summer JJAS maximum temperature (Figure 1.15) shows a strong altitudinal gradient, with higher maximum temperatures (above 25°C) observed in the southern lowlands and progressively cooler temperatures (below 10°C) toward the high- altitude northern regions. This spatial variability is consistent with the country's complex topography and elevation- dependent climate.

Future projections consistently indicate an increase in maximum temperature, with a clear north- south warming gradient. Under SSP1, temperature increases range from 0.6°C to 0.75°C, while SSP2 shows a slightly higher rise from 0.65°C to 0.80°C. SSP3 projects the most significant warming, particularly in northern and central regions, exceeding 0.75°C. These projections highlight the growing warming trend across the country with higher elevation areas expected to experience greater warming.

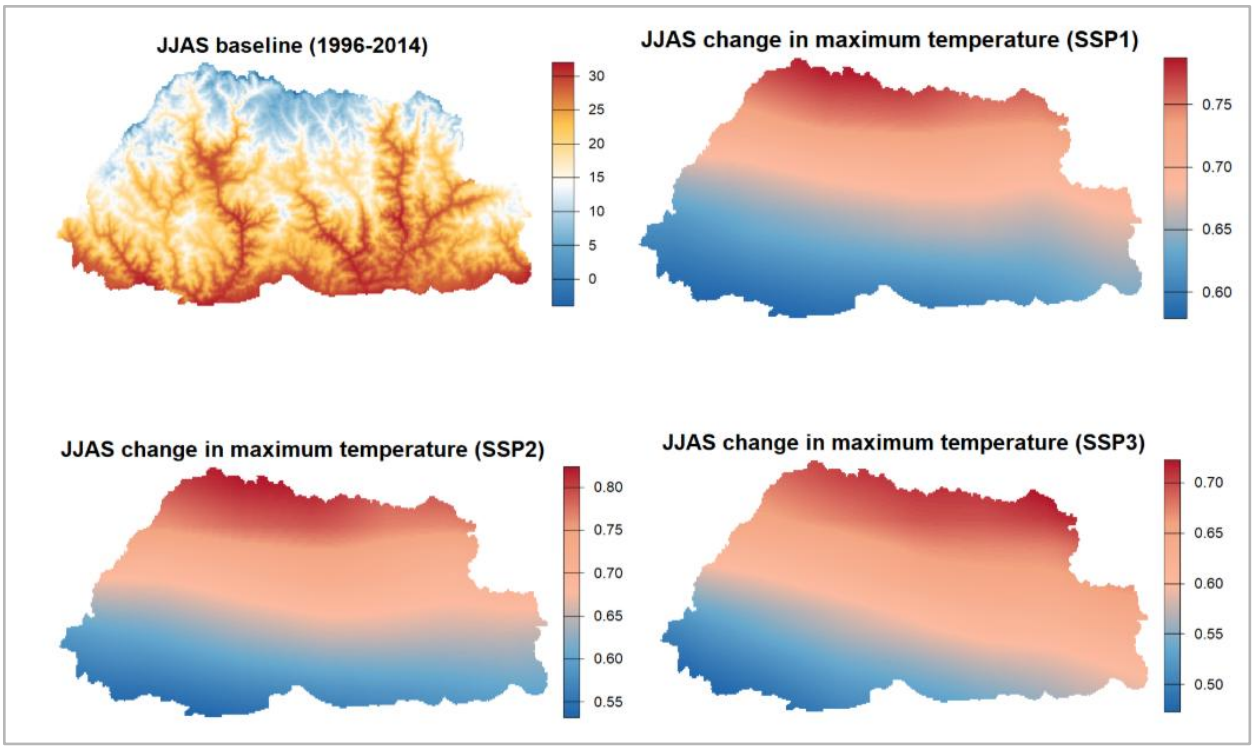

Figure 2.15: Near- term spatial patterns of baseline (top left) and projected changes in summer maximum temperature (degC) under SSP1 (top right), SSP2 (bottom left) and SSP3 (bottom right)

Winter (DJF) maximum temperature changes

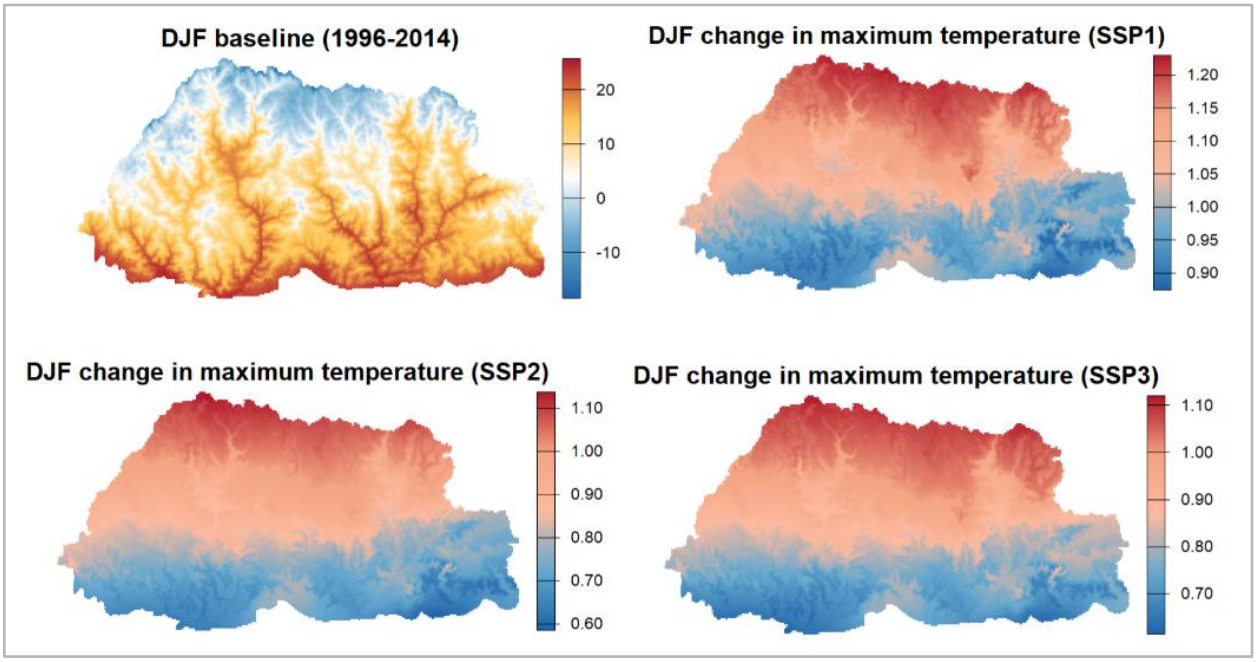

Figure 2.16: Near- term spatial patterns of baseline (top left) and projected changes in winter maximum temperature (degC) under SSP1 (top right), SSP2 (bottom left) and SSP3 (bottom right)

The winter DJF historical map (Figure 2.16) shows that maximum temperatures during winter range from above 20°C in the southern lowlands to below 0°C in the northern highlands, reflecting Bhutan's steep elevation gradient.

Future projections show widespread warming across the country, with a north- south pattern of change. Under SSP1 projected warming ranges from about 0.90°C in the south to over 1.20°C in the north. SSP2 projects slightly higher increases (up to 1.15°C), while SSP3 shows warming exceeding 1.10°C in the northern regions and around 0.70- 0.90°C in the south. Compared to the JJAS season, winter warming is more pronounced, especially over higher elevations. This enhanced warming could have significant implications for snow cover, glacial stability, and winter agriculture.

2.3.2.2. Mid- term scenario

Annual maximum temperature changes

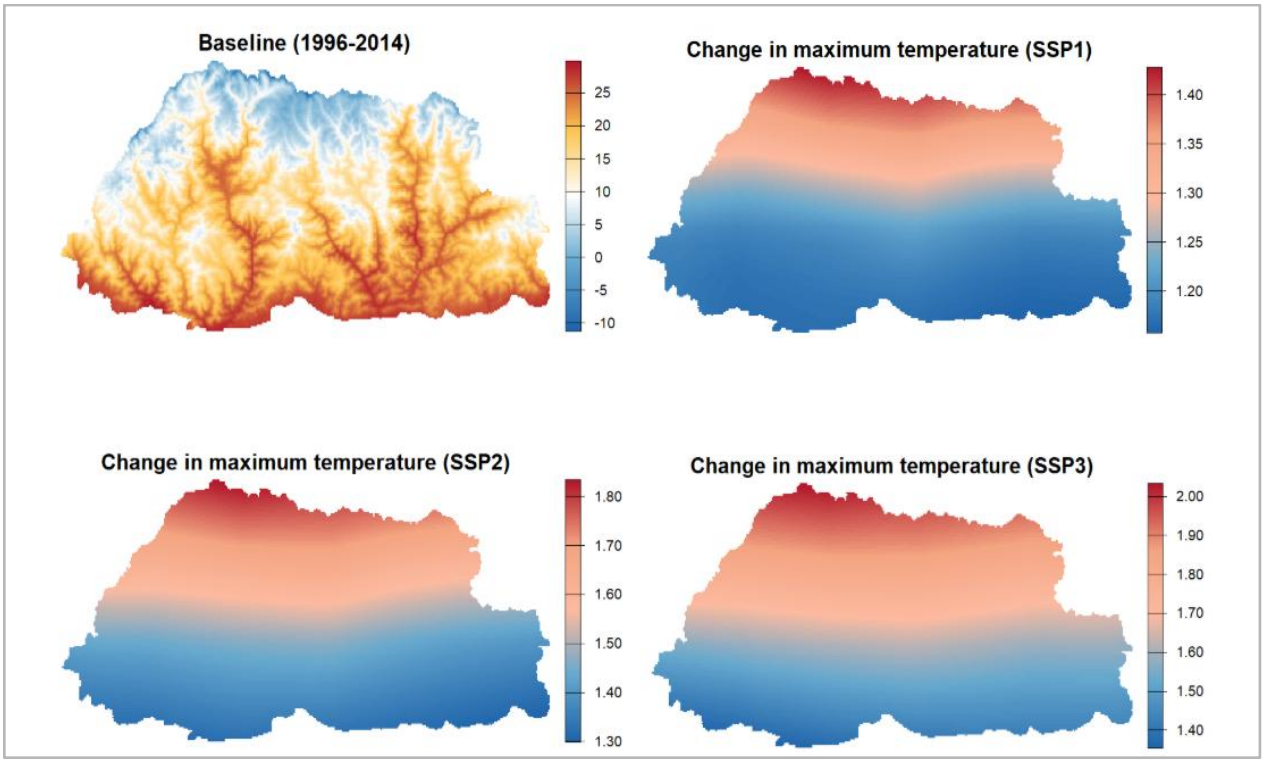

Figure 2.17: Mid- term spatial patterns of baseline (top left) and projected changes in annual maximum temperature (degC) under SSP1 (top right), SSP2 (bottom left) and SSP3 (bottom right)

Under projected climate scenarios, all three SSPs indicate a consistent warming trend, with the magnitude of temperature change increasing from SSP1 to SSP3. In SSP1 the projected change in maximum temperature ranges between 1.20°C and 1.40°C. This scenario suggests

relatively moderate warming concentrated more heavily in the northern regions, following a north-south gradient. SSP2 shows increased warming compared to SSP1, with projected changes ranging from 1.40°C to 1.80°C. Similar to SSP1, the spatial pattern of warming shows intensified changes in the north, indicating continued vulnerability of higher-latitude or higher-elevation regions. SSP3 projects the most substantial increases, with changes between 1.60°C and 2.00°C. The spatial pattern of SSP3 mirrors previous scenarios but with greater overall magnitude, suggesting that warming intensifies progressively with increasing emissions.

Summer (JJAS) maximum temperature changes

Under future scenarios, all projections show a consistent warming trend, intensifying from SSP1 to SSP3 (Figure 2.18). SSP1 shows an increase of about 1.00°C to 1.25°C, primarily concentrated in the northern and central regions. SSP2 shows a more significant rise of around 1.25°C to 1.55°C, while SSP3 exhibits the highest projected warming, ranging from 1.25°C in the south to over 1.65°C in the north. These results indicate an elevation-dependent warming pattern, with greater warming at higher elevations. The increased warming during the monsoon season under high-emission scenarios may exacerbate glacial melt, hydrological extremes, and pose risks to agriculture and ecosystem services

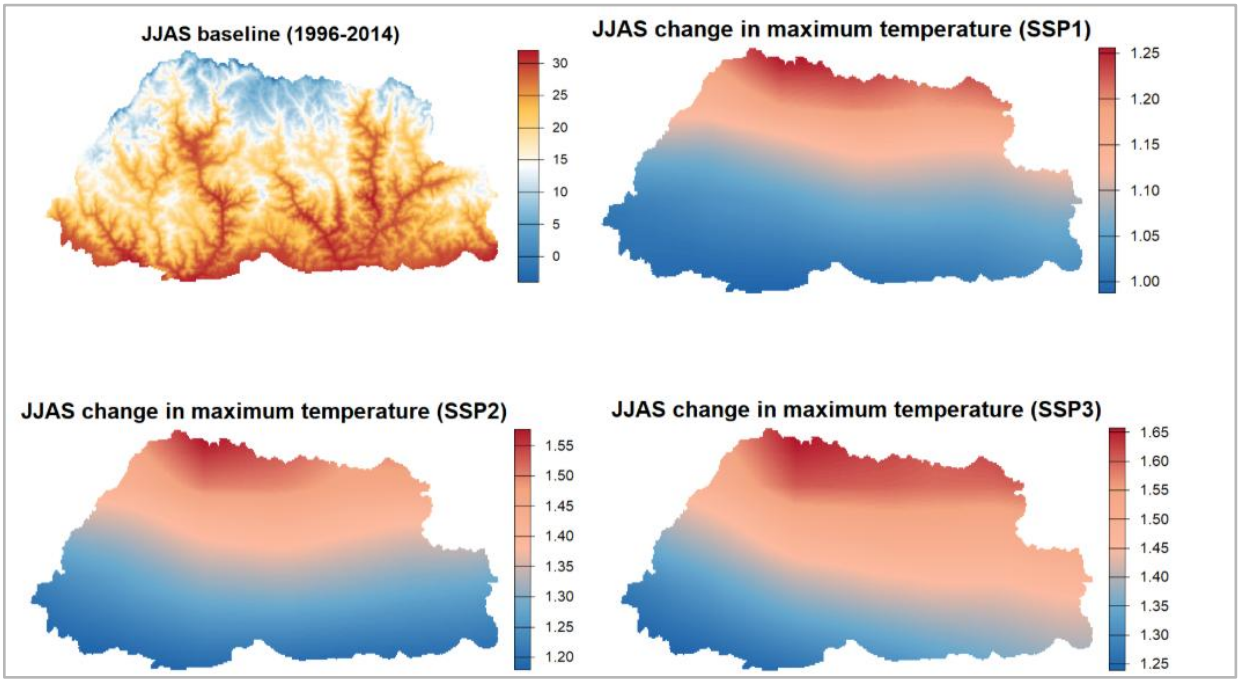

Figure 2.18: Mid- term spatial patterns of baseline (top left) and projected changes in summer maximum temperature (degC) under SSP1 (top right), SSP2 (bottom left) and SSP3 (bottom right)

Winter (DJF) maximum temperature changes

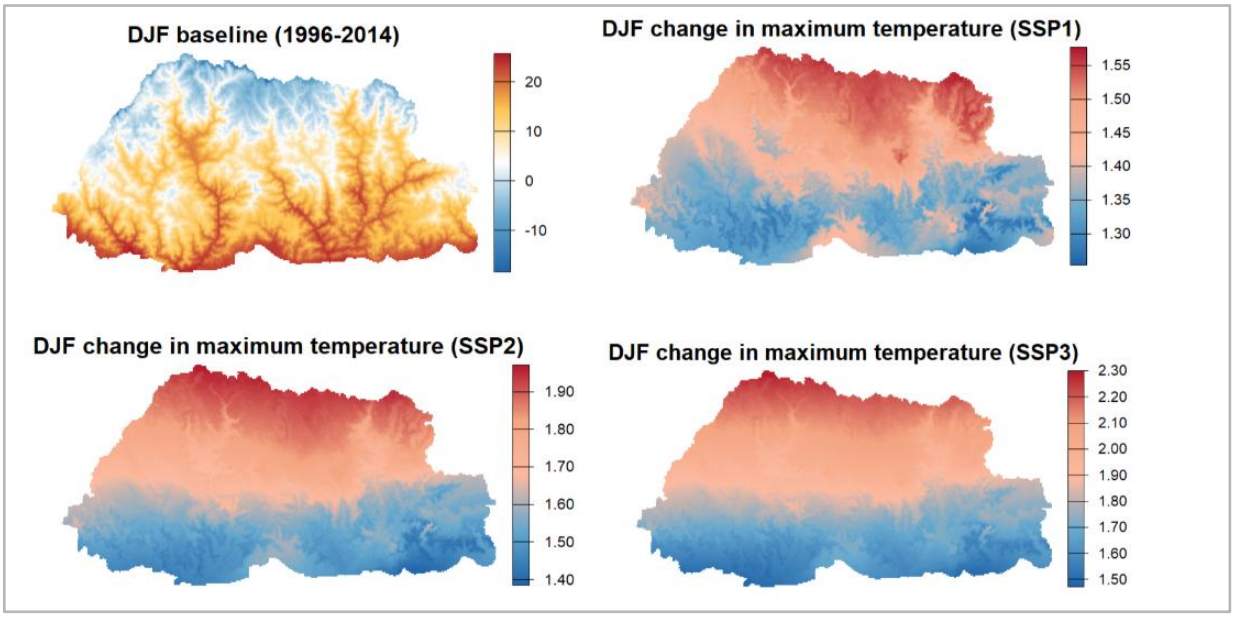

Figure 2.19: Mid- term spatial patterns of baseline (top left) and projected changes in winter maximum temperature (degC) under SSP1 (top right), SSP2 (bottom left) and SSP3 (bottom right)

Projected changes across all SSPs indicate widespread warming, with greater increases in the colder northern regions (Figure 2.19). SSP1 shows a relatively moderate increase in maximum temperature (1.30–1.55°C), while SSP2 and SSP3 project stronger warming, reaching up to 1.90°C and 2.30°C respectively. The spatial pattern suggests elevation-dependent warming, with the northern highlands consistently experiencing higher temperature increases. This could have significant implications for snow cover, glacial melt, and water availability during winter months, particularly under higher- emission scenarios.

2.3.2.3. Long- term scenario

The projected changes in maximum temperature under different SSPs indicate a clear warming trend over the long term, with magnitude increasing from SSP1 to SSP3 (Figure 2.20). Under SSP1 the maximum temperature increases range from approximately 1.35°C to 1.65°C. The warming pattern displays a gradient, with the greatest increases in the northern and central parts of the region. Under SSP2 projected temperature increases range from 2.40°C to 2.90°C. The spatial gradient remains consistent, with more pronounced warming in the northern areas. This scenario reflects the amplified warming expected under more gradual global mitigation efforts. SSP3 projects the most severe warming. Temperature increases range from 3.40°C to 4.40°C, with the northern half of the region experiencing the most extreme changes.

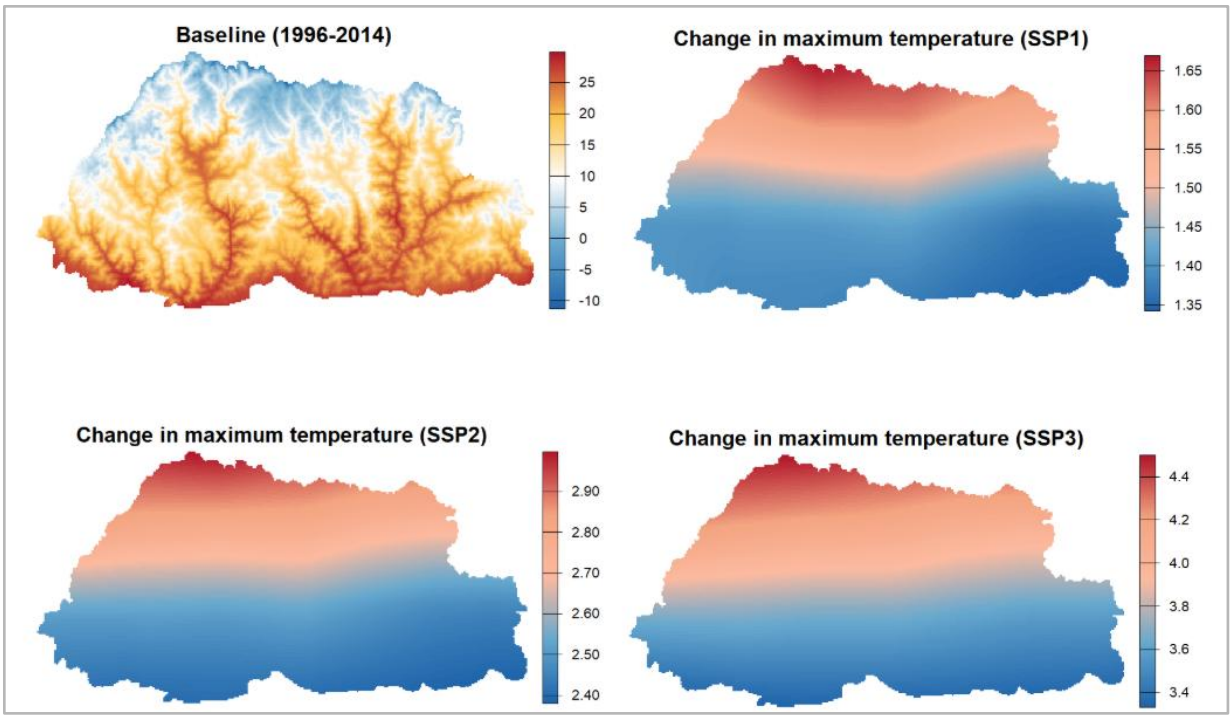

Figure 2.20: Long- term spatial patterns of baseline (top left) and projected changes in annual maximum temperature (degC) under SSP1 (top right), SSP2 (bottom left) and SSP3 (bottom right)

Summer (JJAS) maximum temperature changes

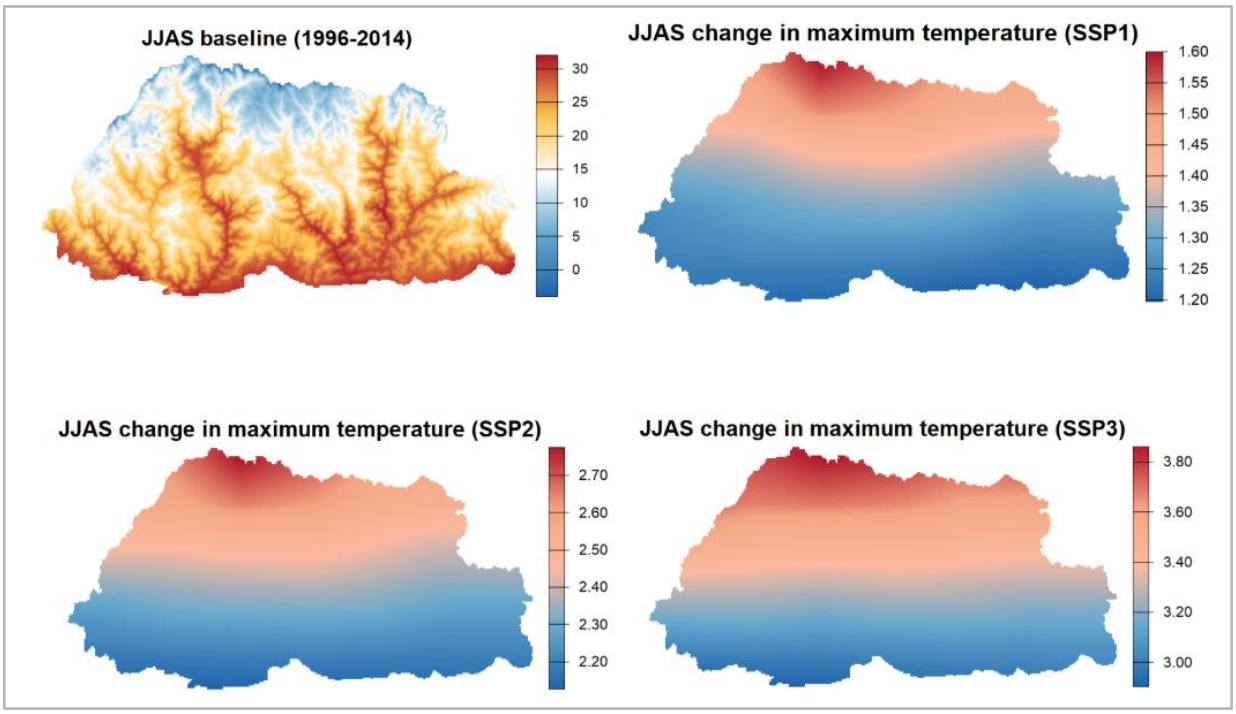

Figure 2.21: Long- term spatial patterns of baseline (top left) and projected changes in summer maximum temperature (degC) under SSP1 (top right), SSP2 (bottom left) and SSP3 (bottom right)

Projected changes under all SSP scenarios show a clear warming trend (Figure 2.21), with the greatest temperature increases concentrated in the northern highlands. SSP1 projects the lowest increase in maximum temperatures (1.20- 1.60°C), followed by SSP2 (2.20- 2.70°C), and SSP3 showing the most significant warming, with increases up to 3.80°C. Notably, under SSP3, warming is more spatially extensive and intense, particularly in central and northern regions. These projected increases in JJAS maximum temperatures may exacerbate heat stress, alter monsoon dynamics, and impact agriculture and water resources, particularly under high- emission scenarios.

Winter (DJF) maximum temperature changes

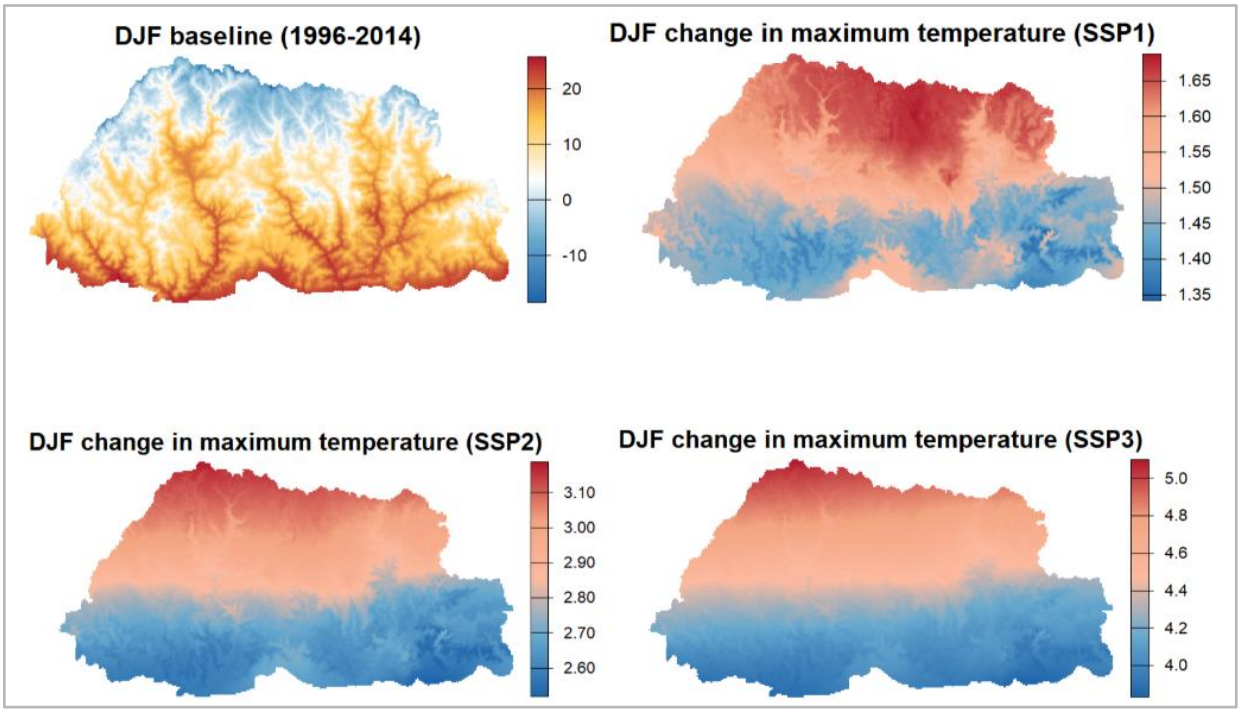

Figure 2.22: Long- term spatial patterns of baseline (top left) and projected changes in winter maximum temperature (degC) under SSP1 (top right), SSP2 (bottom left) and SSP3 (bottom right)

Future changes indicate consistent warming across all scenarios, with the greatest increases occurring in the colder northern regions (Figure 2.22). Under SSP1, the warming is relatively modest (1.35- 1.65°C), while SSP2 shows stronger warming (2.60- 3.10°C), and SSP3 projects the most extreme changes, with increases reaching up to 5.0°C. The spatial pattern of warming highlights elevation-dependent warming, with larger changes in the high-altitude zones.

2.3.3. Minimum Temperature changes

2.3.3.1. Near- term scenario

Annual minimum temperature changes

The historical minimum temperature (Figure 2.23) shows a distinct elevation- driven gradient, with warmer minimum temperatures in the southern lowlands and cooler temperatures dropping below -20°C in the high-altitude northern regions.

Projections under SSP1, SSP2, and SSP3 indicate a consistent warming trend in annual minimum temperatures, particularly in the northern part of the country. The projected increases range from approximately 0.85- 1.15°C under SSP1, up to around 1.20°C under SSP3. The warming is most pronounced in the colder northern and central regions, suggesting a narrowing of the temperature gradient between high and low elevations.

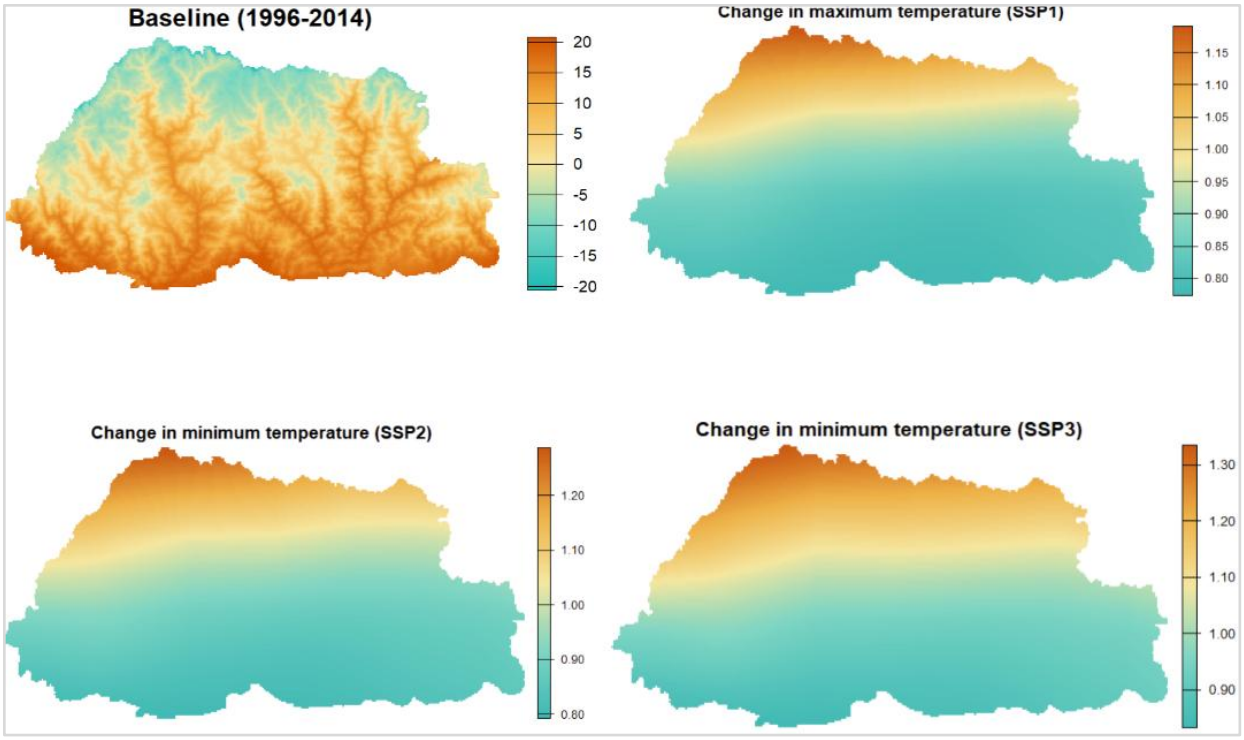

Figure 2.23: Near- term spatial patterns of baseline (top left) and projected changes in annual minimum temperature (degC) under SSP1 (top right), SSP2 (bottom left) and SSP3 (bottom right)

Summer (JJAS) minimum temperature changes

Historical summer JJAS minimum temperature shows a typical elevation gradient, with warmer minimum temperatures above 20°C in the southern lowlands and much cooler values, often below 0°C, in the northern highlands.

Future changes under SSP1, SSP2, and SSP3 (Figure 2.24) show a consistent warming trend, although the magnitude of change remains relatively modest. Under SSP1, the projected

increases range from approximately 0.75°C to 1.05°C, while SSP2 and SSP3 show slightly higher changes, reaching up to around 1.15°C and 1.20°C, respectively. The warming is most pronounced in the higher elevation northern regions, aligning with patterns of elevation-dependent warming. Even slight increases in summer minimum temperatures can influence night time cooling, plant respiration, and heat stress thresholds, potentially affecting both natural ecosystems and agricultural productivity.

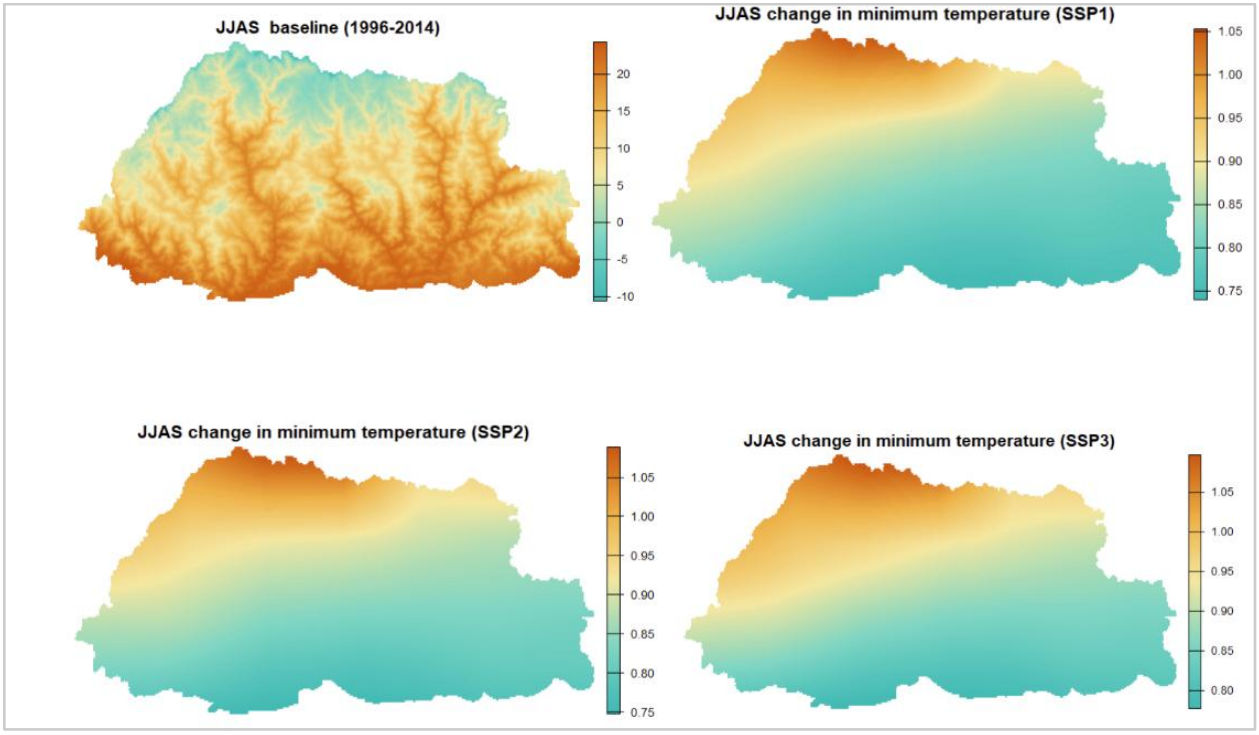

Figure 2.24: Near- term spatial patterns of baseline (top left) and projected changes in summer minimum temperature (degC) under SSP1 (top right), SSP2 (bottom left) and SSP3 (bottom right)

Winter (DFJ) minimum temperature changes

Historical winter DJF minimum temperature shows elevation dependent gradient, with minimum temperatures dropping below -30°C in the northern highlands and rising above 0°C in the southern lowlands.

Across all scenarios, a consistent warming trend is observed (Figure 2. 25), with the most significant increases (up to 1.40°C) in the northern and higher elevation areas. SSP1 shows a relatively moderate warming, while SSP2 and SSP3 suggest slightly greater and more widespread warming. This pattern implies elevation-dependent warming, which could have important implications for snowpack, hydrology, and ecosystem dynamics in the region.

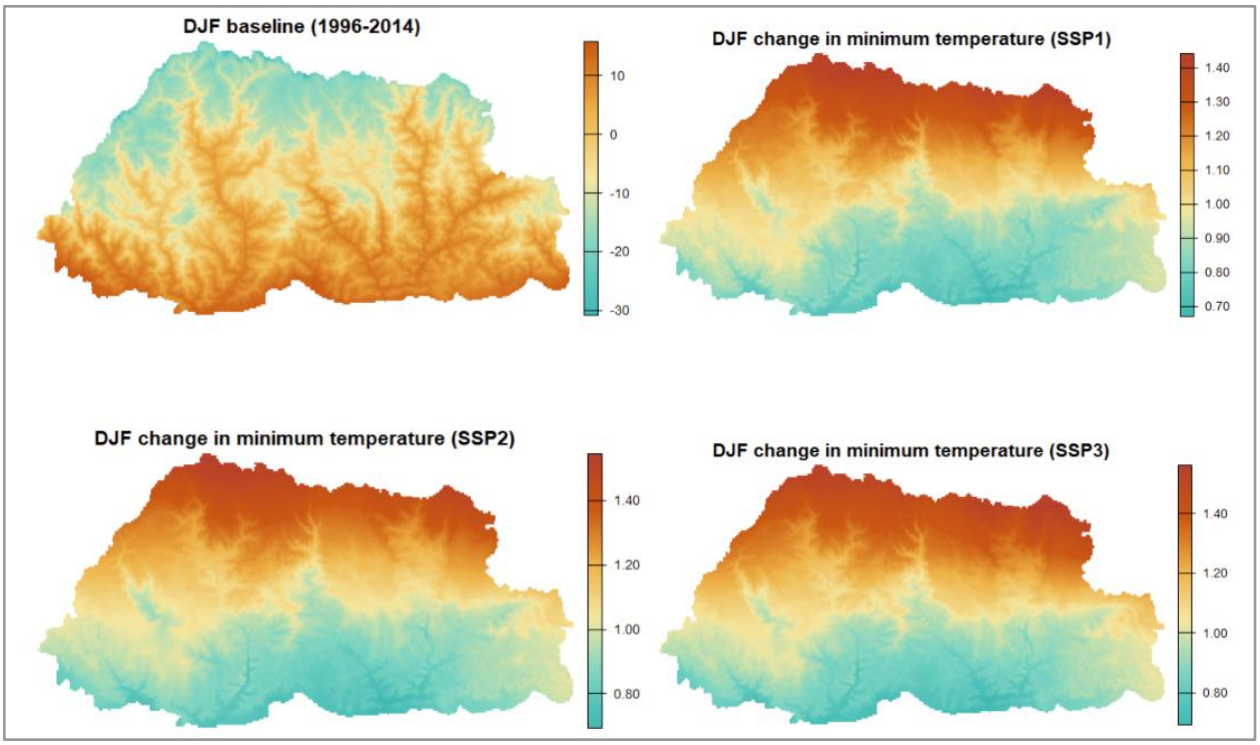

Figure 2.25: Near- term spatial patterns of baseline (top left) and projected changes in winter minimum temperature (degC) under SSP1 (top right), SSP2 (bottom left) and SSP3 (bottom right)

2.3.3.2. Mid- term scenario

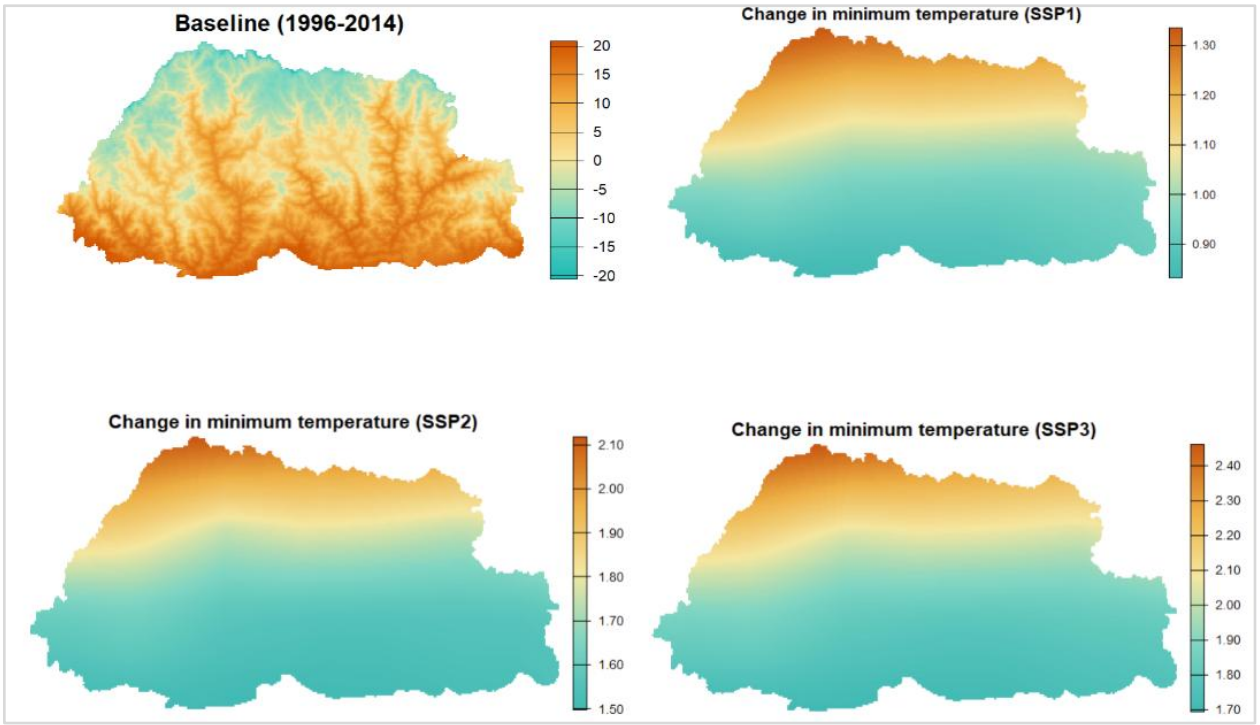

Figure 2.26: Mid- term spatial patterns of baseline (top left) and projected changes in annual minimum temperature (degC) under SSP1 (top right), SSP2 (bottom left) and SSP3 (bottom right)

Changes in annual minimum temperature (Figure 2.26) show a consistent warming trend across all SSPs, with increasing magnitude from SSP1 to SSP3. Under SSP1, temperature increases range from approximately 1.40°C to 1.80°C, while SSP2 and SSP3 show more pronounced warming, reaching up to 2.10°C and 2.40°C respectively. The warming is spatially concentrated in the colder northern regions, highlighting a pattern of elevation-dependent warming.

Summer (JJAS) minimum temperature changes

Projected changes in JJAS minimum temperature (Figure 2.27) indicate a clear warming trend across all SSPs, with more substantial increases under higher- emission scenarios. Under SSP1, the minimum temperature increases range from approximately 1.20°C to 1.50°C. This warming intensifies under SSP2 (1.40- 1.80°C) and SSP3 (1.60- 2.10°C), particularly in the northern mountainous areas. The spatial consistency of warming across scenarios suggests potential impacts on nighttime temperatures, which could reduce diurnal temperature ranges, alter plant physiology, and influence monsoon-season hydrology and crop productivity.

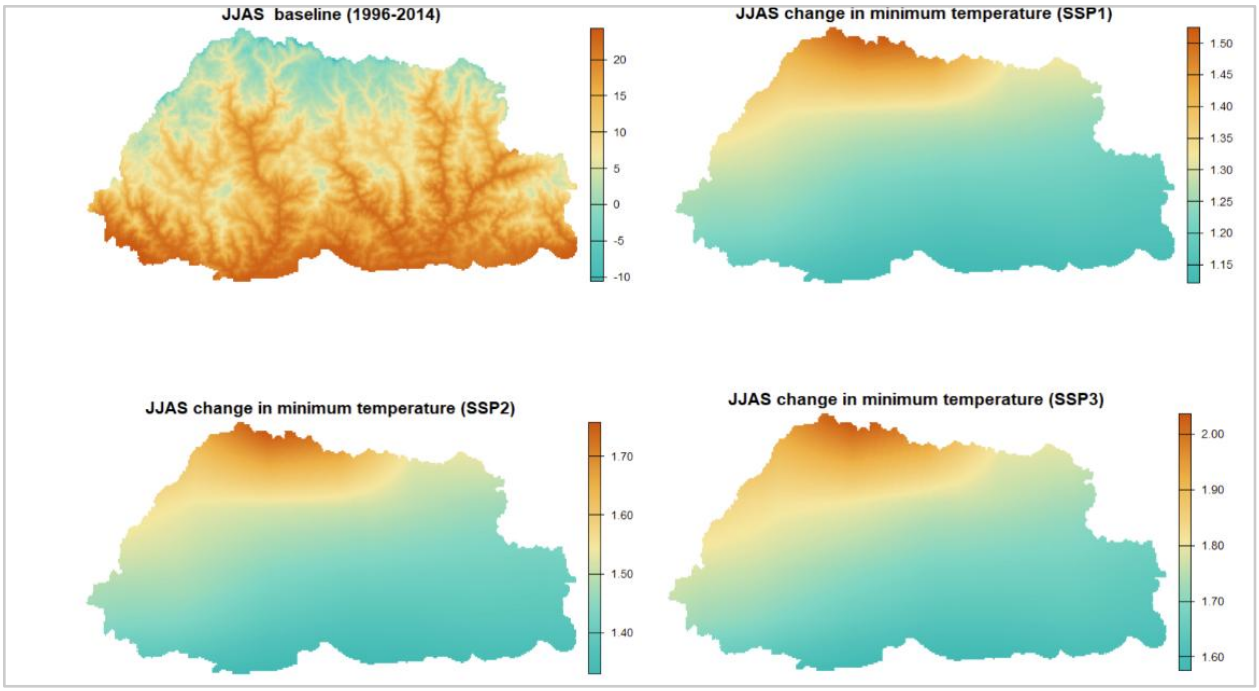

Figure 2.27: Mid- term spatial patterns of baseline (top left) and projected changes in summer minimum temperature (degC) under SSP1 (top right), SSP2 (bottom left) and SSP3 (bottom right)

Winter (DFJ) minimum temperature changes

The future scenario shows a clear warming trend (Figure 2.28). Under SSP1, minimum temperatures are projected to increase by approximately 1.10°C to 1.90°C, with the greatest warming in the northern and high- altitude area. SSP2 shows a stronger warming pattern, with increases ranging from 1.40°C to 2.40°C, again concentrated in elevated regions. The highest warning is seen under SPP3, with projected increases between 1.80°C and 2.80°C.

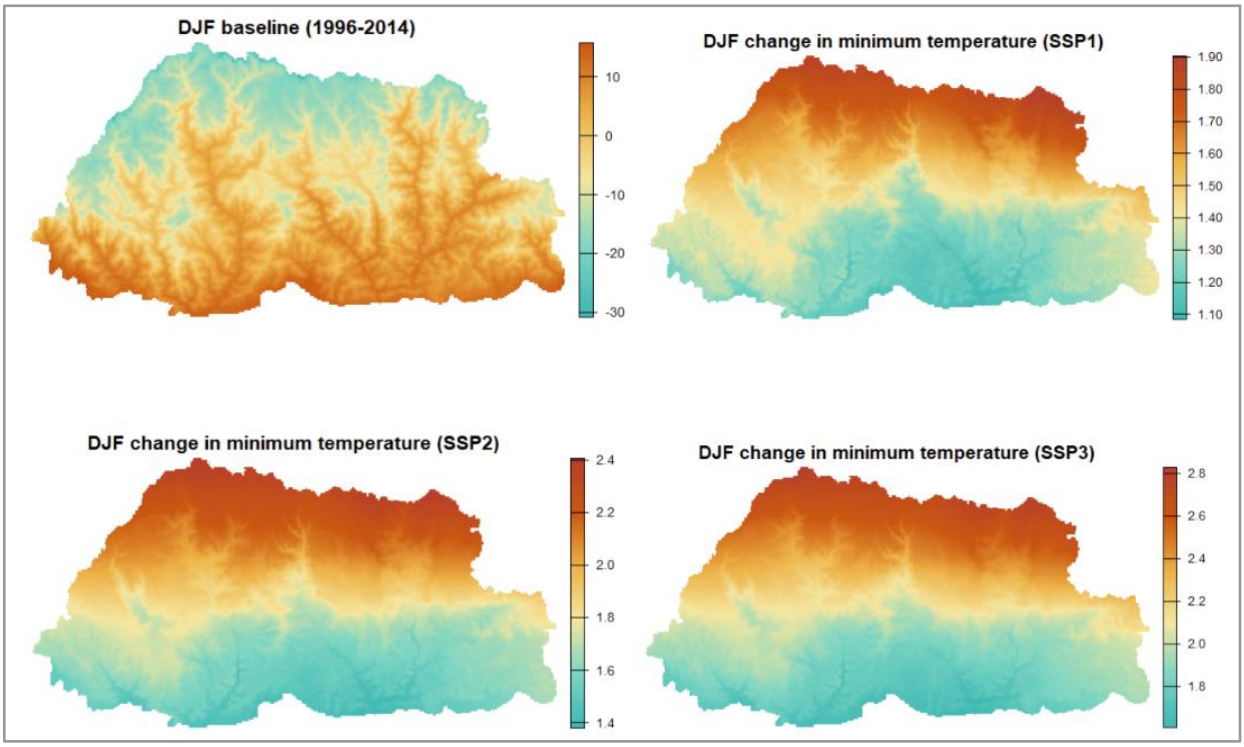

Figure 2.28: Mid- term spatial patterns of baseline (top left) and projected changes in winter minimum temperature (degC) under SSP1 (top right), SSP2 (bottom left) and SSP3 (bottom right)

2.3.3.3. Long- term scenario

Annual minimum temperature changes

The changes in annual minimum temperature under SSP scenarios (Figure 2.29) show a clear increase across the country, with the magnitude of warming intensifying from SSP1 to SSP3. SSP1 indicates moderate warming, with temperature increases up to 1.75°C, particularly in the northern and central regions. SSP2 presents a stronger warming signal, with maximum temperature changes reaching approximately 3.40°C. The highest warming is projected under SSP3 with values exceeding 5.20°C in the northern and central zones.

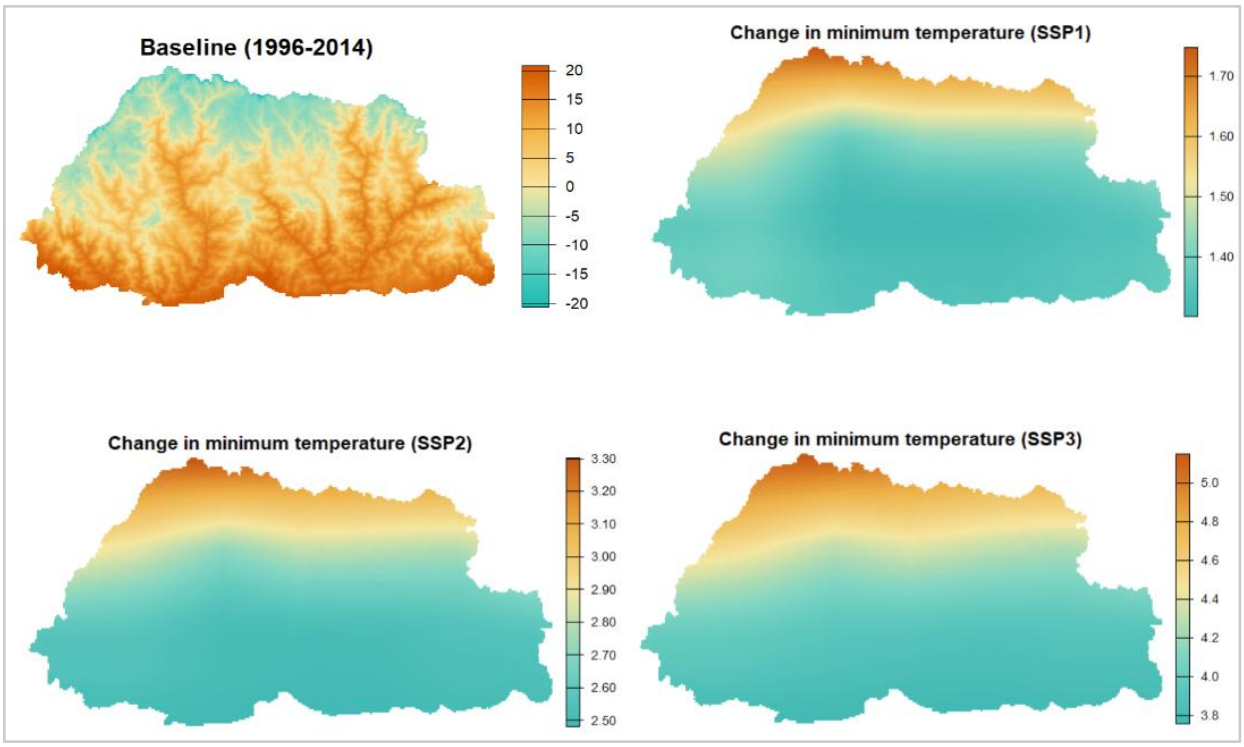

Figure 2.29: Long- term spatial patterns of baseline (top left) and projected changes in annual minimum temperature (degC) under SSP1 (top right), SSP2 (bottom left) and SSP3 (bottom right)

Summer (JJAS) minimum temperature changes

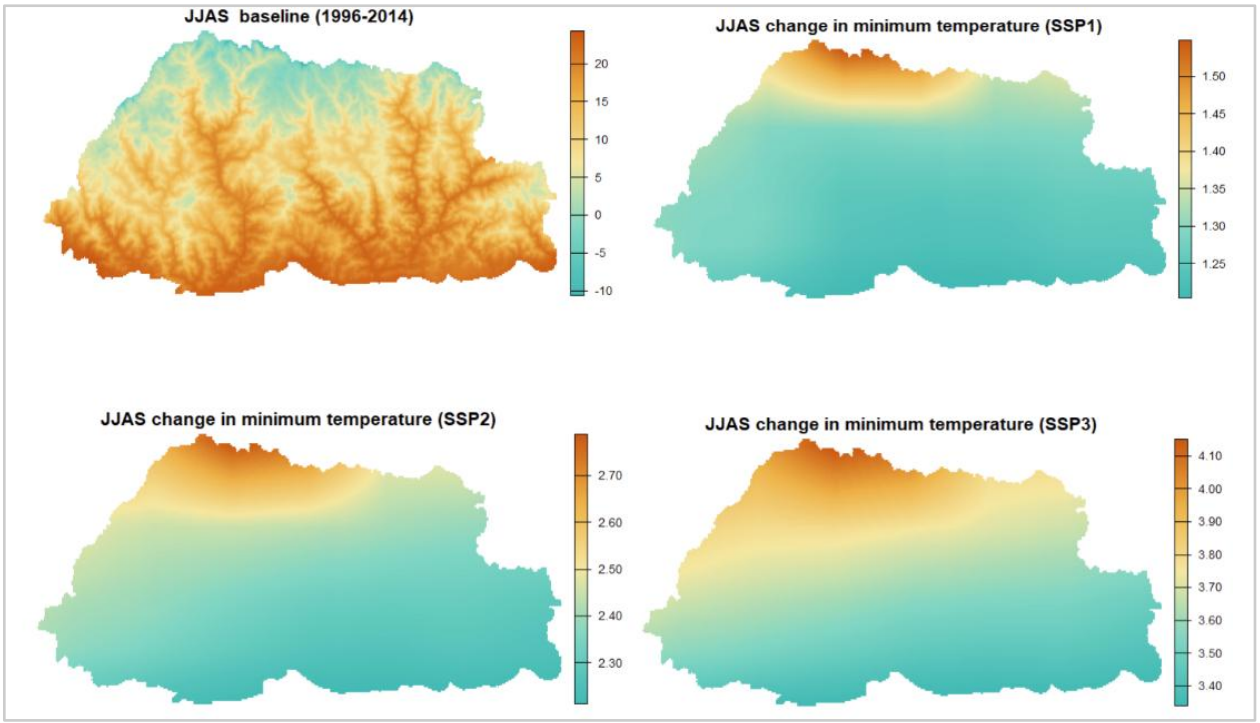

Figure 2.30: Long- term spatial patterns of baseline (top left) and projected changes in summer minimum temperature (degC) under SSP1 (top right), SSP2 (bottom left) and SSP3 (bottom right)

Projected changes in summer minimum temperature (Figure 2.30) reveal a consistent warming trend under all SSP scenarios. Under SSP1 temperature increases are relatively moderate, ranging from around 1.20°C to 1.60°C. SSP2 projects a stronger warming, which increases up to approximately 2.80°C, particularly in the northern and western regions. The most pronounced warming is observed under SSP3 where increases exceed 4.40°C in the highlands. The spatial trend suggests more intense warming in the northern parts of the country.

Winter (DFJ) minimum temperature changes

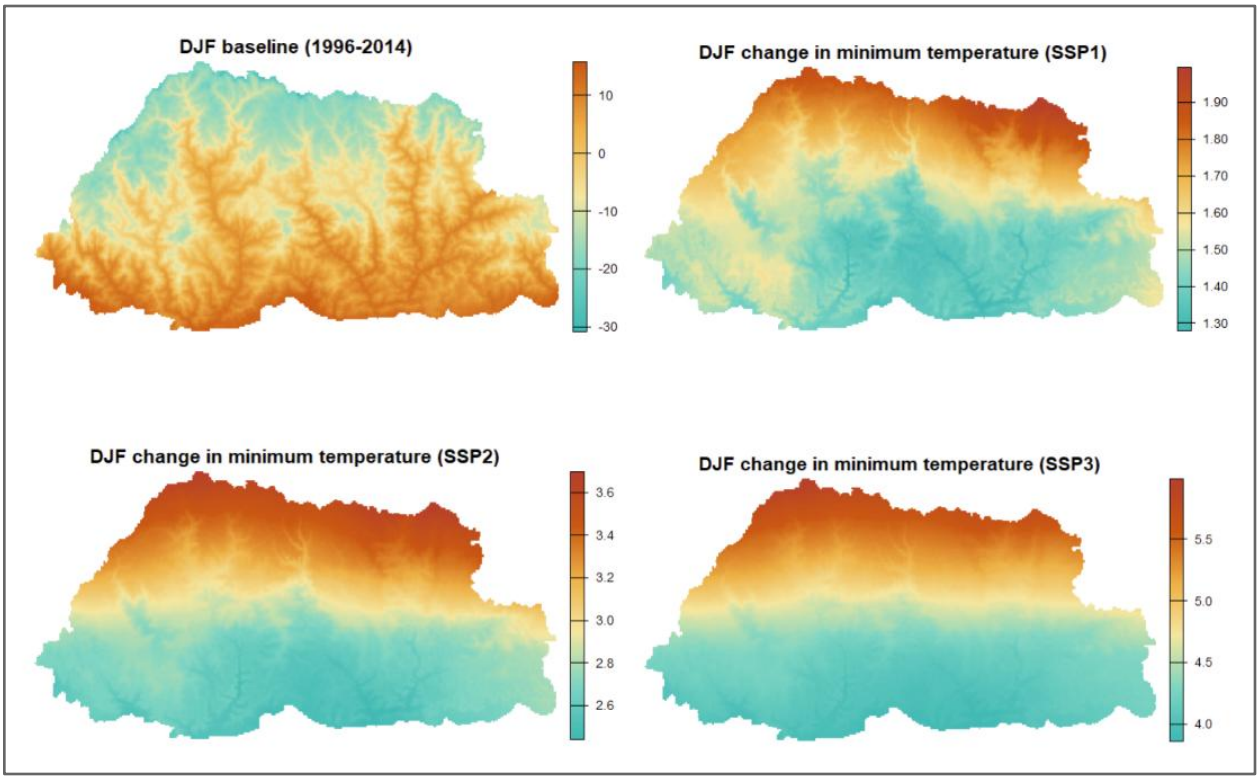

Figure 2.31: Long- term spatial patterns of baseline (top left) and projected changes in winter minimum temperature (degC) under SSP1 (top right), SSP2 (bottom left) and SSP3 (bottom right)

The maps (Figure 2.31) show a consistent warming trend across scenarios, with the magnitude of warning increasing progressively from SSP1 to SSP3. Under SSP1, the minimum temperature increases ranges from 1.30°C to 2.20°C, while SPP2 shows a rise between 2.4°C to 3.6°C. The most dramatic warming is observed in SSP3, where winter minimum temperatures are projected to increase by 4.0°C to almost 6.0°C. These changes are mostly seen in the northern and elevated regions, indicating elevation- dependent warming.

2.4. Discussion

Climate projections for Bhutan indicate a consistent trend of increasing precipitation and rising maximum and minimum temperatures, with the magnitude of change intensifying over time and under higher- emission scenarios. Spatially, these changes are most pronounced in the southern regions for precipitation and the northern highlands for temperature, highlighting both topographic and elevation- dependent climate responses.

In the near- term, all SSP scenarios (SSP1–3) project moderate increases in annual and summer (JJAS) precipitation, particularly in the south, with SSP3 showing the largest changes: annual increases over 300 mm and summer gains above 350 mm. Winter (DJF) precipitation remains low with minimal change. Meanwhile, maximum temperatures are projected to rise by 0.6- 1.0°C annually, with slightly higher increases during winter (up to 1.2°C) in the north. Minimum temperatures show a similar warming pattern, ranging from 0.8- 1.2°C annually, with the most notable increases in cold, high- elevation areas. DJF minimum temperatures increase up to 1.4°C, signaling potential impacts on frost frequency and snowpack.

By the mid- term, changes intensify. Annual precipitation increases up to 500 mm under SSP1 and 2, and over 600 mm under SSP3, with JJAS rainfall exceeding 500 mm in southern areas. DJF precipitation begins to show a drying trend, particularly under SSP2 and SSP3. Maximum temperatures increase to 1.2- 2.0°C annually, and summer maximum temperature reaches over 1.65°C in northern regions. Winter maximum temperature increases are even higher, up to 2.3°C, raising concerns for glacial stability. Minimum temperatures continue to rise, with annual increases reaching 2.4°C under SSP3, and winter minimums up to 2.8°C, especially in the north. These trends indicate increasing risks of hydrological shifts, snowpack loss, and ecological disruption.

In the long term, projections under SSP3 show dramatic changes. Annual precipitation increases by over 2000 mm, and summer rainfall by up to 1500 mm, while winter precipitation declines by over 15 mm, intensifying dry- season water stress. Maximum annual temperatures rise up to 4.4°C, with winter maximum temperature increases reaching 5.0°C in the northern regions. Minimum annual temperatures exceed 5.2°C under SSP3, with DJF minimums rising as high as 5.5°C. This extreme warming could accelerate glacial melt, reduce winter snow cover, and stress agricultural and ecological systems, particularly in the country's mountainous regions.

Overall, these projections underscore the urgent need for climate adaptation and mitigation, particularly for water resource management, glacier and snow monitoring, and high-altitude ecosystem resilience, as the country faces increasingly severe climate impacts across all timeframes and pathways.

3. Assessment of Hydrological Changes

Bhutan is characterized by a complex river system originating primarily from its alpine and glacial regions. Numerous high-altitude lakes, formed due to increased glacial melt, are situated in remote mountainous areas and pose a risk of GLOFs, which can cause devastating flash floods downstream. The country's major rivers generally flow from north to south, originating in the alpine zone and draining into the tropical lowlands at the border with India. These rivers, flowing through steep and narrow valleys, occasionally open into small flat areas suitable for cultivation. Their steep longitudinal gradients and high annual runoff provide significant potential for hydropower development (Yangzom and Choden, 2021). Bhutan's river systems exhibit strong seasonal flow variations, driven by distinct monsoon and dry seasons (NWRED, 2011). During the monsoon, rivers carry high volumes of water and sediment, while snowmelt contributes significantly at the end of the dry season. In addition to the major rivers, a dense network of perennial and rain- fed tributaries descend steeply from the mountains, often forming waterfalls before joining the main rivers.

Bhutan's hydrological system is broadly categorized into four major river basins: the Amochu, Wangchu, Punatsangchu, and Manas basins. The Amochu, a transboundary river originating in China, flows through the Ha and Samtse districts before entering India via Phuntsholing. The Jaldhaka, another transboundary river, originates from southeastern Sikkim and enters Bhutan through Samtse. The Wangchu River includes three major tributaries from the Thimphu, Paro, and Ha valleys, and flows southward through Chukha into India. The Punatsangchu, also known as the Sankosh River, is formed by the confluence of the Phochu and Mochu rivers from Gasa, which merge at Punakha Dzong and flow through Wangdue Phodrang, Tsirang, and Sarpang before reaching India. The Manas River is the largest river basin, draining much of central and eastern Bhutan, and includes four major sub-basins: Mangde Chu, Chamkhar Chu, Kuri Chu, and Dangmechu. Kuri Chu and Gongri, sub-tributaries of the Manas, are transboundary rivers originating in the Tibetan Autonomous Region of China. Additionally, three minor rivers Nyera Ama Ri, Nonori Chu, and Jomo Chu (Dhansari)drain the southeastern corner of the country.

3.1. Punatshangchu and Wangchu River Basins

Punatshangchu River Basin (PRB) and Wangchu River Basin (WRB) located in the western part of Bhutan (Figure 3.1) covers most of the river system in the country. PRB is the largest river basin in the country with an area of 9,645 km^2, whereas the WRB is the third largest basin with an area of 4,596 km^2. The elevation of these bains ranges from 100- 7,500 meters with alpine, temperate and subtropical climatic zones (Katwal et al., 2020). PRB and WRB constitute the largest urban area of 9.36 km^2 and 26.03 km^2 respectively. PRB covers five districts of the country namely Gasa, Punakha, Wangdue Phodrang (largest district in the country), Dagana and Tsirang. WRB included Thimphu (capital city of the country), Paro (international airport), Haa and Chukha (largest commercial hub) districts. Together, these basins represent some of the most densely populated regions in Bhutan. According to the 2017 Population and Housing Census (NSB, 2018), the PRB had a population of 122,219, while the WRB had 240,012, out of the national total of 735,533.

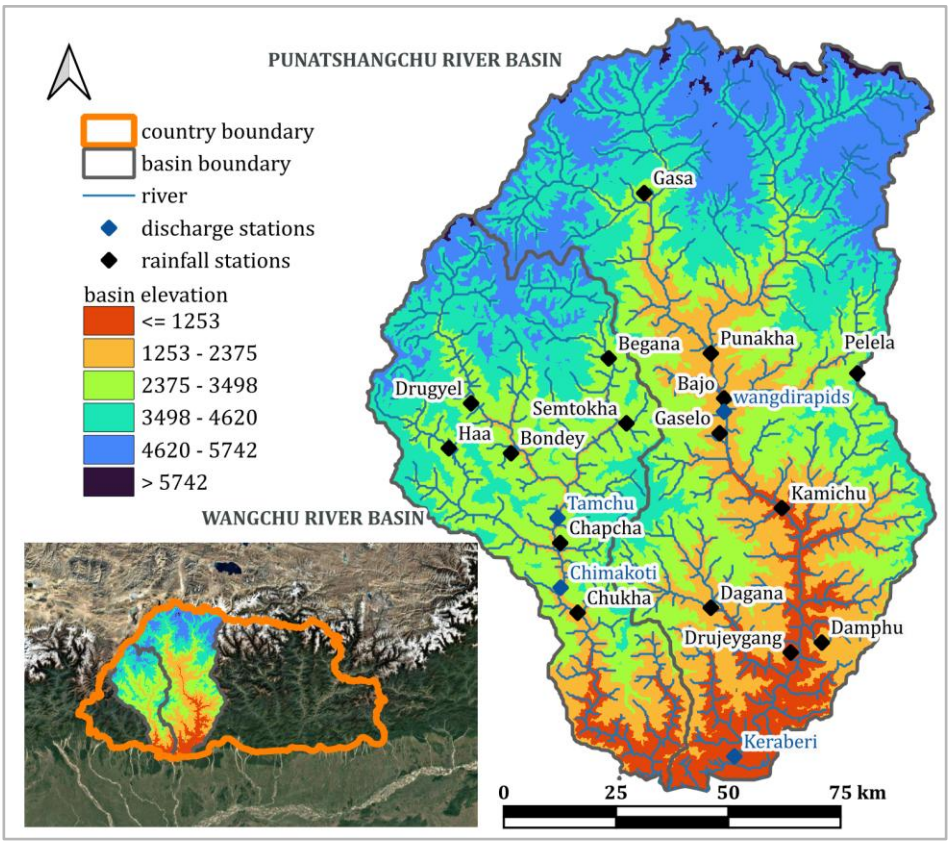

Figure 3.1: Location of Punatshangchu and Wangchu River Basin

The basins are important for water supply for domestic use and economic development (Zam et, al. 2021 and Chhogyel, et al., 2020, Dahal, et.al., 2025)). They are agricultural zones with the largest rice crop areas with 231.85 km^{2}and 103.88 km^2 (NSB,2025) respectively, contributing significantly to the country's rice cultivation. Furthermore, the basins host the country's important hydropower projects such the Punatshangchu I and II, Tala, Chukha and Dagachu projects. These basins contribute significantly to the country's national revenue and energy, making their hydrology critical for economic development and stability.

3.2. Methodology

The changes in precipitation patterns will change the river flows in the country. In order to understand the changes in the river flow, precipitation from the nine GCM models from the *3. Assessment of Climate under CMIP6 scenario*, were input to the hydrological model. The river flow was simulated for baseline year (1996-2014), and future scenarios of near- term (2021-2040), mid- term (2041-2060) and long- term (2081-2100) for three SSPs namely SSP 1 2.6, SSP2 4.5, and SSP3 7.0. The nine models are shown in Table 2.1.

3.2.1. Rainfall- Runoff Inundation Model

Hydrological and hydraulic models are employed to simulate key flood characteristics, including inundation extent, depth, and duration. Accurate calibration of these models is essential to enhance the reliability of flood assessments for the area of interest. In this study, the two-dimensional Rainfall-Runoff-Inundation (RRI) model (Sayama et al., 2012) was

applied to PRB and the WRB to simulate the river discharge, with rainfall input from the GCMs.

The RRI model has been widely utilized in a variety of geographic settings, ranging from mountainous terrains to lowland floodplains (Bhagabati and Kawasaki, 2017; Nastiti et al., 2015; Nguyen et al., 2021; Sayama et al., 2015; Shrestha, 2019; Shrestha et al., 2015; Shrestha et al., 2016; Try et al., 2020, Syldon et al., 2024). This model allows for simultaneous simulation of rainfall- runoff processes and river discharge by discretely accounting for slopes and river channels. The model was configured using topographic inputs sourced from the HydroSHEDS database, developed by the United States Geological Survey (USGS). These inputs included a Digital Elevation Model (DEM) with a spatial resolution of 15 arc-seconds (approximately 450 × 450 meters), along with datasets for flow direction and flow accumulation. Land cover and soil characteristics were integrated through the RRI_BUILDER.exe tool, which utilizes global land use and soil distribution datasets to facilitate discharge simulations and model calibration. Daily rainfall records from nine meteorological stations within the PRB and seven within the WRB were incorporated, in addition to discharge measurements from two hydrological stations in each basin, all provided by NCHM. Station details are shown in Table 3.1.

Table 3.1: Rainfall stations at PRB and WRB

Sl no	Station	Latitude	Longitude	Sl no	Station	Latitude	Longitude
Rainfall station at PRB				Rainfall station at WRB			
1	Bajo	27.49	89.90	1	Begana	27.57	89.64
2	Dagana	27.07	89.87	2	Bondey	27.38	89.42
3	Damphu	27.00	90.12	3	Chapcha	27.19	89.53
4	Drujeygang	26.98	90.05	4	Chukha	27.06	89.57
5	Gasa	27.90	89.72	5	Drugyel	27.48	89.33
6	Gaselo	27.42	89.89	6	Haa	27.39	89.28
7	Kamichu	27.27	90.03	7	Semtokha	27.44	89.68
8	Pelela	27.54	90.20				

9	Punakha	27.58	89.87				

A comparative analysis of observed versus simulated discharge at the Wangdirapids and Keraberi stations within the PRB was conducted for both calibration and validation periods (Figure 3.2 and 3.3). The model calibration utilized hydrological data from the 2019 flood event. At Wangdirapids, performance metrics during calibration were as follows: NSE of 0.68, RMSE of 141.7m^3/s, and R^2 of 0.81. At the Keraberi station, the model demonstrated a slightly higher NSE of 0.78, with RMSE and R^2 values of 164.14 m^3/s and 0.89, respectively. Model validation was conducted using discharge records from the 2015 flood event. At Wangdirapids, validation results were comparable to the calibration phase, yielding an NSE of 0.72, RMSE of 124.82 m^3/s, and R^2 of 0.78. The Keraberi station exhibited a modest decrease in performance, with corresponding metrics of NSE = 0.76, RMSE = 172.24 m^3/s, and R^2 = 0.83. Overall, these statistical indicators suggest that the model performed within acceptable to good accuracy ranges. Despite the satisfactory overall performance, the model exhibited a tendency to underestimate peak discharges, which may be attributed to topographic resolution constraints in the digital elevation model used for this high relief terrain.

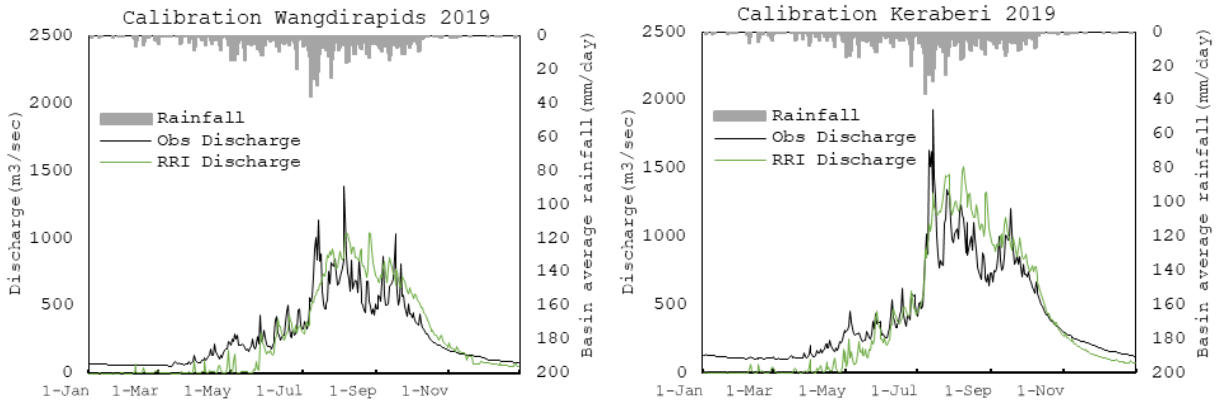

Figure 3.2: Calibration of RRI model for PRB for flood event 2019 (left: Wangdirapids station and right: Keraberi station)

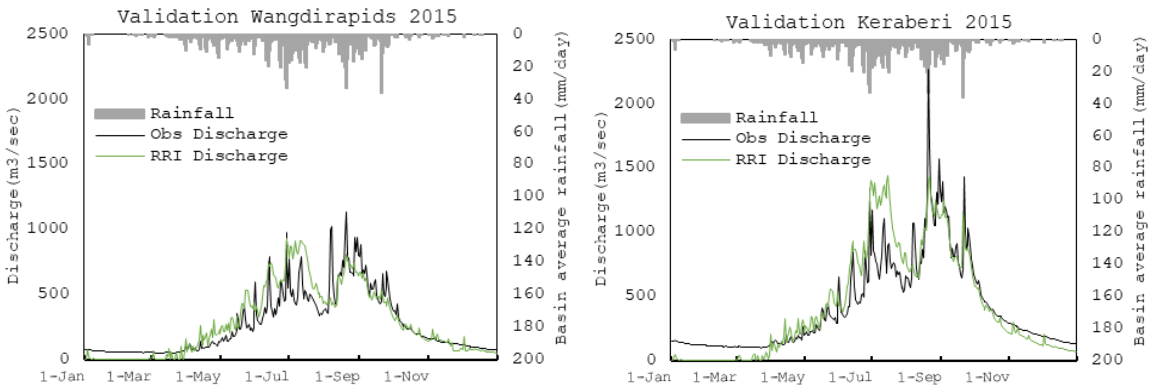

Figure 3.3: Validation of RRI model for PRB for flood event 2015 (left: Wangdirapids station and right: Keraberi station)

The WRB model was calibrated using the 2010 flood event for Chimakoti and Tamchu stations. Figure 3.4 and 3.5 presents the observed and simulated discharge comparisons at Chimakoti and Tamchu station across calibration and validation periods. During the calibration phase, the model yielded an NSE of 0.77 and an RMSE of 47.23 m^3/s at Chimakoti, with an R^2 of 0.83. At the Tamchu station, NSE was 0.61, RMSE was 50.07 m^3/s, and R^2 was 0.73. Validation was carried out using hydrological data from the 2017 flood event. The model produced NSE values of 0.83 at Chimakoti and 0.80 at Tamchu, with corresponding RMSE values of 33.35 m^3/s and 25.23 m^3/s. R^2 values during validation were 0.87 and 0.84, respectively. The validation results confirm that the model effectively reproduced peak flows and overall discharge trends across different hydrological conditions.

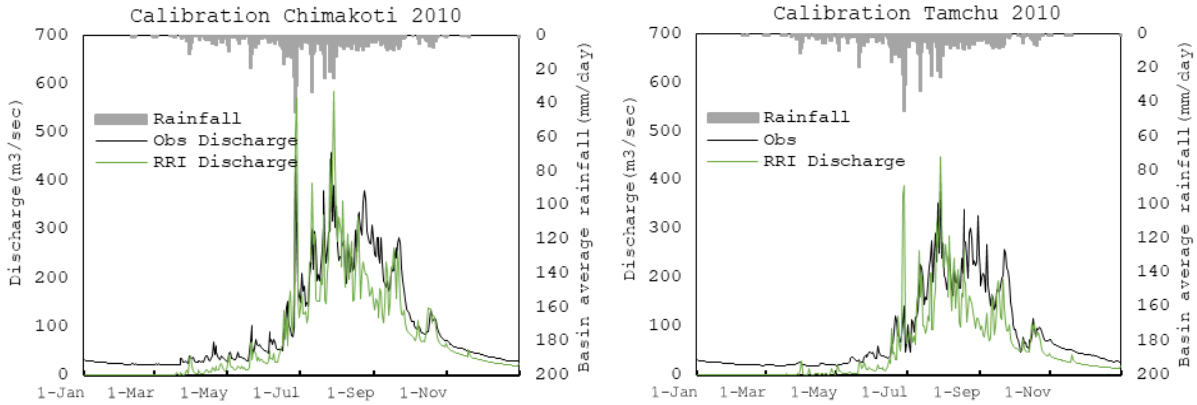

Figure 3.4: Calibration of RRI model for WRB for flood event 2010 (left: Chimakoti station and right: Tamchu station)

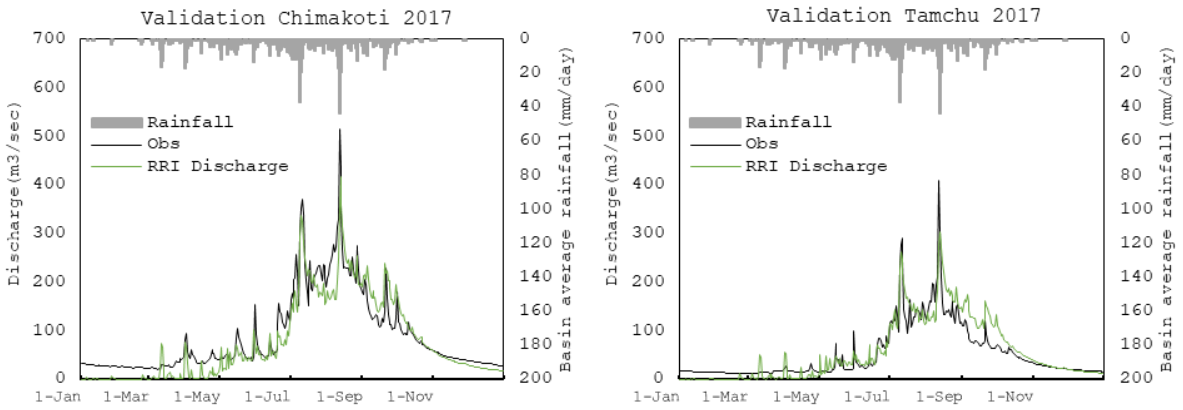

Figure 3.5: Validation of RRI model for WRB for flood event 2017 (left: Chimakoti station and right: Tamchu station)

The model's parameter sensitivity analysis identified lateral saturated hydraulic conductivity (ka), soil depth (d), and unsaturated effective porosity (γm) as the most influential parameters affecting model performance. The calibrated values for these and other model parameters used in the RRI simulation framework are summarized in Table 3.2.

Table 3.2: Calibrated values of RRI model for PRB and WRB

Parameter	**Symbol**	**Calibrated value**
Channel roughness coefficient ($m^{-1/3}s$)	$ns_{\_river}$	0.03
Hillslope roughness coefficient ($m^{-1/3}s$)	$ns_{\_slope}$	0.3
Soil depth (m)	D	3
Soil porosity	γ_a	0.475
Lateral saturated hydraulic conductivity (m/s)	k_a	0.01
Unsaturated effective porosity	γ_m	0.1
Width parameter C (m)	C_W	2.5
Width parameter S (m)	S_W	0.35

Depth parameter C (m)	C_D	0.95
Depth parameter S (m)	S_D	0.2

3.3. Historical river flow

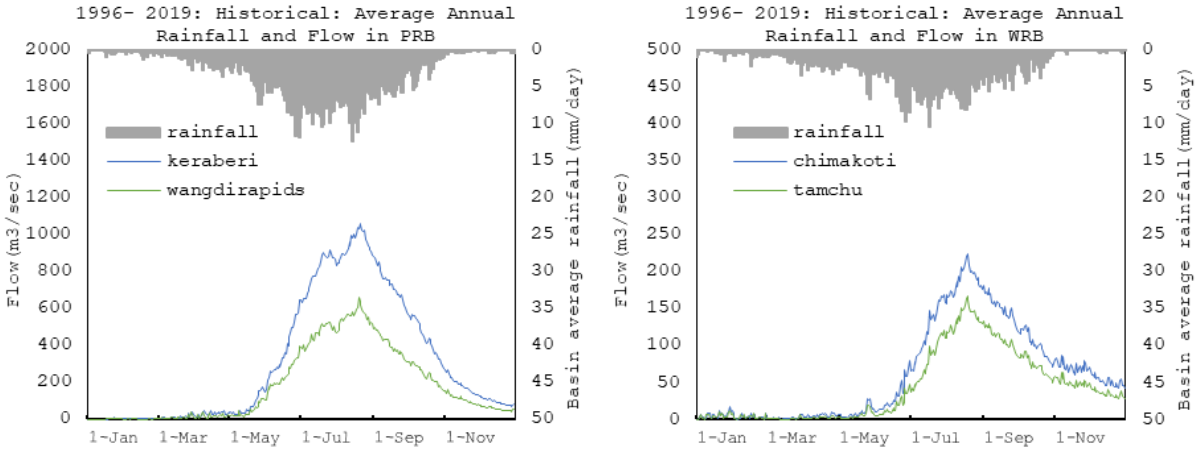

Figure 3.6: Historical (1996- 2019) average annual rainfall and flow in PRB (left) and WRB (right)

The historical analysis of average annual rainfall and streamflow for the period 1996– 2014 in the PRB and WRB reveals a strong seasonal dependency on monsoonal rainfall. In both basins, rainfall increases sharply from late May, peaks during July- September, and gradually declines toward the end of the year. Correspondingly, river flows at Kerabari and Wangdirapids (PRB), and Chimakoti and Tamchu (WRB) follow similar trends, with peak flows occurring in sync with peak rainfall. The PRB experiences higher rainfall intensity (exceeding 35 mm/day) and significantly greater flow (peaking around 1,100 m^3/sec at Kerabari), whereas in WRB the rainfall peaks at around 25 mm/day and discharge remains below 250 m^3/sec. The average annual flow at Wangdi rapids and Keraberi are 180 m^3/sec and 308 m^3/sec respectively. Tamchu and Chimakoti are 43 m^3/sec and 62 m^3/sec respectively. Overall, it confirms that rainfall is the dominant driver of river discharge in both basins, with minimal lag between precipitation and runoff.

3.4. Future river flow

3.4.1. Near- term scenario

a. Punatshangchu River Basin

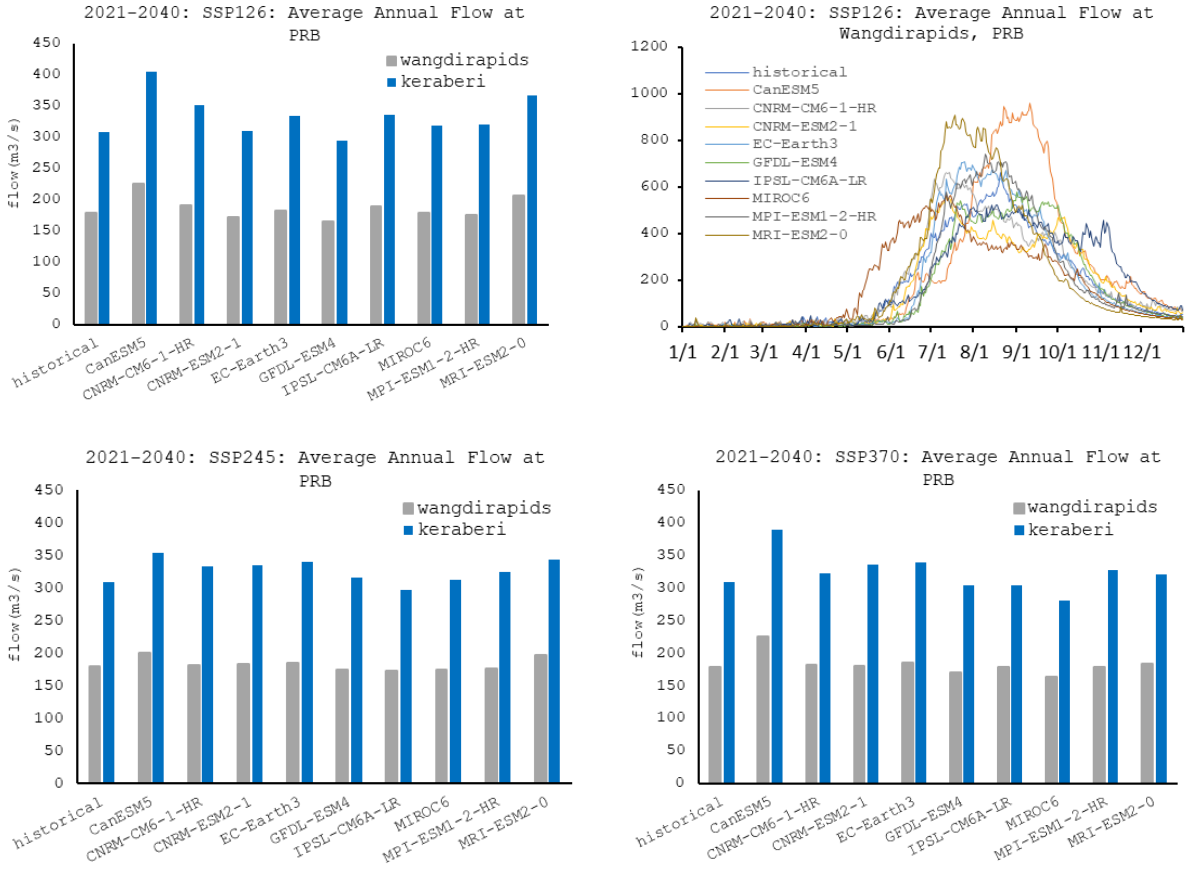

Figure 3.7: Near- term average annual flow at Wangdirapids and Keraberi in PRB under SSP1 (top left), SSP2 (bottom left) and SSP3 (bottom right). Hydrograph of average annual flow at PRB from 9 GCMs (top right)

Hydrological simulations for the period near- term (Figure 3.7) reveal consistent increases in river flow within the PRB under all three SSP scenarios. At both Wangdirapids and Kerabari stations, the projected average annual flow exceeds the historical baseline, with Kerabari consistently exhibiting higher discharge. Under SSP1 streamflow at Kerabari generally ranges from 290 to 350 m^3/s, while Wangdirapids show a smaller increase, ranging from 180 to 250 m^3/s across models. These values gradually intensify under SSP2. The largest increases are observed under SSP3, where Kerabari flow exceeds 360 m^3/s in several models, suggesting the influence of greater precipitation intensity or increased snow and glacier melt due to elevated warming. These inter-model differences reflect the inherent uncertainties in future climate projections, but the consistent direction of change suggests a robust signal of increasing river flow.

Seasonal analysis at Wangdirapids further supports these findings, with most models capturing the dominant monsoonal pattern, peaking between June and September. While the overall shape of the seasonal hydrograph remains consistent with historical behavior, many models simulate higher peak flows during the monsoon season, with some projections exceeding 1000 m^3/s. This suggests a potential intensification of hydrological extremes, particularly under higher- emission pathways. The dry season (December- February) flow

patterns remain largely unchanged, indicating that projected changes are mostly concentrated in the wet season.

Table 3.4: Near- term projected percentage changes in river flow at PRB

Near- term: 2021-2040: percentage change						
GCM	SSP1		SSP2		SSP3	
	Wangdi rapids	keraberi	Wangdi rapids	keraberi	Wangdi rapids	keraberi
CanESM5	26	31	12	14	26	26
CNRM-CM6-1-HR	6	14	1	8	1	5
CNRM-ESM2-1	-4	0	2	8	1	9
EC-Earth3	2	8	3	10	3	10
GFDL-ESM4	-8	-5	-2	3	-5	-1
IPSL-CM6A-LR	6	9	-3	-4	0	-2
MIROC6	0	4	-3	1	-9	-9
MPI-ESM1-2-HR	-2	4	-2	5	0	6
MRI-ESM2-0	15	19	10	11	2	4
Mean increase	**11**	**13**	**4**	**8**	**5**	**8**

The projected percentage changes in river flow for the near- term period (Table 3.4) show a general tendency toward increased flow at both Wangdirapids and Kerabari stations, although with considerable inter- model variability. Under the SSP1, the mean projected increase in flow is 11% at Wangdirapids and 13% at Kerabari. CanESM5 and MRI-ESM2-0 simulate the largest increases at both stations (26- 31%), while some models such as GFDL-ESM4 and CNRM-ESM2-1 show slight reductions in flow. This suggests that although the majority of models predict an increase, uncertainties still exist, particularly in models with weaker or negative signals.

Under SSP2 the mean projected increases are 4% for Wangdirapids and 8% for Kerabari, indicating a more subdued hydrological response compared to SSP1. The reduced mean values, despite continued warming and emissions in SSP2, may reflect differences in precipitation seasonality or model sensitivity. CanESM5 and MRI-ESM2-0 again show consistent increases, while models like MIROC6 and IPSL-CM6A-LR simulate slight declines in flow at Wangdirapids. Under SSP3 the projected mean increase is 5% at Wangdirapids and 8% at Kerabari, which, while greater than SSP2, does not surpass the values seen under SSP1. This somewhat counterintuitive result may be due to complex regional climatic dynamics or model structural differences, particularly regarding monsoon behavior and snowmelt processes.

b. Wangchu River Basin

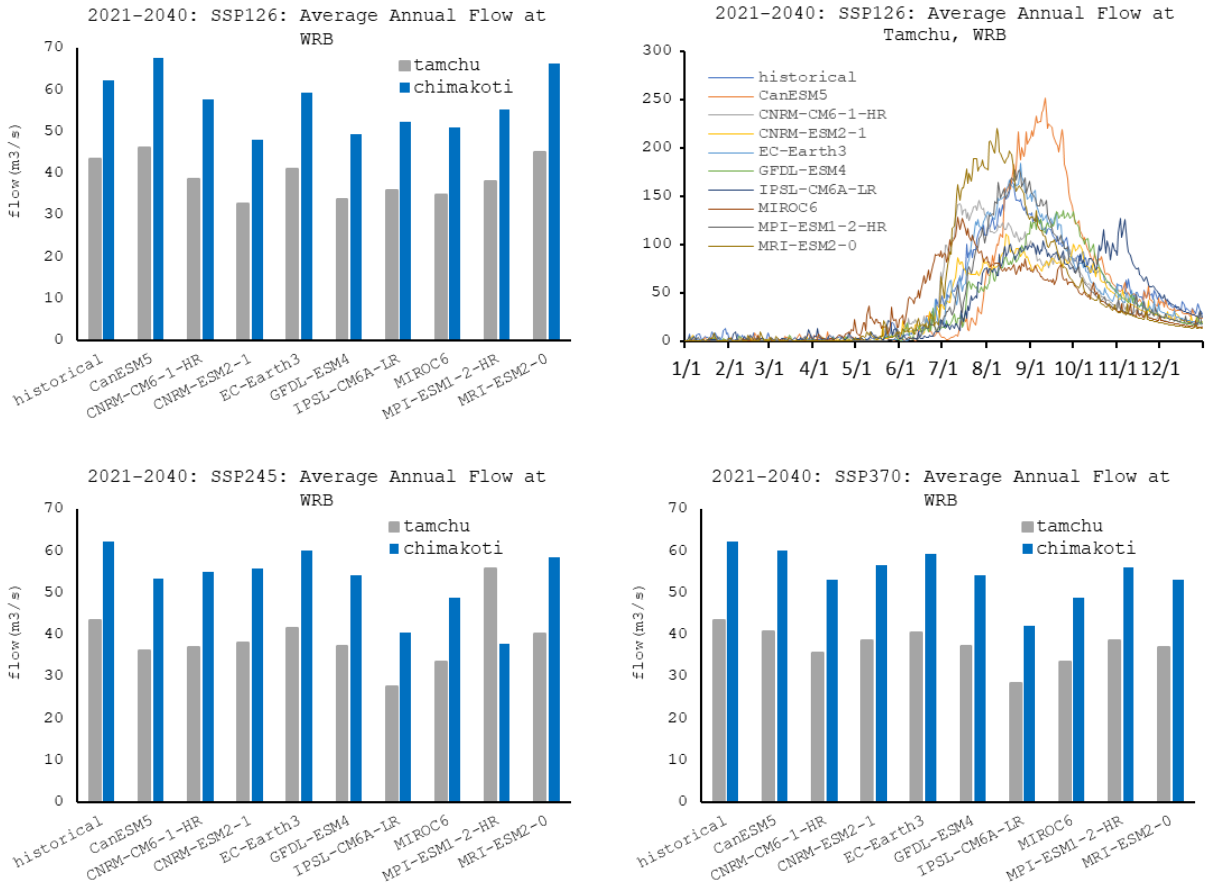

Figure 3.8: Near- term average annual flow at Tamchu and Chimakoti in WRB under SSP1 (top left), SSP2 (bottom left) and SSP3 (bottom right). Hydrograph of average annual flow at WRB from 9 GCMs (top right)

Across all scenarios, Chimakoti consistently shows higher average annual flows than Tamchu, with historical values around 65 m^3/s and 45 m^3/s, respectively (Figure 3.8). While individual climate models vary, general patterns suggest that under SSP1 and SSP2, flow at Chimakoti and Tamchu may decrease. Notably, the SSP3 scenario projects a marginal

reduction in Chimakoti flows across several models, potentially reflecting reduced precipitation or snowmelt in higher emissions conditions.

The time- series plot for SSP1 at Tamchu illustrates strong seasonality, with peak flows occurring between July and September, aligning with the monsoon season. Most climate models project an increase in peak flows compared to the historical baseline, with some models (e.g., GFDL-ESM4, CanESM5) showing significant enhancements, indicating greater runoff intensity during the monsoon.

Table 3.5: Near- term projected percentage changes in river flow at WRB

Near-term: 2021-2040: percentage change						
Models	SSP1		SSP2		SSP3	
	tamchu	chimakoti	tamchu	chimakoti	tamchu	chimakoti
CanESM5	7	9	-17	-14	-6	-3
CNRM-CM6-1-HR	-11	-7	-15	-12	-18	-15
CNRM-ESM2-1	-25	-23	-12	-10	-11	-9
EC-Earth3	-6	-5	-4	-3	-7	-5
GFDL-ESM4	-22	-21	-14	-13	-14	-13
IPSL-CM6A-LR	-17	-16	-37	-35	-34	-32
MIROC6	-19	-18	-23	-22	-23	-22
MPI-ESM1-2-HR	-12	-11	29	-39	-11	-10
MRI-ESM2-0	4	6	-7	-6	-15	-15
Mean decrease	**-16**	**-14**	**-11**	**-17**	**-15**	**-14**

Across most models and scenarios, a general decline in streamflow is evident (Table 3.5). Under SSP1 only CanESM5 and MRI-ESM2-0 project increases at both sub- basins, while all other models show declines, leading to a mean decrease of -16% at Tamchu and -14% at

Chimakoti. This suggests that even low emission pathways may not entirely offset reductions in flow.

In SSP2 the declines are slightly more pronounced at Chimakoti, with a mean decrease of -17%, compared to -11% at Tamchu. IPSL-CM6A-LR shows the most severe reductions under this scenario (-37% at Tamchu, -35% at Chimakoti), indicating strong sensitivity to climatic and hydrological changes in this model. While some models (like MPI-ESM1-2-HR) exhibit anomalous values, possibly due to local variability, the consistent negative trends across models underscore a robust signal of decreasing water availability. Overall, SSP3 maintains similar reductions with mean decreases of -15% and -14% at Tamchu and Chimakoti respectively. These consistent declines across all pathways highlight potential climate-induced stress on regional water resources.

3.4.2. Mid- term scenario

a. Punatshangchu River Basin

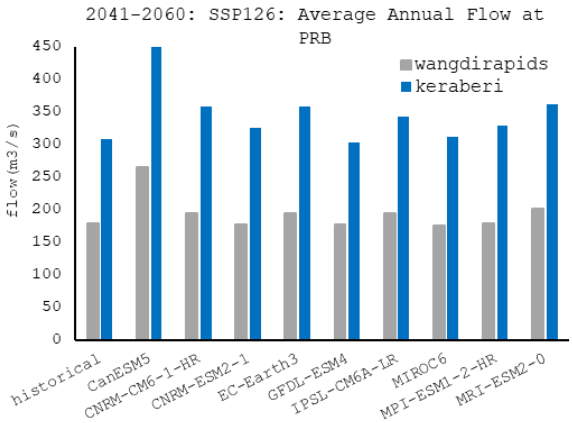

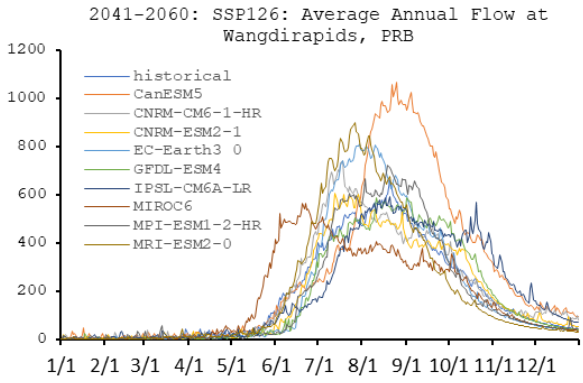

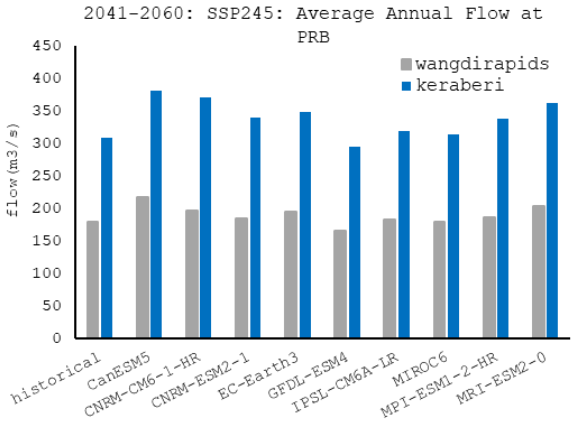

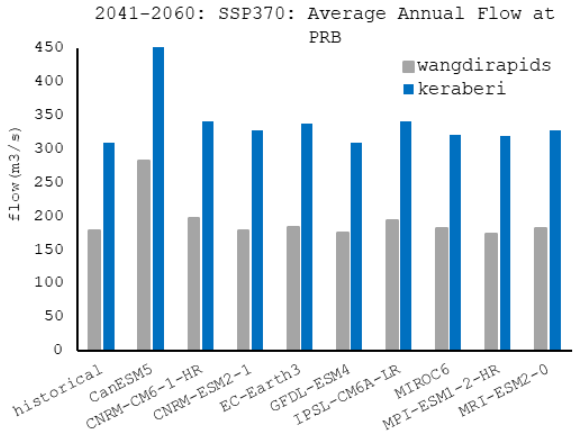

Figure 3.9: Mid- term average annual flow at Wangdirapids and Keraberi in PRB under SSP1 (top left), SSP2 (bottom left) and SSP3 (bottom right). Hydrograph of average annual flow at PRB from 9 GCMs (top right)

Across all scenarios (Figure 3.9), Kerabari exhibits significantly higher annual average flow compared to Wangdirapids, indicating a consistently wetter hydrological regime in the upstream catchment. Under SSP1, both stations show relatively stable flow conditions with slight increases over the historical baseline, while the seasonal hydrograph illustrates intensified monsoon flows, particularly in July to September, with peak discharges exceeding historical norms in most models.

Under SSP2, model spread becomes more pronounced; Wangdirapids flow shows reductions in some models (e.g., EC-Earth3, IPSL-CM6A-LR), while Kerabari maintains or increases flow levels, suggesting localized climate response differences within the basin. In the SSP3 scenario, the contrast between the two stations becomes more evident, Kerabari exhibits robust increases in flow (reaching over 500 m^3/s in some models), whereas Wangdirapids show stagnation or decline, highlighting downstream vulnerability to potential drying or altered runoff generation. These findings imply that mid century hydrological conditions in the PRB are likely to be dominated by stronger seasonality and elevated peak flows during the monsoon, with model uncertainty growing under higher forcing pathways.

Table 3.6: Mid- term projected percentage changes in river flow at PRB

Mid- term: 2041-2060: percentage change						
Models	SSP1		SSP2		SSP3	
	Wangdi rapids	keraberi	Wangdi rapids	keraberi	Wangdi rapids	keraberi
CanESM5	48	54	21	24	57	59
CNRM-CM6-1-HR	9	16	10	20	10	10
CNRM-ESM2-1	-1	5	3	10	-1	6
EC-Earth3	9	16	9	13	2	9
GFDL-ESM4	-2	-2	-7	-4	-2	0
IPSL-CM6A-LR	8	11	2	3	8	10

MIROC6	-2	1	0	2	2	4
MPI-ESM1-2-HR	0	7	4	10	-3	3
MRI-ESM2-0	12	17	14	17	2	6
Mean increase	**17**	**16**	**9**	**12**	**13**	**13**

The projected percentage change in discharge for the mid- term period (Table 3.6) under three climate scenarios indicates a general increasing trend across both Wangdirapids and Keraberi. Under SSP1 the mean discharge increase is 17% for Wangdirapids and 16% for Keraberi, with the CanESM5 model projecting exceptionally high increases of 48% and 54%, respectively. Most models under this scenario show moderate to strong positive changes, though a few (e.g., GFDL-ESM4 and MIROC6) indicate slight reductions.

Under SSP2 the projected changes are slightly lower, averaging 9% for Wangdirapids and 12% for Keraberi. While CanESM5 continues to project relatively higher increases (21% and 24%), other models such as GFDL-ESM4 and MIROC6 show negative or marginal changes, suggesting greater uncertainty under this pathway. The results under SSP3 show a mean increase of 13% for both sites. CanESM5 again shows extreme increases (57% and 59%), while other models display more moderate projections, with some (like MPI-ESM1-2-HR and CNRM-ESM2-1) showing minimal or even negative change.

b. Wangchu River Basin

Across all scenarios (Figure 3.10), Chimakoti consistently shows higher flow than Tamchu, indicating stronger hydrological response or greater catchment contribution. Under SSP1, mean flows for both stations are generally higher than historical levels, with noticeable inter-model variability. In contrast, under SSP2 and SSP3, projected flows remain relatively stable for Chimakoti but decline or remain subdued for Tamchu, especially under SSP3, suggesting possible drying or reduced runoff in that region.

The seasonal hydrograph for Tamchu under SSP1 shows a pronounced monsoon peak around mid July to August, with all models indicating a sharp rise followed by rapid recession. Compared to the historical baseline, most models simulate enhanced peak flows and slightly earlier onset of the monsoon season, highlighting a potential shift in hydrological regime due to climate change.

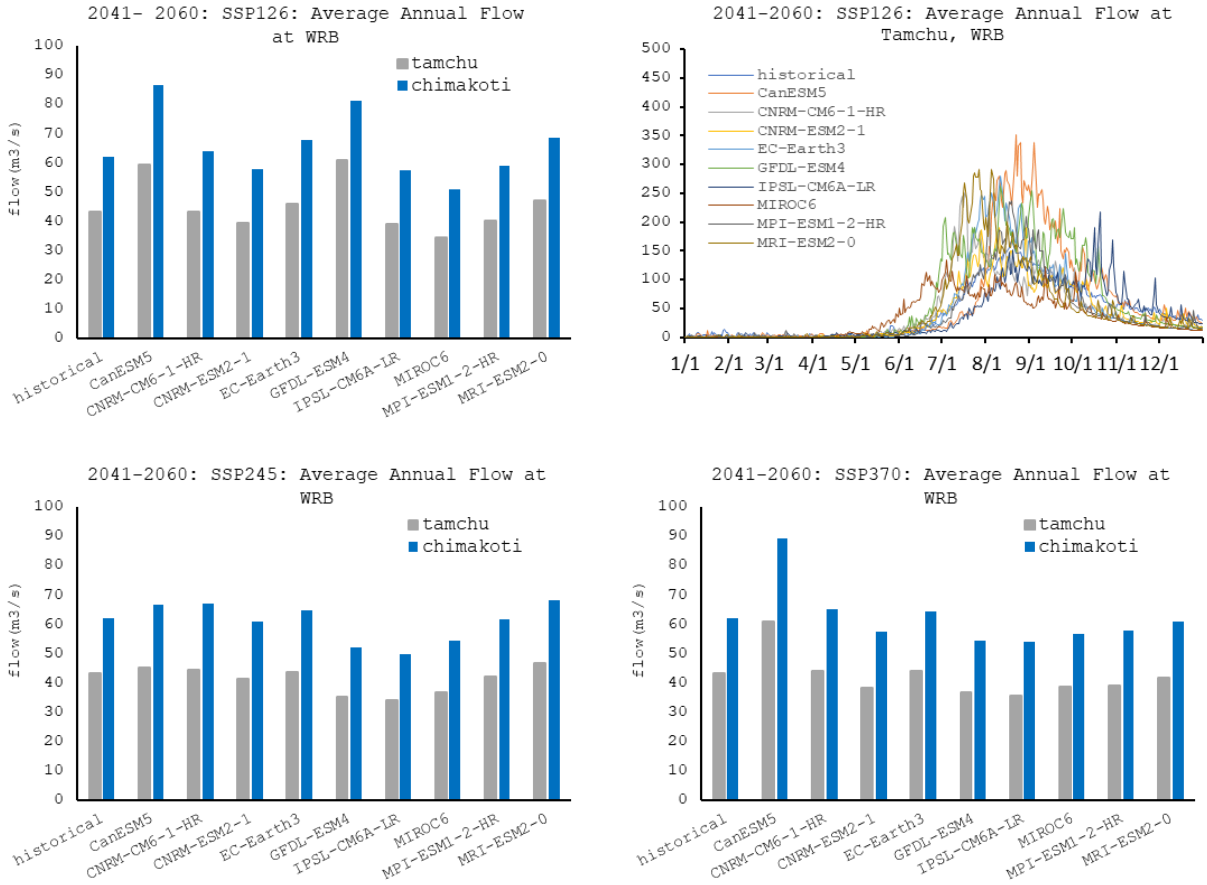

Figure 3.10: Mid- term average annual flow at Tamchu and Chimakoti in WRB under SSP1 (top left), SSP2 (bottom left) and SSP3 (bottom right). Hydrograph of average annual flow at Tamchu from 9 GCMs (top right)

Table 3.7: Mid- term projected percentage changes in river flow at WRB

Mid-term: 2041- 2060: percentage change						
Models	SSP1		SSP2		SSP3	
	tamchu	chimakoti	tamchu	chimakoti	tamchu	chimakoti
CanESM5	37	39	4	7	40	44
CNRM-CM6-1-HR	0	3	2	8	2	5
CNRM-ESM2-1	-9	-7	-5	-2	-12	-8

EC-Earth3	6	9	1	4	2	3
GFDL-ESM4	40	30	-19	-17	-15	-13
IPSL-CM6A-LR	-10	-8	-21	-20	-17	-13
MIROC6	-21	-18	-15	-13	-11	-9
MPI-ESM1-2-HR	-8	-5	-3	-1	-10	-7
MRI-ESM2-0	8	10	8	9	-3	-2
Mean increase	**23**	**18**				
Mean decrease			**-13**	**-10**	**-11**	**-9**

Under SSP1 both Tamchu and Chimakoti show significant increases in flow, with mean increases of 23% and 18%, respectively. Models like CanESM5 and GFDL-ESM4 project the highest increases (up to 40%), while a few models (e.g., MIROC6 and IPSL-CM6A-LR) suggest moderate declines. This indicates that a low- emission pathway may enhance water availability, particularly during peak flow seasons.

In contrast, SSP2 and SSP3 scenarios exhibit a more consistent pattern of declining flows. For SSP2, the mean change is -13% at Tamchu and -10% at Chimakoti, while SSP3 shows slightly smaller average decreases (-11% and -9%, respectively). This suggests that under moderate to high emission futures, river flows may decrease due to potential warming driven reductions in snow and glacier contributions and increased evapotranspiration. The consistent direction of change across models under SSP2 and SSP3 implies a greater likelihood of water stress in mid- to long- term planning horizons.

3.4.3. Long- term scenario

a. Punatshangchu River Basin

Across all three SSP scenarios, both Wangdirapids and Keraberi are projected to experience an increase in average annual flow compared to the historical baseline (Figure 3.11). Under SSP1, flows at Keraberi are consistently higher than Wangdirapids across all models, with values reaching above 400 m^3/s in models such as CanESM5, CNRM-ESM2-1, and MRI-ESM2-0. Wangdirapids shows a more modest increase, typically between 200- 300 m^3/s, with slightly less inter-model variability.

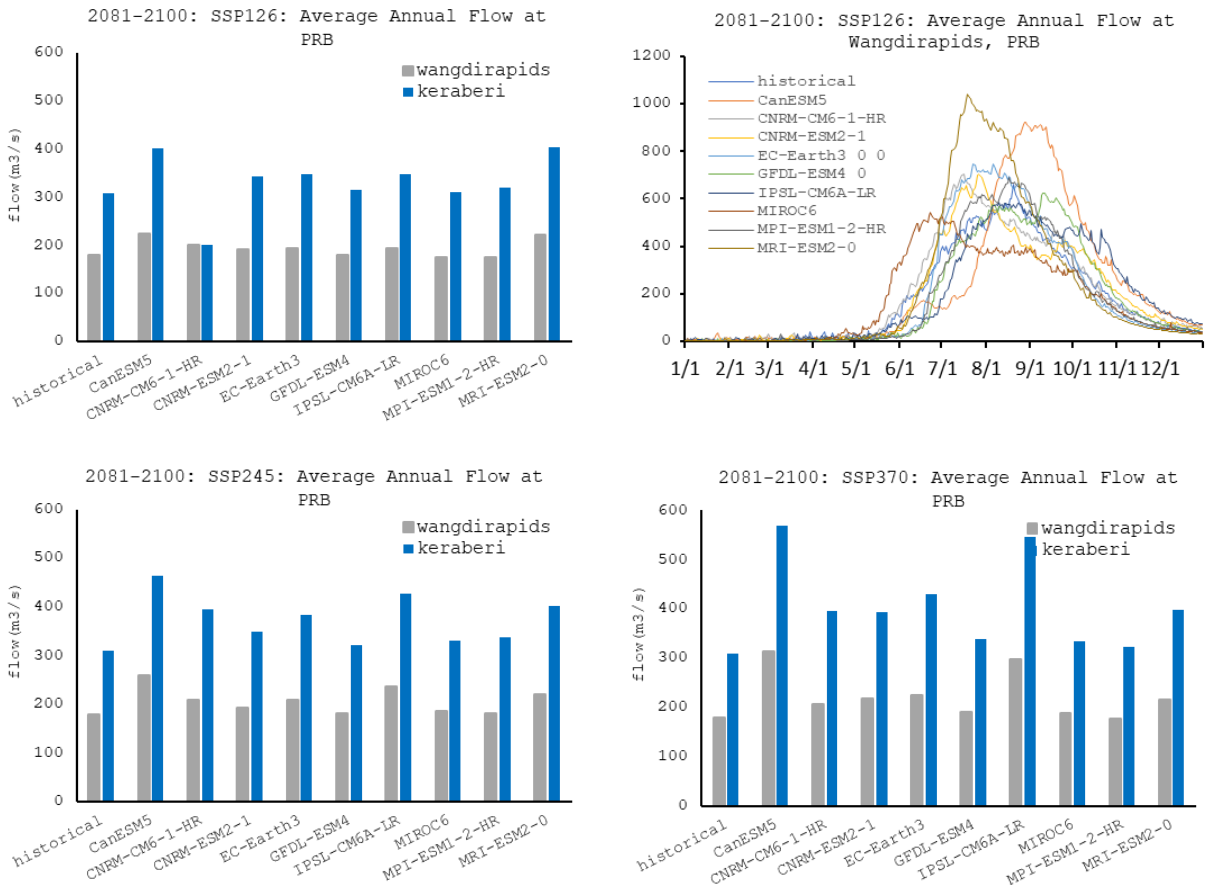

Figure 3.11: Long- term average annual flow at Tamchu and Chimakoti in WRB under SSP1 (top left), SSP2 (bottom left) and SSP3 (bottom right). Hydrograph of average annual flow at Tamchu from 9 GCMs (top right)

Under SSP2, a similar pattern is observed: Keraberi maintains higher projected flows (in the range of 350- 450 m^3/s) while Wangdirapids remains lower (around 200- 300 m^3/s), although model spread slightly widens. The MRI-ESM2-0 and CanESM5 models again show the highest values at both stations. Under SSP3, projected flows increase further, especially for Wangdirapids, with some models projecting up to 300 m^3/s. Keraberi continues to show the highest mean flows (close to or exceeding 400 m^3/s) under most models. This indicates that higher emissions could lead to more intensified runoff and streamflow conditions in the basin.

The hydrograph for SSP1 at Wangdirapids reveals a clear seasonal pattern across models, with peak flow occurring in July and August corresponding to the monsoon season. CanESM5 projects significantly higher peaks (~1100 m^3/s), while other models vary between 500-900 m^3/s. The sharp increase in June and rapid recession after August suggests intensified monsoonal influence, which could amplify flood risks in the future.

Table 3.8: Long- term projected percentage changes in river flow at PRB

Long- term: 2081-2100: percentage change						
Models	SSP1		SSP2		SSP3	
	Wangdi rapids	keraberi	Wangdi rapids	keraberi	Wangdi rapids	keraberi
CanESM5	25	30	44	50	75	84
CNRM-CM6-1-HR	12	-35	16	28	15	28
CNRM-ESM2-1	6	11	7	13	21	27
EC-Earth3	8	13	16	24	26	39
GFDL-ESM4	0	2	1	4	6	10
IPSL-CM6A-LR	8	12	32	38	66	77
MIROC6	-2	0	3	7	5	9
MPI-ESM1-2-HR	-2	3	1	10	-2	5
MRI-ESM2-0	23	31	23	30	20	29
Mean increase	**14**	**15**	**16**	**23**	**29**	**34**

Overall, the results show a clear increasing trend in percentage change from SSP1 to SSP3, with SSP3 exhibiting the highest increases (Table 3.8), particularly in Keraberi. While mean increases for Wangdirapids range from 14% (SSP1) to 29% (SSP3), Keraberi shows even higher changes, from 15% to 34%, indicating spatial variation in climate impact between the two sites. This suggests that Keraberi may be more sensitive to climate change effects, especially under higher emissions scenarios.

Among the models, CanESM5, IPSL-CM6A-LR, and MRI-ESM2-0 consistently show strong positive changes, whereas MIROC6, MPI-ESM1-2-HR, and GFDL-ESM4 show smaller or even negative changes under SSP1. Notably, the CNRM-CM6-1-HR model shows a significant -35% change for Keraberi under SSP1, standing out as a potential outlier. Despite some variation,

the ensemble average indicates a consistent increase in hydrological variables under higher emissions scenarios.

b. Wangchu River Basin

Under SSP1, Chimakoti continues to exhibit consistently higher annual flows than Tamchu, with most models projecting flows above 60 m^3/s. Tamchu flows remain stable or slightly increase compared to historical levels, with some inter- model variation. The hydrograph reveals a strong monsoon peak in August, with some models projecting daily flows approaching 300- 350 m^3/s, suggesting intense but short-lived flood periods in the late monsoon.

In the SSP2, both stations experience moderate increases over historical flows. Chimakoti again shows higher overall discharge, but Tamchu also demonstrates improvement in flow relative to SSP126 for some models. The spread among models narrows slightly, indicating more agreement on future flow conditions under this pathway.

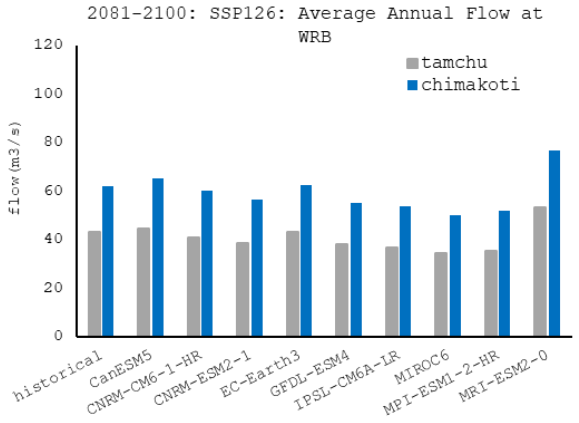

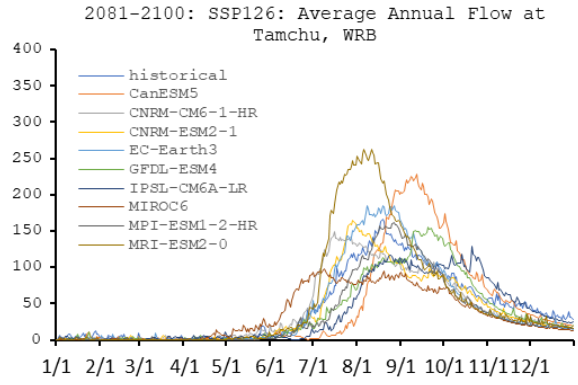

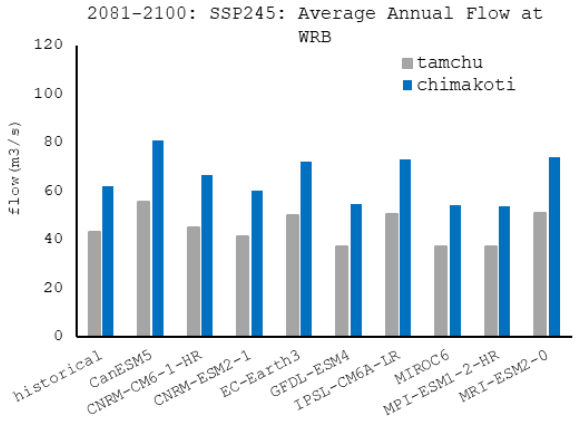

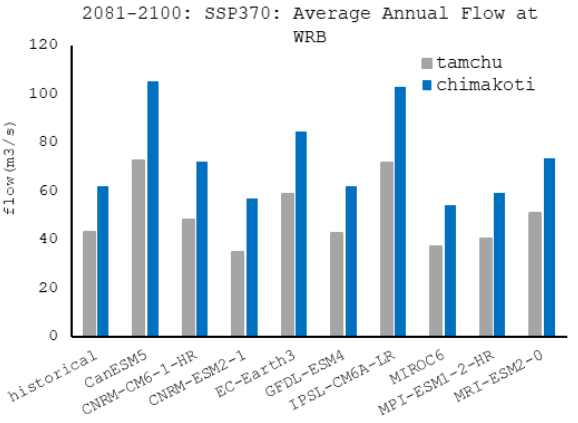

Figure 3.12: Long- term average annual flow at Tamchu and Chimakoti in WRB under SSP1 (top left), SSP2 (bottom left) and SSP3 (bottom right). Hydrograph of average annual flow at Tamchu from 9 GCMs (top right)

Under SSP3 both stations, especially Chimakoti, show significant increases in average annual flow, with several models projecting flows above 100 m^3/s. Tamchu also sees an increase in flow magnitude, with many models showing flows of 60- 80 m^3/s, indicating a climate-intensified hydrological regime likely driven by enhanced glacier melt, precipitation increases, or both.

Table 3.9: Long- term projected percentage changes in river flow at WRB

Long- term: 2081-2100: percentage change						
Models	SSP1		SSP2		SSP3	
	tamchu	chimakoti	tamchu	chimakoti	tamchu	chimakoti
CanESM5	3	5	28	30	68	69
CNRM-CM6-1-HR	-6	-4	4	7	12	16
CNRM-ESM2-1	-11	-9	-5	-3	-19	-8
EC-Earth3	0	0	15	16	35	36
GFDL-ESM4	-12	-11	-14	-12	-2	0
IPSL-CM6A-LR	-15	-14	16	17	65	66
MIROC6	-20	-19	-14	-13	-14	-13
MPI-ESM1-2-HR	-19	-16	-15	-13	-7	-5
MRI-ESM2-0	22	23	17	19	18	18
Mean increase			**13**	**18**	**40**	**41**
Mean decrease	**-14**	**-12**				

Under SSP1, most models project decreases in flow for both stations. Tamchu sees a mean decrease of -14%, and Chimakoti shows a -12% decline, with models like MIROC6 and IPSL-CM6A-LR showing the most significant reductions. Only MRI-ESM2-0 projects a notable increase (22- 23%). This suggests that even under low- emission pathways, some models anticipate reduced snowmelt and glacier contributions to streamflow over the long term.

Under the SSP2 projections shift toward positive trends, with a mean increase of 13% at Tamchu and 18% at Chimakoti. Several models (e.g., CanESM5, EC-Earth3, MRI-ESM2-0) project strong increases, indicating improved water availability under moderate warming. However, other models (e.g., MIROC6 and MPI-ESM1-2-HR) still suggest declines, revealing inter-model uncertainty.

The most dramatic change is under SSP3, with Tamchu and Chimakoti showing mean increases of 40% and 41%, respectively. Notably, CanESM5 and IPSL-CM6A-LR project very high increases (up to 68- 69%), highlighting the potential for intensified hydrological cycles, possibly due to enhanced glacier melt, heavier monsoon rains, or both. While a few models still indicate slight decreases, the majority suggest substantial increases in flow, which may pose challenges for flood risk management and water infrastructure.

3.5. Discussion

Hydrological projections across PRB and WRB revealS distinct spatial and temporal patterns under different emission scenarios. In the near term, the PRB shows consistent increases in river flow at both Kerabari and Wangdirapids stations across all scenarios, especially during the monsoon season. Kerabari generally records higher discharges, with peak flows under SSP3 exceeding 360 m^3/s. While there is inter- model variability, most simulations suggest stronger peak flows and a potential rise in hydrological extremes during the wet season. In contrast, the WRB shows a declining trend in streamflow. Both Chimakoti and Tamchu are projected to experience reductions in annual flow across most models, even under SSP1, pointing to possible water stress in this basin.

By the mid- term, the PRB continues to see increased flows, particularly at Kerabari. Under SSP1, both sites show moderate gains (up to 17%), with stronger monsoonal peaks. However, under SSP2 and SSP3, Wangdirapids show reduced or stagnant flows in some models, highlighting downstream vulnerability. In the WRB, only SSP1 shows increased flow, especially during the monsoon, with Tamchu and Chimakoti experiencing gains of 23% and 18%, respectively. Under SSP2 and SSP3, declining trends reemerge, indicating increased sensitivity to warming and reduced snowmelt contributions.

In the long term, the PRB is projected to experience substantial increases in flow, especially under SSP3. Kerabari may see average flows exceeding 400 m^3/s, while Wangdirapids reaches up to 300 m^3/s, with intensified monsoonal peaks. Although model uncertainty persists, the overall trend suggests a wetter future for the basin. Conversely, long-term projections for the WRB vary more. Under SSP1, most models still show declining flows, while SSP2 brings moderate increases. Under SSP3, both Tamchu and Chimakoti exhibit sharp rises in flow over 40%, potentially driven by glacier melt and heavier rainfall. These increases may help alleviate water shortages but also raise flood management concerns.

4. Conclusion

Projections of future climate for Bhutan indicate a consistent warming trend across all emission scenarios (SSP1, SSP2, SSP3), with substantial increases in both precipitation and temperature, particularly under higher emission pathways and over longer timeframes. These changes are not uniform across space or time. Southern regions are projected to receive significantly more precipitation, especially during the summer monsoon (JJAS), while the high-altitude northern areas are expected to experience more intense warming, especially during the winter months (DJF). These elevation- dependent and seasonally skewed climate responses have critical implications for Bhutan's water resources, ecosystems, and infrastructure.

In the near term (2021- 2040), precipitation increases are modest but notable especially under SSP3, where southern regions may receive over 300 mm more annual rainfall. Summer precipitation is projected to rise by more than 350 mm in some areas. Winter precipitation, however, remains low with minimal change. Maximum temperatures are projected to increase by 0.6- 1.0°C annually, with winter warming reaching up to 1.2°C in the north. Minimum temperatures follow a similar trend, with annual increases of 0.85- 1.2°C and winter increases up to 1.4°C, potentially reducing frost frequency and impacting snow cover.

By the mid term (2041- 2060), the magnitude of change intensifies. Annual precipitation increases by up to 500 mm under SSP1 and SSP2 and over 600 mm under SSP3. JJAS rainfall exceeds 500 mm in southern Bhutan, indicating a stronger monsoonal influence. In contrast, DJF precipitation begins to decline, particularly under SSP2 and SSP3, raising concerns about dry-season water stress. Temperature increases are more pronounced, with annual maximum temperatures rising by 1.2- 2.0°C, and winter Tmax reaching up to 2.3°C in the north. Minimum temperatures could rise by as much as 2.8°C in winter under SSP3, which may accelerate glacier melt and alter alpine ecosystems.

In the long term (2081- 2100), climate change impacts become more severe and potentially disruptive. Under SSP3, annual precipitation increases by more than 2000 mm in some areas, with summer rainfall increasing by up to 1500 mm greatly intensifying runoff and flood risk. Simultaneously, winter precipitation declines by over 15 mm, heightening dry-season vulnerability. Annual maximum temperatures may rise by up to 4.4°C, with winter Tmax increases reaching 5.0°C in the north. Minimum temperatures show similar trends, exceeding 5.2°C annually and reaching 5.5°C in DJF, potentially leading to rapid snowpack decline and permafrost degradation.

These projected changes in temperature and precipitation are expected to fundamentally reshape the country's hydrological systems. In the Punatshangchu River Basin (PRB), increased precipitation and warming temperatures drive consistent increases in river flow, particularly at the Kerabari station. These gains are most evident during the monsoon season, with peak flows intensifying under SSP3. Even in the near term, most models show increases in flow, and by the long term, Kerabari may see average flows exceeding 400 m^3/s. While this indicates enhanced water availability, it also poses risks of increased flooding and sediment transport, especially if infrastructure is not adapted.

In contrast, the Wangchu River Basin (WRB) displays a more uncertain and potentially adverse hydrological response. In the near and mid-term, flows at Tamchu and Chimakoti generally decline, even under low- emission scenarios. These reductions are likely due to warming- driven decreases in snow and glacier contributions, as well as increased evapotranspiration. Only under SSP3 in the long term do flows increase significantly, with some models projecting gains over 40%, possibly due to accelerated glacier melt and intensified rainfall. These shifts suggest that the WRB may face water scarcity in the short to mid term, followed by potential flood risks in the future.

While the findings provide valuable insight, several limitations must be acknowledged. The projections rely on a limited ensemble of climate models, which introduces uncertainty- especially at local and sub- basin scales. Glacier dynamics and snow processes are not fully resolved, which may underestimate or misrepresent meltwater contributions. Land use changes, human interventions (e.g., dam construction, irrigation), and groundwater dynamics were also not incorporated, potentially limiting the applicability of results for long-term planning. Lastly, biases in climate models, particularly in simulating monsoonal variability and extreme events, could affect the precision of hydrological estimates.

Nevertheless, to manage the growing risks and opportunities presented by these changes, several targeted actions are recommended. In the PRB, flood preparedness and sediment management should be prioritized, given the projected increases in monsoon runoff. Adaptive infrastructure design such as flexible reservoir operation and enhanced early warning systems will be essential. In the WRB, the focus should be on water conservation, seasonal storage, and integrated watershed management, particularly in light of potential dry- season shortfalls.

Nationally, the country should expand hydrometeorological monitoring, especially in glacier fed systems and high altitude catchments, to better track climate and runoff changes. Glacier and snowpack monitoring programs should be enhanced to support real time risk assessments. Climate projections must also be mainstreamed into water resource planning, urban development, agriculture, and disaster management policies, ensuring climate resilience is built into long- term national strategies.

In summary, the country's climate future is marked by both intensified water abundance and growing variability. Preparing for this dual reality through proactive, science- based policies will be key to securing sustainable water resources, safeguarding communities, and protecting ecosystems in the decades ahead.

5. References

ADPC & UNDRR. (2020). Disaster Risk Reduction in Bhutan: Status Report 2020. Asian Disaster Preparedness Center and United Nations Office for Disaster Risk Reduction.

Bhahabati, S.S., Kawasaki, A., (2017). Consideration of the rainfall-runoff-inundation (RRI) Model for Flood Mapping in a Deltaic Area of Myanmar. Hydrol. Res. Lett. 11 (3), 155–160. https://doi.org/10.3178/hrl.11.155.

Chhogyel, N., Kumar, L., Bajgai, Y., (2020). Spatio-temporal landscape changes and the impacts of climate change in mountainous Bhutan: A case of Punatsang Chhu Basin. Remote Sensing Applications: Society and Environment, Volume 18, 100307, https://doi.org/10.1016/j.rsase.2020.100307

Dahal, D.; Kojima, T., (2025). Evaluating the Performance of Hydrological Models for Flood Discharge Simulation in the Wangchu River Basin, Bhutan. Hydrology. 12, 51. https://doi.org/10.20944/preprints202502.0052.v1

Dawa, T., Shrestha, A., Aryal, A., (2015). Impact of topography on rainfall variability in Bhutan. Journal of Hydrology and Meteorology, 12(2), 45–56.

Dorji, T., B. J. L. Ona., and S. V. Raghavan., (2021). Statistical analyses on the seasonal rainfall trend and annual rainfall variability in Bhutan. SOLA, 17, 202–206, doi:10.2151/sola. 2021-035

Dorji, U., Olesen, J., Bøcher, Peder., Seidenkrantz, Marit-Solveig,. (2016). Spatial Variation of Temperature and Precipitation in Bhutan and Links to Vegetation and Land Cover. Mountain Research and Development. 36. 66-79. 10.1659/MRD-JOURNAL-D-15-00020.1.

Frieler, K., Lange, S., Piontek, F., Reyer, C. P. O., Schewe, J., Warszawski, L., et al. (2017). Assessing the impacts of 1.5 °C global warming – simulation protocol of the Inter-Sectoral Impact Model Intercomparison Project (ISIMIP2b), Geosci. Model Dev., 10, 4321–4345, https://doi.org/10.5194/gmd-10-4321-2017

Hijmans, R.J., Cameron, E. S., Parra, L. J., Jones, J. P., Jarvis, A., (2005). Very high resolution interpolated climate surfaces for global land areas. International Journal of Climatology. Volume 25, Issue 15 pp. 1965-1978. https://doi.org/10.1002/joc.1276

Katwal, T.B., Bazile, D., (2020). First adaptation of quinoa in the bhutanese mountain agriculture systems. PLoS ONE 15 (1), 18. https://doi.org/10.1371/journal.pone.0219804.

Mahanta, C., Mahagaonkar, A., Choudhury, R., (2018). Climate Change and Hydrological Perspective of Bhutan. In: Mukherjee, A. (eds) Groundwater of South Asia. Springer Hydrogeology. Springer, Singapore. https://doi.org/10.1007/978-981-10-3889-1_33

Maraun, D., (2016). Bias Correcting Climate Change Simulations - A Critical Review. Current Climate Change Reports.Volume 2, pages 211–220, https://link.springer.com/article/10.1007/s40641-016-0050-x
Ministry of Work and Human Settlement. (2015). Flood Hazard Assessment of Thimphu Dzongkhag a Detailed Assessment of Flooding Problems in Thimphu Dzongkhag, Bhutan. Retrieved from https://www.mowhs.gov.bt/en/publications/des-2/femd/

Ministry of Economic Affairs and the World Bank. (2015). Modernizing Weather, Water, and Climate Services: A Road Map for Bhutan. Washington, DC: The World Bank. Retrieved from https://www.nchm.gov.bt/home/pageMenu/32

National Centre for Hydrology and Meteorology. (2024). Climate Change Projection Report, Insights from CMIP6.

National Center for Hydrology and Meteorology. (2021). State of Climate in Bhutan 2021. Retrieved from from https://www.nchm.gov.bt/home/pageMenu/1003

National Centre for Hydrology and Meteorology. (2019). Analysis of Historical Climate and Climate Projection for Bhutan.

National Statistics Bureau. (2025). Statistical Yearbook of Bhutan 2025. Retrieved from https://www.nsb.gov.bt/publications/statistical-yearbook/

National Statistics Bureau. (2020). National Accounts Statistics 2020. Retrieved from https://www.nsb.gov.bt/publications/national-account-report/

National Statistics Bureau Of Bhutan. (2018). 2017 Population and Housing Census of Bhutan National Report. Retrieved from https://www.nsb.gov.bt/publications/census-report/

Nastiti, K.D., Kim, Y., Jung, K., An, H., (2015). The application of rainfall-runoff-inundation (RRI) model for inundation case in upper Citarum Watershed, West Java- Indonesia. Procedia Eng. 125, 166–172. https://doi.org/10.1016/j.proeng.2015.11.024.

Norwegian Water Resources and Energy Directorate. (2011). Climate change impacts on the flow regimes of rivers in Bhutan and possible consequences for hydropower development.

Nguyen, T.T., Nakatsugawa, M., Yamada, T.J., Hoshino, T., (2021). Flood inundation assessment in the low-lying river basin considering extreme rainfall impacts and topographic vulnerability. Water 13 (896), 1–21. https://doi.org/10.3390/w13070896.

Phili-Sihvola, H., et al. (2014). Assessment of hydro-meteorological risks in the Eastern Himalayas. ICIMOD Working Paper.

Poff, L. N., Zimmerman, H.K. J., (2019). Ecological responses to altered flow regimes: a literature review to inform the science and management of environmental flows. Freshwater BiologyVolume 55, Issue 1 pp. 194-205. https://doi.org/10.1111/j.1365-2427.2009.02272.x

Rupa Kumar, K., Sahai, A. K., & Krishna Kumar, K., (2006). High-resolution climate change scenarios for Bhutan based on ENSO and monsoon simulations. Current Science, 90(3), 334–345.

Saji, N. H., Goswami, B. N., Vinayachandran, P. N., & Yamagata, T., (1999). A dipole mode in the tropical Indian Ocean. Nature, 401(6751), 360–363. https://doi.org/10.1038/43854

Sayama, T., Tatebe, Y., Tanaka, S., (2015). An emergency response-type rainfall-runoff-inundation simulation for 2011 Thailand Floods. J. Flood Risk Manag 10, 65–78. https://doi.org/10.2208/jscejhe.69.14.

Sayama, T., Ozawa, G., Kawakami, T., Nabesaka, S., Fukami, K., (2012). Rainfall-runoff-inundation analysis of the 2010 Pakistan flood in the Kabul River basin. Hydrol. Sci. J. 57 (2), 298–312. https://doi.org/10.1080/02626667.2011.644245.

Shrestha, B.B., (2019). Assessment of flood hazard and agriculture damage under climate change in the Bagmati River Basin of Nepal. Int. J. Environ. 8, 55–69. https://doi.org/10.3126/ije.v8i2.25508

Shrestha, B.B., Sawano, H. & Kuribayashi, D., (2016). Assessment of Disaster Damage due to Flood Hazard in the Solo River Basin of Indonesia. The 7th International Conference on Water Resources and Environment Research, Kyoto, Japan, g10–30-1- g10–03-6.

Shrestha, B.B., Sawano, H., Ohara, M., Nagumo, N., (2015). Rice crops flood damage assessment in the pampanga river basin of the Philippines. Adv. River Eng. 21, 497–502. https://doi.org/10.11532/river.21.0_497.

Shrestha, U. B., et al. (2018). Influence of ENSO on Bhutan's rainfall variability. Journal of Climate Research, 23(4), 229–240

Syldon, P., Shrestha, B.B., Miyamoto, M., Tamakawa, K., Nakamura, S., (2024). Assessing the impact of climate change on flood inundation and agriculture in the Himalayan Mountainous Region of Bhutan. Journal of Hydrology: Regional Studies. 52 (101687). https://doi.org/10.1016/j.ejrh.2024.101687

Teutschbein , C., Seibert, J., (2012). Bias correction of regional climate model simulations for hydrological climate-change impact studies: Review and evaluation of different methods. Journal of Hydrology. s 456–457:12–29. http://dx.doi.org/10.1016/j.jhydrol.2012.05.052

Try, S., Tanaka, S., Tanaka, K., Sayama, T., Lee, S., Oeurng, C., (2020). Assessing the effects of climate change on flood inundation in the lower mekong basin using high-resolution AGCM outputs. Prog. Earth. Planet. Sci. 7 (34), 1–16. https://doi.org/10.1186/s40645-020-00353-z.

Wangchuk, S., Dorji, T., & Wangchuk, T. (2020). Spatial climate variability over Bhutan. International Journal of Climatology, 40(5), 2569–2582.

Wang, H., L. Long, A. Kumar, W. Wang, J.-K.E. Schemm, M. Zhao, G.A. Vecchi, T.E. LaRow, Y.-K. Lim, S.D. Schubert, D.A. Shaevitz, S.J. Camargo, N. Henderson, D.Y. Kim, J.A. Jonas, and K.J.E. Walsh., (2014). How well do global climate models simulate the variability of Atlantic tropical cyclones associated with ENSO? J. Climate, 27, no. 15, 5673-5692, https://doi.org/10.1175/JCLI-D-13-00625.1

Warszawski, L., Frieler, K., Huber, V., Piontek, F., Serdeczny, O., Schewe, J., (2014). The Inter-Sectoral Impact Model Intercomparison Project (ISI-MIP): project framework. Proc Natl Acad Sci U S A. 111(9):3228-32. https://doi.org/10.1073/pnas.1312330110

Yangzom, K., Choden, P., (2021). Climate change and water resources in Bhutan. Journal of the Bhutan Ecological Society. 9, 25- 38. https://bes.org.bt/issue-4/

Zam, P., Shrestha, S., Budhathoki, A., (2021). Assessment of climate change impact on hydrology of a transboundary river of Bhutan and India. Journal of Water and Climate Change Vol 12 No 7, 3224 doi: 10.2166/wcc.2021.338